



**British  
Geological Survey**

NATURAL ENVIRONMENT RESEARCH COUNCIL

# Consolidation and rebound properties of Opalinus clay: A long-term, fully-drained test

Environmental Protection Programme

Commissioned Report CR/05/128N





BRITISH GEOLOGICAL SURVEY

TECHNICAL REPORT CR/05/128

# Consolidation and rebound properties of Opalinus Clay: A long-term, fully-drained test

S.T. Horseman, J.F. Harrington, D.J. Birchall,  
D.J. Noy and R.J. Cuss

## *Keywords*

Nagra, Mont Terri, Opalinus Clay, URL, Switzerland, shale, triaxial, consolidation, creep, permeability, drained, undrained, elastic properties, Lemaitre, hydro-mechanical, radioactive waste.

## *Front cover*

Photograph of BGS elastimeter apparatus prior to testing.

## *Bibliographical reference*

S.T. HORSEMAN, J.F.  
HARRINGTON, D.J. BIRCHALL,  
D.J. NOY AND R.J. CUSS  
Consolidation and rebound  
properties of Opalinus Clay: A  
long-term, fully-drained test.  
*British Geological Survey  
Technical Report CR/05/128,*  
60 p.

## BRITISH GEOLOGICAL SURVEY

The full range of Survey publications is available from the BGS Sales Desks at Nottingham and Edinburgh; see contact details below or shop online at [www.thebgs.co.uk](http://www.thebgs.co.uk)

The London Information Office maintains a reference collection of BGS publications including maps for consultation.

The Survey publishes an annual catalogue of its maps and other publications; this catalogue is available from any of the BGS Sales Desks.

*The British Geological Survey carries out the geological survey of Great Britain and Northern Ireland (the latter as an agency service for the government of Northern Ireland), and of the surrounding continental shelf, as well as its basic research projects. It also undertakes programmes of British technical aid in geology in developing countries as arranged by the Department for International Development and other agencies.*

*The British Geological Survey is a component body of the Natural Environment Research Council.*

### **Keyworth, Nottingham NG12 5GG**

☎ 0115-936 3241 Fax 0115-936 3488  
e-mail: [sales@bgs.ac.uk](mailto:sales@bgs.ac.uk)  
[www.bgs.ac.uk](http://www.bgs.ac.uk)  
Shop online at: [www.thebgs.co.uk](http://www.thebgs.co.uk)

### **Murchison House, West Mains Road, Edinburgh EH9 3LA**

☎ 0131-667 1000 Fax 0131-668 2683  
e-mail: [scotsales@bgs.ac.uk](mailto:scotsales@bgs.ac.uk)

### **London Information Office at the Natural History Museum (Earth Galleries), Exhibition Road, South Kensington, London SW7 2DE**

☎ 020-7589 4090 Fax 020-7584 8270  
☎ 020-7942 5344/45 email: [bgs london@bgs.ac.uk](mailto:bgs london@bgs.ac.uk)

### **Forde House, Park Five Business Centre, Harrier Way, Sowton, Exeter, Devon EX2 7HU**

☎ 01392-445271 Fax 01392-445371

### **Geological Survey of Northern Ireland, 20 College Gardens, Belfast BT9 6BS**

☎ 028-9066 6595 Fax 028-9066 2835

### **Maclea Building, Crowmarsh Gifford, Wallingford, Oxfordshire OX10 8BB**

☎ 01491-838800 Fax 01491-692345

### *Parent Body*

### **Natural Environment Research Council, Polaris House, North Star Avenue, Swindon, Wiltshire SN2 1EU**

☎ 01793-411500 Fax 01793-411501  
[www.nerc.ac.uk](http://www.nerc.ac.uk)

# Acknowledgements

The study was undertaken by staff of the Environmental Protection Programme of the BGS using the experimental facilities of the Transport Properties Research Laboratory (TPRL). Funding for the study was provided by the Mont Terri Project, Switzerland.

It is with great sadness that we report that, before this programme of work could be completed, Dr Steve Horseman died. Steve was a much respected scientist whose encyclopaedic knowledge, enthusiasm and energy for his science will be greatly missed by all those who knew and worked with him.

# Contents

<b>Acknowledgements</b> .....	<b>i</b>
<b>Contents</b> .....	<b>i</b>
<b>Figures</b> .....	<b>iii</b>
<b>Tables</b> .....	<b>v</b>
<b>Executive summary</b> .....	<b>vii</b>
<b>1 Scope of the work</b> .....	<b>1</b>
<b>2 Experimental geometry</b> .....	<b>2</b>
2.1 Test material .....	2
2.2 Apparatus.....	2
2.3 Calibration and data acquisition .....	5
2.4 Testing for compliance in apparatus.....	5
2.5 Specimen preparation .....	7
2.6 Basic physical properties .....	8
2.7 Experimental history.....	8
<b>3 Description of test history</b> .....	<b>10</b>
3.1 Initial loading of test specimen.....	10
3.2 Experimental history.....	10
<b>4 Interpretation</b> .....	<b>22</b>
4.1 Consolidation behaviour.....	22
4.2 Parameter estimates from consolidation data .....	25
4.3 Creep analysis.....	27
4.3.1 Methods of studying creep .....	27
4.3.2 Experimental procedure .....	28
4.3.3 Experimental results.....	28
4.3.4 General qualitative observations .....	31
4.3.5 Complexity of measured parameters.....	33

4.3.6	Quantitative approaches to interpreting creep.....	33
4.4	Hydro-mechanical modelling .....	39
4.4.1	The data .....	39
4.4.2	Model definition and boundary conditions .....	40
4.4.3	Modelling of Phase 1 data.....	41
4.4.4	Modelling of Phase 2 data.....	43
<b>5</b>	<b>Conclusions .....</b>	<b>52</b>
	<b>References .....</b>	<b>55</b>
<b>Appendix 1</b>	<b>Glossary .....</b>	<b>57</b>

# Figures

Figure 1 – Schematic of test and data acquisition systems. ....	3
Figure 2 – Schematic of triaxial cell and sample assembly. ....	4
Figure 3 – Vertical (1) and horizontal (2) fractures running through the supplied core. ....	7
Figure 4 – Initial loading of specimen LTFD-1 prior to the start of test stage [1]. ....	10
Figure 5 – Complete test history showing test stages [1] through [16]. Negative strains represent swelling of the specimen. ....	11
Figure 6 – Strain responses during initial reloading of the specimen in test stages [1] and [2]. Initial exposure to backpressure results in swelling of the specimen. Consolidation occurs in stage [2] as effective stress is increased. ....	11
Figure 7 – Time-dependent evolution in water saturation during test stages [1] and [2]. Rapid hydration occurs in the early section of the test, followed by a slow progressive increase in water saturation. ....	13
Figure 8 – Visco-plastic strain and stress deviator during drained creep test stages [3], [4], [5] and [6]. Instantaneous loading strains have been subtracted from the data. ....	14
Figure 9 – Cross-plot of radial and axial strain for the determination of the principal strain ratio during creep deformation. ....	15
Figure 10 – Corrected volumetric strain data for creep stages [3], [4], [5] and [6]. As differential stress increases, dewatering of the clay is clearly observed. ....	15
Figure 11 – Axial strain, radial strain and average effective stress plotted against elapsed time for test stage [7] to [11] inclusive. The strain transients are clearly delineated and approach well-defined asymptotes. ....	16
Figure 12 – Principal strain ratio analysis for test stages [1] to [9] inclusive. Arrows indicate the direction of the test history. ....	17
Figure 13 – Volumetric strain data from volume change and porewater displacement measurements during test stages [7] to [11] inclusive. ....	17
Figure 14 – Axial strain and average effective stress plotted against elapsed time for test stages [12], [13] and [14]. The length of the strain transients for each stage has doubled compared to earlier test stages. ....	18
Figure 15 – Volumetric strain data from volume change and porewater displacement measurements for test stages [12], [13] and [14] inclusive. ....	19
Figure 16 – Cross-plot of cumulative porewater displacement against mean normal effective stress. The convergence of the linear trend lines between 20 MPa and 25 MPa may provide an estimation of the preconsolidation stress. ....	19
Figure 17 – Axial strain and average effective stress plotted against elapsed time for test stages [15] and [16]. ....	20
Figure 18 – Volumetric strain (from porewater displacement measurements) and average effective stress data for test stages [15] and [16]. ....	21
Figure 19 – Post-test photograph of specimen LTFD-1 showing inclined failure planes. ....	21
Figure 20 – Void ratio against logarithm of effective stress for volume change and porewater displacement measurements. ....	23

Figure 21 – Cross-plot of alpha ( $\alpha$ ) values for test stages [2] and [7] to [14] inclusive. Data shows a general trend of increasing $\alpha$ values as average effective stress rises suggesting the onset of plastic yield. ....	24
Figure 22 – A series of void ratio – vertical effective stress curves for a range of geological materials. The preconsolidation stress for a specimen in similar porosity-stress space (shown by red trend lines) suggests a value of around 20 MPa. ....	24
Figure 23 – Specific storage against average effective stress for test stages [2] and [7] to [14] inclusive. ....	26
Figure 24 – Results of the complete creep study, showing the axial strain for the four stages of creep investigation. ....	29
Figure 25 – Creep results for test stage [3] of the experiment (creep stage C1). ....	29
Figure 26 – Creep results for test stage [4] of the experiment (creep stage C2). ....	30
Figure 27 – Creep results for test stage [5] of the experiment (creep stage C3). ....	30
Figure 28 – Creep results for test stage [6] of the experiment (creep stage R1). ....	31
Figure 29 – Lemaitre’s model fitted to triaxial creep data for the shaly facies of the Opalinus Clay. The confining pressure was 0.6 MPa. Test data from Kharchafi and Descoedres (1995) and the data fit from Boidy <i>et al.</i> (2002). ....	35
Figure 30 – The application of the Lemaitre model to the current study. The experimental parameters published by Boidy <i>et al.</i> (2002) are shown, along with a fit produced for the current study [Lemaitre: $N = 15.7$ ; $M = -13.3$ ; $A = 3 \times 10^{-61}$ ; $\alpha = 0.07$ ; $\beta = 1.1$ ; $a = 7.42 \times 10^{-5}$ ]. ....	36
Figure 31 – Comparing the form of the Lemaitre result with the strain data from the current study. [Lemaitre: $N = 15.7$ ; $M = -13.3$ ; $A = 3 \times 10^{-61}$ ; $\alpha = 0.07$ ; $\beta = 1.1$ ; $a = 7.42 \times 10^{-5}$ ]. ...	37
Figure 32 – The fit of each creep stage using a power-law relationship. ....	38
Figure 33 – Data for Phase 1 of the hydro-mechanical testing during which the confining pressure is held constant while the axial stress is changed. The steps in the test are numbered for ease of reference. ....	39
Figure 34 – Data for Phase 2 of the hydro-mechanical testing during which the confining and axial pressures are changed together in steps of 4 MPa. The stages in the test are numbered for ease of reference. ....	40
Figure 35 – Schematic diagram of the main elements of the model and boundary conditions. ...	41
Figure 36 – A comparison of data for the axial strain during Phase 1 of the test with the model response. The model parameters were set for fitting to stage [2]. ....	42
Figure 37 – A comparison of data for the radial strain during Phase 1 of the test with the model response. ....	42
Figure 38 – A comparison of data for the porewater flow during Phase 1 of the test with the model response. ....	43
Figure 39 – Comparison of model to axial strain data for test stage [8]. ....	44
Figure 40 – Comparison of model to axial strain data for test stage [9]. ....	44
Figure 41 – Comparison of model to axial strain data for test stage [10]. ....	45
Figure 42 – Comparison of model to axial strain data for test stage [11]. ....	45
Figure 43 – Comparison of model to axial strain data for test stage [12]. ....	46
Figure 44 – Comparison of model to axial strain data for test stage [13]. ....	46

Figure 45 – Comparison of model to axial strain data for test stage [14].	47
Figure 46 – Comparison of model to radial strain data for test stage [8].	47
Figure 47 – Comparison of model to radial strain data for test stage [9].	48
Figure 48 – Comparison of model to porewater flow data for test stage [8].	48
Figure 49 – Comparison of model to porewater flow data for test stage [9].	49
Figure 50 – Comparison of model to porewater flow data for test stage [10].	49
Figure 51 – Comparison of model to porewater flow data for test stage [11].	50
Figure 52 – Comparison of model to porewater flow data for test stage [12].	50
Figure 53 – Comparison of model to porewater flow data for test stage [13].	51
Figure 54 – Comparison of model to porewater flow data for test stage [14].	51

## Tables

Table 1 – Results for compliance testing experiments with aluminium alloy bar.	6
Table 2 – Modelled axial displacements resulting from stress changes. The final column gives changes of axial displacement from the first modelled state.	7
Table 3 – Dimensions and properties of the test specimen based on a measured grain density for the mineral phases of $2695 \text{ kg.m}^{-3}$ . The value in parentheses is derived from the axial strain measurement recorded at an elapsed time of 532 days.	8
Table 4 - Summary of experimental history showing stage number, description of stage, axial stress and confining stress.	8
Table 5 – Summary of axial and radial strain parameters, cumulative porewater displacement measurements and duration of test stages for specimen LTFD-1.	12
Table 6 – Summary of average effective stress and volumetric strain data from volume change and porewater displacement measurements for each test stage. From stage [11] onwards, volumetric strains determined from volume change observations are based on an assumed principal strain ratio of 0.2764.	13
Table 7 – Average effective stress, void ratio and $\alpha$ parameters for each test stage.	23
Table 8 – Estimates for specific storages based on $\alpha$ values derived from consolidation measurements. For calculation purposes the bulk modulus of water is taken as 2.2 GPa.	25
Table 9 – Drained elastic constants determined for each loading stage. Values in parentheses are based on porewater displacement measurements. PSR values marked # denote average values derived from previous test stages (Section 3).	26
Table 10 – Average undrained elastic constants determined from each load stage.	26
Table 11 – Summary of the experimental conditions for each of the four creep stages of investigation.	28
Table 12 – Lemaitre viscoplastic model parameters for the Opalinus Clay based on gallery convergence and a laboratory creep test performed at ÉPFL. Parameter Set No. 2 gives the best representation of the measured gallery convergences (from Boidy <i>et al.</i> , 2002).	36
Table 13 – Parameter values determined for each stage of Phase 2.	43



## Executive summary

A specimen of Opalinus clay from Mont Terri has been subjected to stress testing over a period of 532 days. Testing was undertaken by changing either (or both) of the axial and confining stresses in sharp steps followed by periods of between 4 and 82 days during which time the specimen was allowed to adjust to the new stress state. In this way, the drained consolidation, creep and rebound behaviour of an Opalinus clay specimen was examined. The test material was subjected to a maximum average effective stress of 38.3 MPa.

Volumetric strain data for both volume change and porewater displacement measurements indicate a small inflection in the standard geotechnical plot of void ratio against the logarithm of average effective stress at a value between 20 and 22 MPa. The negative slope of the consolidation curve ( $\alpha$ ) based on volume change measurements exhibits a general trend of increasing magnitude as effective stress rises. Even though the data do not exhibit the sharp increase in  $\alpha$  indicative of classic virgin consolidation behaviour, it would appear that plastic yielding is occurring at an average effective stress below 20 MPa. Analysis of net porewater flow measurements suggest original interstitial fluid was not expelled from the specimen until average effective stress exceeded 20 MPa. Given the data available, an estimate for the preconsolidation stress in the region of 20 to 25 MPa seems reasonable.

As effective stress rises the duration of the strain transients lengthen. As the induration state of the mudrock increases, strain traces are characterised by less well-defined transients, indicative of time-dependent plastic yielding at high effective stresses. The volumetric strain data for both volume change and porewater displacement shows similar transient behaviour. These results give an average principal strain ratio of 0.252, suggesting the material is either mechanically anisotropic or behaving as a non-ideal elastic medium.

Specific storage values derived from porewater displacement measurements show a general decreasing trend with increasing average effective stress and are in the range 1.5 to  $12.5 \times 10^{-6} \text{ m}^{-1}$ . Data from volume change measurements are less sensitive to changes in effective stress and are in the range 1.2 to  $17.5 \times 10^{-6} \text{ m}^{-1}$ .

Elastic constants derived for undrained quantities are significantly higher than those for drained conditions by approximately one order of magnitude. Data suggests there is a transition in behaviour centred around an average effective stress of approximately 20 MPa.

Analysis of creep curves can be broken down into three distinct responses. The Lemaitre model, as applied to Opalinus clay by Boidy (Boidy *et al.*, 2002), was applied to the current test data. However the published model parameters failed to adequately fit the current data. Minor alteration of these parameters enabled modelling of the longer-term volumetric responses to be undertaken. The Lemaitre model did not predict the initial stage of creep very effectively. A much slower response time was seen in the current data, which was absent in the work by previous researchers.

A power-law creep model was established. In general the fit was adequate for the volumetric strain observed, although these data exhibited some noise. In contrast, the fit of the axial strain data was not adequate and even the subdividing of the data into the individual creep stages failed to give an acceptable fit. A combination of power-law for the initial response and Lemaitre for the longer response may achieve a better prediction for this test stage.

A numerical simulation was run using the 2-dimensional coupled flow and deformation code STAFAN. Two phases of the testing were modelled separately. During Phase 1, the model was used in an attempt to fit the creep data. A reasonable fit was made to the first step axial strain data, but the extrapolation to later stages showed a progressive deviation from the data. In addition, the model made poor predictions for the radial strain and porewater flow data in all

steps. These observations indicate that both the assumptions of linear elasticity and isotropic deformation are probably invalid for this specimen.

During the second phase of testing, the axial and confining stresses were raised synchronously in a series of seven 4 MPa steps. In view of the results of the Phase 1 modelling, it was decided to treat each step of Phase 2 as a separate test and to use the model to parameterise the changing state of the specimen. Young's modulus was significantly lower than those derived from volume and porewater displacement measurements, which can be explained by the over prediction of radial strain due to the simple linear-elastic assumption in the STAFAN model.

It has been shown that the linear elastic deformation model is not a good analogue for the behaviour of this specimen. There are clear indications of non-linear responses to stress changes in the data and it seems likely that some form of viscoelastic or viscoplastic model should be adopted. In addition, the axial and radial strain responses would seem to be anisotropic, bringing further complexity to the model that should be employed.

# 1 Scope of the work

The British Geological Survey was approached by the Mont Terri Consortium to measure and report the drained consolidation and rebound properties of Opalinus clay (OPA) as part of the Phase 8 R&D activities at the Mont Terri Underground Research Laboratory. This long-term hydro-mechanical test was performed using the BGS Elastimeter, a high pressure triaxial apparatus designed to measure the poroelastic properties of cylindrical core plugs. Monitored quantities in the test are axial strain, radial strain, volumetric strain and net porewater displacement. Controlled quantities are confining pressure, axial stress and porewater pressure. The test history comprised a series of fixed increments and decrements in effective stress to provide information on the drained consolidation and rebound properties of the clay, creep behaviour, preconsolidation yield stress, the slope of void ratio – effective stress plot and the stress-dependent specific storage (Wood, 1990; Horseman et al., 1993). Information derived from this experimental study will be used in a number of further activities including assessment of the long-term evolution of the geological barrier (Horseman 2001; 2002) and stress path analysis (Karig and Morgan, 1994).

## 2 Experimental geometry

### 2.1 TEST MATERIAL

The Opalinus Clay is a Jurassic (Aalenian) marine clayshale. The formation, named after the ammonite *Leioceras opalinum*, consists of indurated dark grey micaceous claystones (shales) that are subdivided into several lithostratigraphic units. Some of them contain thin sandy lenses, limestone concretions, or siderite nodules. The clay-mineral content ranges from 40-80 wt% (9-29% illite, 3-10% chlorite, 6-20% kaolinite, and 4-12% illite/smectite mixed layers in the ratio 70/30). Other minerals are quartz (15-30%), calcite (6-40%), siderite (2-3%), ankerite (0-3%), feldspars (1-7 %), pyrite (1-3 %), and organic carbon (<1%). The total water content ranges from 4-19% (Gautschi, 2001).

### 2.2 APPARATUS

The elastimeter apparatus comprises 5 main components (Figure 1):

- 1) The specimen, surrounded by a flexible Hoek sleeve and main pressure vessel body.
- 2) An axial load system comprising of an Enerpac single acting hydraulic ram pressurised by an ISCO-500 series D syringe pump. This is connected via an axial strain jig to a Global Digital Systems optical encoder for measuring linear displacement accurate to 0.003 mm.
- 3) A confining pressure system using an ISCO-100 series D syringe pump allowing radial strain measurements to be calculated through volume change.
- 4) A backpressure system using a second ISCO-100 series D syringe pump allowing the measurement of porewater displacement from the specimen.
- 5) A state-of-the-art custom designed data acquisition system facilitating the remote monitoring and control of all experimental parameters.

A cylindrical rock specimen is positioned between two stainless steel platens and jacketed in a flexible Hoek sleeve to exclude the confining fluid (Figure 2). The inlet and outlet zones for water flow to and from the specimen are provided by stainless-steel discs, nominally 38 mm in diameter and 2 mm thick. The face of each disc was etched with a spiral pattern leading to a central hole with a diameter of 0.36 mm.

Stainless steel platens are in direct contact with these discs transmitting the axial force generated by the Enerpac ram directly to the specimen. Each platen has two ports facilitating flushing of the system and the removal of residual air prior to testing. Retaining collars and axial tie-rods lock the system components together to provide a rigid test rig. Compliance effects are discussed in Section 2.4.

Axial displacement is measured using the GDS optical encoder connected to stainless steel push rods terminating a short distance behind the load-bearing face of each platen to minimise compliance effects. Data from the optical encoder is processed through a multiplexer to provide a continuous measure of axial strain. The confining system provides an indirect measurement of radial strain by monitoring changes in volume while porewater displacement is monitored via the backpressure system.

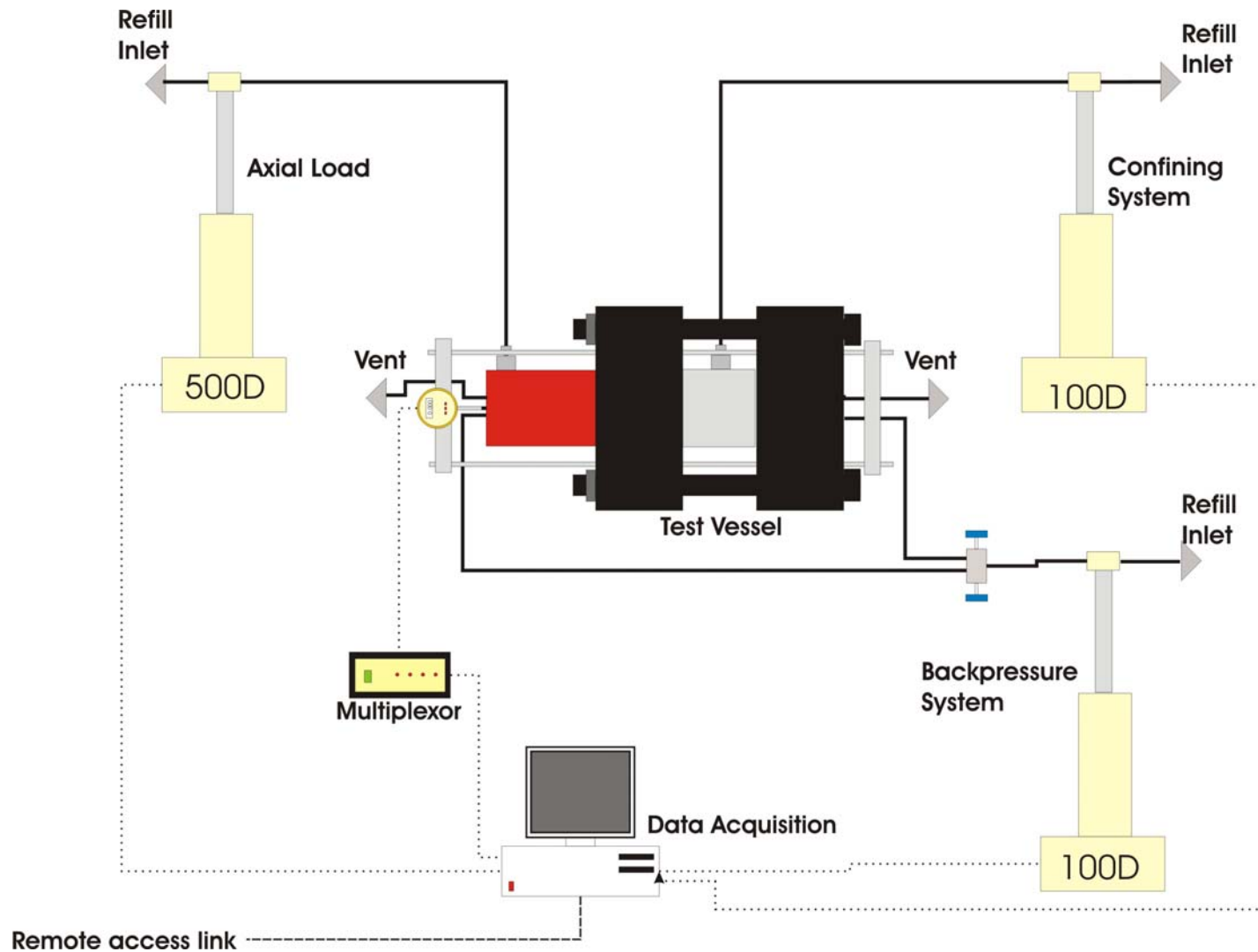


Figure 1 – Schematic of test and data acquisition systems.

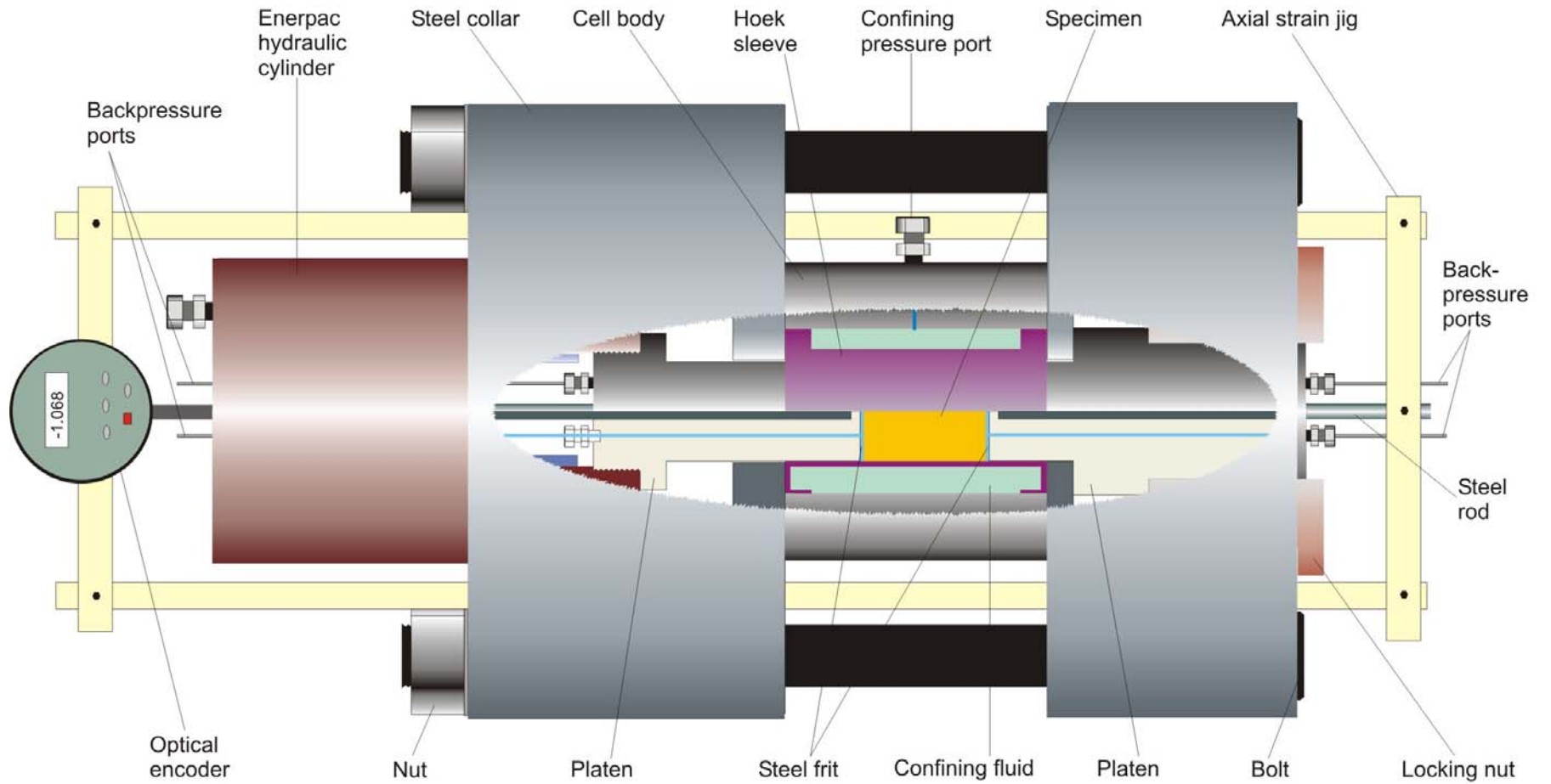


Figure 2 – Schematic of triaxial cell and sample assembly.

## 2.3 CALIBRATION AND DATA ACQUISITION

Confining and backpressure syringe pumps were calibrated using a Druck PTX610 pressure transmitter. Linear regression of data was undertaken to provide calibration values. In order to determine the axial load applied to the specimen through the surface of the platen at any given pump pressure, it is essential to accurately calibrate the ISCO pump used to pressurise the Enerpac ram. To minimise residual error between calibrated and measured values a second order polynomial fit was applied to the data. Calibration values were then multiplied by the ratio of surface areas between the ram piston and platen.

Each ISCO pump controller has an RS232 serial port that allows volume and pressure data to be transmitted to an equivalent port of a 32-bit personal computer. A state-of-the-art data acquisition system was specifically developed for this test using National Instruments LabVIEW™ software. The system allows both remote access to test parameters and control of all ISCO pumps via a LAN based telemetry link. The software prompts the pump controller and multiplexer unit to transmit data to the computer at pre-set time intervals. Data can be downloaded at any time without physical access to the laboratory, minimising thermal variations due to personnel working in the laboratory environment.

## 2.4 TESTING FOR COMPLIANCE IN APPARATUS

In order to try to assess the degree to which compliance of the apparatus might be affecting the results, the deformation of a “standard” aluminium alloy bar was measured within the apparatus under a series of applied axial and radial stresses. These measured deformations were then compared to those calculated using the STAFAN code (INTERA, 1983).

The test bar measured 85.66 mm in length and 38.19 mm in diameter. Its Young’s modulus was certified as 61.8 GPa, but its Poisson’s ratio was unknown. This bar was subjected to a series of increasing and then decreasing axial stresses at constant confining pressure followed by a series of increasing and then decreasing confining pressures under constant axial stress. The axial displacement was observed during these changes and the results are given in Table 1. It can be seen that increasing the axial stress from 39.63 MPa to 91.77 MPa, whilst holding the confining pressure at 34.99 MPa, gives an axial displacement of 45  $\mu\text{m}$  which drops back to a residual displacement of 3  $\mu\text{m}$  when the axial stress is reduced again to 39.43 MPa. Resetting the axial stress to 91.76 MPa with the confining pressure at 34.98 MPa for the start of the second series of measurements gives an axial displacement of 47  $\mu\text{m}$ . This reduces to 30  $\mu\text{m}$  as the confining pressure is raised to 68.83 MPa and increases again to 44  $\mu\text{m}$  when the confining pressure is reduced back to 35.0 MPa.

A simple cylindrically symmetric finite element model of the tests has been set up using the STAFAN code. A mesh of 817 elements with radial and axial dimensions of about 1 mm was used with axial and radial forces applied in three stages. In the first stage, axial stress was set at 39.6 MPa and radial stress at 35 MPa to simulate the initial state of the sample. For the second stage, axial stress was raised to 91.8 MPa, corresponding to the maximum stress applied to the test bar during the first series of measurements. For the third modelled stage the axial stress was maintained at 91.8 MPa while the radial stress was raised to 68.8 MPa - the maximum stress applied during the second series of measurements. Since the Poisson’s ratio for the test bar was not specified, the model was run with values of 0.2 and 0.3 to check for sensitivity to this parameter. The resulting modelled values of axial displacement are shown in Table 2.

It can be seen that the modelled axial displacement in response to a change of axial stress of 52.2 MPa was 72  $\mu\text{m}$ . The measured change was only about 45  $\mu\text{m}$  and it is suggested that the difference is due to compliance of the apparatus. This difference represents an error in the axial strain of 0.032%. When testing clay specimens with this apparatus, it was found that stress

changes of 4 MPa gave rise to strain changes of the order of 0.1%. On the basis of the above, it would be expected that compliance in the apparatus might give rise to errors of the order of 0.002% (for a 4 MPa pressure step), and should have little effect on the interpretations made from the data.

<b>Axial stress MPa</b>	<b>Confining pressure MPa</b>	<b>Axial displacement mm</b>
39.63	34.99	0
44.30	34.99	-0.006
49.67	34.99	-0.012
55.04	34.99	-0.015
60.39	34.99	-0.020
65.77	34.99	-0.024
70.30	34.99	-0.028
75.67	34.99	-0.033
81.04	34.99	-0.037
86.40	34.99	-0.042
91.77	34.99	-0.045
86.41	34.99	-0.040
81.08	34.99	-0.035
75.75	34.99	-0.031
70.39	34.99	-0.027
65.01	34.99	-0.023
59.64	34.99	-0.019
54.29	34.99	-0.014
49.33	34.99	-0.010
44.38	34.99	-0.007
39.43	34.99	-0.003
91.76	34.98	-0.047
91.76	39.96	-0.044
91.76	44.953	-0.041
91.76	49.947	-0.039
91.76	54.941	-0.037
91.76	59.937	-0.034
91.76	64.928	-0.031
91.76	68.825	-0.030
91.76	64.937	-0.030
91.76	59.959	-0.031
91.76	54.965	-0.032
91.76	49.974	-0.035

**Table 1 – Results for compliance testing experiments with aluminium alloy bar.**

Poisson's ratio	Axial stress MPa	Radial stress MPa	Axial displacement $\mu\text{m}$	Delta axial displacement $\mu\text{m}$
0.2	-	-	0.0	
	39.6	35.0	-35.5	0.0
	91.8	35.0	-107.7	-72.2
	91.8	68.8	-89.0	-53.5
0.3	-	-	0.0	
	39.6	35.0	-25.8	0.0
	91.8	35.0	-98.0	-72.2
	91.8	68.8	-69.9	-44.1

**Table 2 – Modelled axial displacements resulting from stress changes. The final column gives changes of axial displacement from the first modelled state.**

## 2.5 SPECIMEN PREPARATION

Core samples of Opalinus Clay from the Mont Terri site were shipped to BGS in resin sealed pipe (Inderbitzin and Météille, 2004). However, initial attempts to manufacture a suitable specimen proved problematic as the supplied core was extensively fractured (Figure 3). Following a number of unsuccessful attempts to manufacture a 38mm diameter core plug, a test specimen was finally prepared by a combination of dry core-drilling and diamond slicing. The ends of the core sample were surface ground flat and parallel to minimise “end-effects” during testing. The specimen was accurately measured using a digital micrometer and weighed. Off-cuts from the coring process were also weighed and oven dried to obtain an estimate of moisture content. The dimensions and geotechnical properties of the specimen are given in Table 3.



**Figure 3 – Vertical (1) and horizontal (2) fractures running through the supplied core.**

## 2.6 BASIC PHYSICAL PROPERTIES

Water content was determined by oven drying at 105°C for a period in excess of 24 hours. Porosity, bulk and dry density and degree of saturation were based on a measured grain density (BS1377: Part 2: 1990) of 2.695 Mg.m<sup>-3</sup>. Table 3 shows basic physical properties of the test specimen before and after the testing programme.

Specimen		Length (mm)	Diameter (mm)	Moisture content (%)	Porosity (%)	Bulk density Kg.m <sup>-3</sup>	Dry density Kg.m <sup>-3</sup>	Saturation (%)
LTFD-1	Pre-test	46.9	38.3	7.9	19.0	2355	2182	91
	Post-test	[46.1]	38.4	8.0	17.9	2390	2214	99

**Table 3 –Dimensions and properties of the test specimen based on a measured grain density for the mineral phases of 2695 kg.m<sup>-3</sup>. The value in parentheses is derived from the axial strain measurement recorded at an elapsed time of 532 days.**

Stage number	Description	Axial stress (MPa)	Confining stress (MPa)	Duration of test (days)
1	Saturation and swelling	6	5	7.8
2	Consolidation	8	7	17.0
3	Drained creep	9	7	24.8
4	Drained creep	10	7	38.9
5	Drained creep	11	7	58.8
6	Drained creep	10	7	68.7
7	Consolidation	10	9	72.6
8	Consolidation	14	13	100.8
9	Consolidation	18	17	133.8
10	Consolidation	22	21	166.7
11	Consolidation	26	25	211.6
12	Consolidation	30	29	274.7
13	Consolidation	34	33	348.5
14	Consolidation	38	37	407.4
15	Unloading (rebound)	34	33	489.4
16	Unloading (rebound)	30	29	532.3

**Table 4 - Summary of experimental history showing stage number, description of stage, axial stress and confining stress.**

## 2.7 EXPERIMENTAL HISTORY

Table 4 defines the test programme for specimen LTFD-1. The test history comprised a series of fixed increments and decrements in effective stress to provide information on the drained consolidation and rebound properties of the clay, creep behaviour, preconsolidation yield stress, the slope of void ratio – effective stress plot and the stress-dependent specific storage (Wood, 1990; Horseman et al., 1993). During the saturation and swelling stage the specimen was exposed to distilled water on both faces. Porewater pressure was maintained constant at 1.0 MPa throughout the duration of the entire test history. A consolidation stage was accomplished by raising the axial stress and confining stress in 1.0 MPa increments respectively until the target test conditions were achieved. With each increment in axial or radial stress, axial displacement

was monitored to determine the undrained properties of the specimen. In the drained creep stages, differential stress was increased in 1.0 MPa increments while confining stress and porewater pressure were held constant. In later test stages designed to evaluate the unloading behaviour of the specimen, confining and axial stresses were reduced in 1.0 MPa decrements respectively until the target test conditions were achieved. During the consolidation and unloading (rebound) test stages differential stress was maintained constant at 1.0 MPa.

## 3 Description of test history

### 3.1 INITIAL LOADING OF TEST SPECIMEN

Axial stress and confining pressure were increased in a step-wise manner illustrated in Figure 4. Porewater pressure was maintained at atmospheric pressure for the majority of the loading history. When axial stress and confining pressure had been raised to 6.0 and 5.0 MPa respectively (test stage [1]), porewater pressure was increased in two steps to the target value of 1.0 MPa. By the end of the loading history the specimen had undergone an axial strain of around 0.50%. Assuming a principal strain ratio (PSR) of 0.2794<sup>1</sup>, the volumetric strain during this test cycle is around 0.79%. This equates to a reduction in specimen volume of around 0.43 cm<sup>3</sup>. It seems clear from the data that this early load-history is dominated by compression of dilatant features, probably caused during the initial sampling and subsequent preparation of the test specimen.

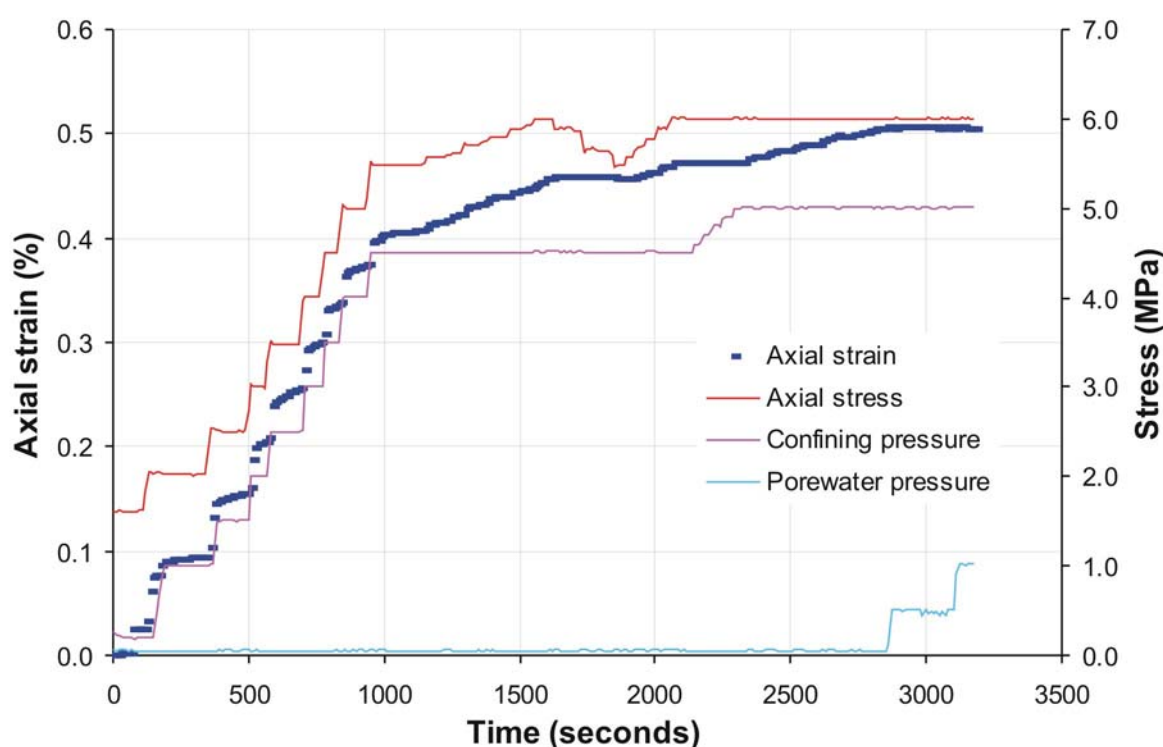


Figure 4 – Initial loading of specimen LTFD-1 prior to the start of test stage [1].

### 3.2 EXPERIMENTAL HISTORY

Data from the initial load-history described in Section 3.1 has not been applied to subsequent test stages. All data and calculated parameters are relative to the start of test stage [1] and to the dimensions of the specimen prior to loading. Figure 5 shows a plot of the entire loading history from test stages [1] to [16] inclusive.

To prevent possible triaxial extension of the specimen during testing, a differential stress of 1.0 MPa was maintained throughout the test history. During the saturation and swelling stage [1], an axial stress of 6.0 MPa and a confining stress of 5.0 MPa were applied to the specimen. A fixed backpressure of 1.0 MPa was applied to both ends of the specimen. There was a net flow of 0.94 cm<sup>3</sup> of porewater solution into the specimen over a period of 7.8 days (Table 5). This

<sup>1</sup> This value is derived from analysis of the strain data for test stage [1].

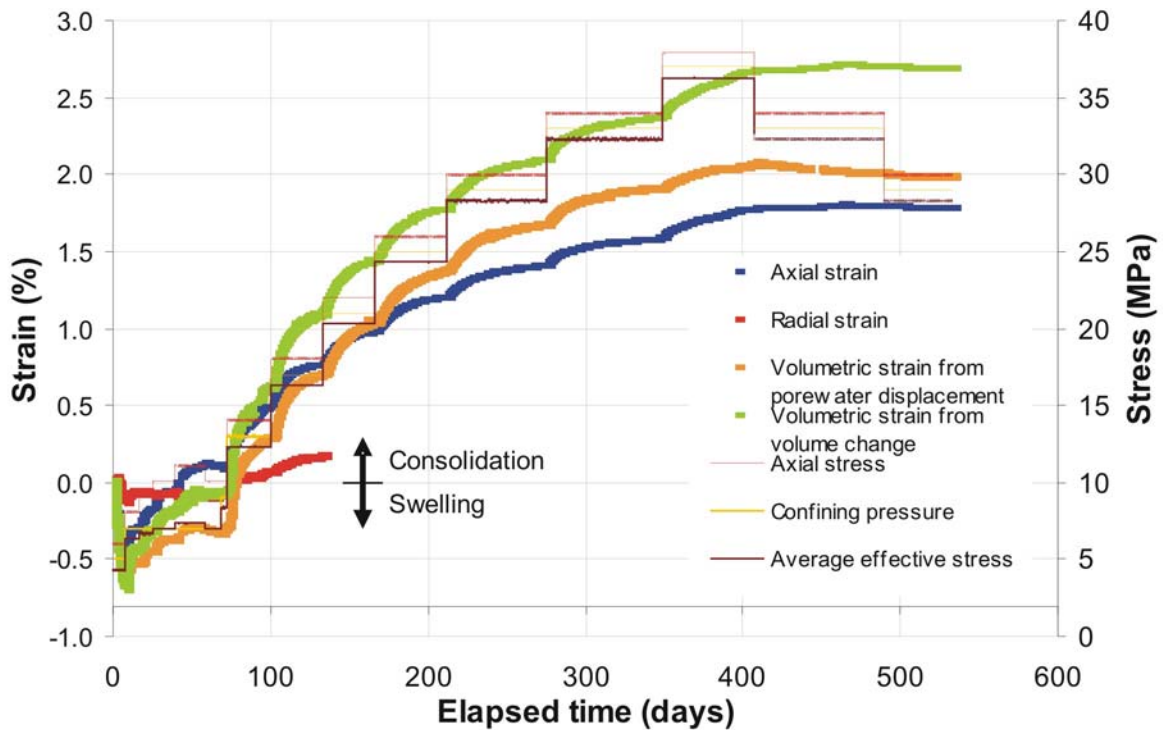


**Figure 5 – Complete test history showing test stages [1] through [16]. Negative strains represent swelling of the specimen.**

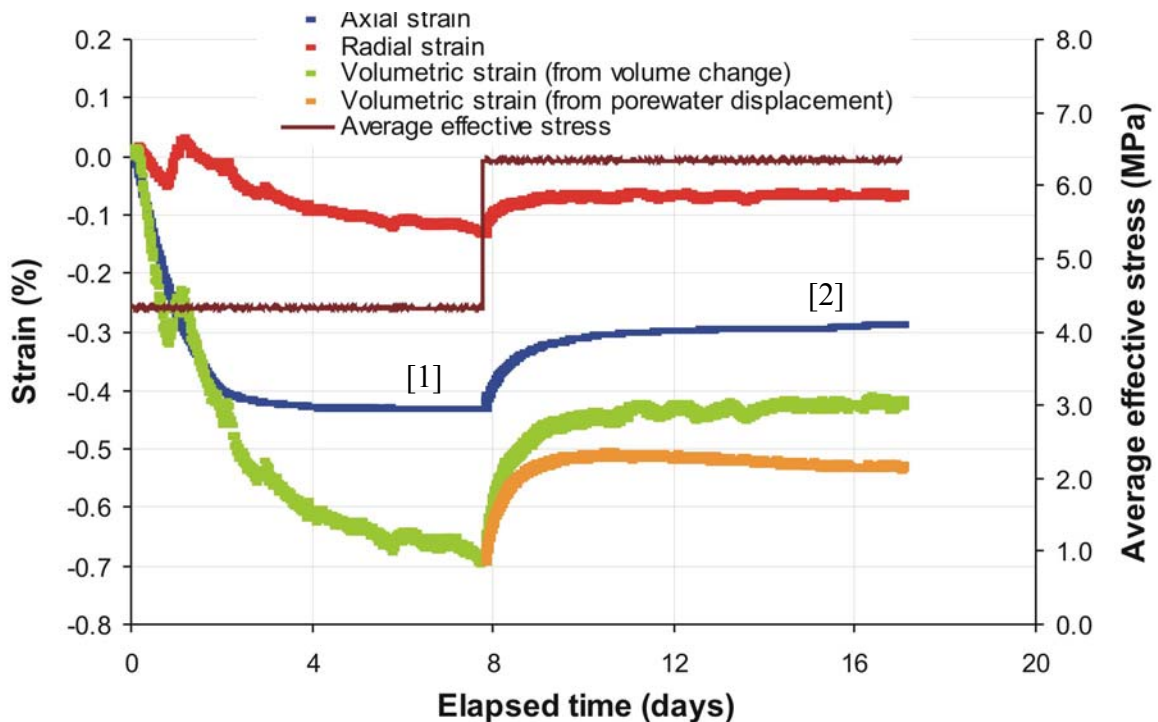


**Figure 6 – Strain responses during initial reloading of the specimen in test stages [1] and [2]. Initial exposure to backpressure results in swelling of the specimen. Consolidation occurs in stage [2] as effective stress is increased.**

represents an apparent volumetric strain of around -1.73% (negative strains represent swelling of the specimen). However, direct measurement of volume change based on axial and radial strain data indicates a volumetric strain of only -0.69% i.e. a change in volume of -0.37 cm<sup>3</sup> (Figure 4, Table 5). This discrepancy can be simply explained by the presence of residual gas trapped in

the specimen at the start of testing. Examination of the geotechnical data (Table 3) shows the specimen contained an initial gas saturation of around 9.1%. This equates to an apparent gas volume of 0.937 cm<sup>3</sup>. Assuming the PSR value applied to the initial loading stage is correct (Section 3.1), the specimen reduced in volume by around 0.43 cm<sup>3</sup>. This suggests that approximately 50% of the air within the specimen was resident within dilatant microfractures which are sensitive to the current level of confining stress and around 50% was located in the remaining pore space of the mudrock; it is uncertain from the data available whether the dilatant microfractures have closed completely.

A second estimate for the gas saturation within the pore space of the mudrock can be obtained from the difference in volumetric strain values quoted above. If the residual gas for test stage [1] is predominantly located within the porosity of the mudrock (rather than dilatant microfractures), then the direct measurement of volumetric strain should be less sensitive to the presence of the gas at low confining pressures. In contrast, volumetric strain estimates based on measurements of porewater displacement will be highly sensitive to both the compressibility of a gas phase and the movement of residual gas into solution. Examination of the data indicates that the difference in these strain values equates to an apparent gas volume of around 0.57 cm<sup>3</sup> suggesting approximately 40% of the gas may reside within the dilatant microfractures and 60% located in the remaining porosity.

Given the uncertainties in the calculation procedure, the assumption of a PSR value, and the sensitivity of the geotechnical calculation for gas saturation, the estimates for gas present in dilatant microfractures are comparable. A correction has therefore been applied to the volumetric strain data based on measurements of porewater displacement to correct for residual gas saturation, such that by the end of stage [1], both values give an apparent volumetric strain of around -0.69%.

Stage number	Axial strain (%)	Radial strain (%)	Porewater displacement (cm <sup>3</sup> )	Duration of stage (days)	Duration of test (days)
1	-0.430	-0.128	-0.940	7.8	7.8
2	-0.289	-0.066	-0.848	9.2	17.0
3	-0.168	-0.074	-0.807	7.8	24.8
4	-0.046	-0.072	-0.764	14.1	38.9
5	0.128	-0.093	-0.724	19.9	58.8
6	0.113	-0.092	-0.739	9.9	68.7
7	0.089	-0.061	-0.710	3.9	72.6
8	0.488	0.067	-0.402	28.2	100.8
9	0.771	0.170	-0.183	33	133.8
10	0.976	0.227	0.000	32.9	166.7
11	1.197	0.288	0.181	44.9	211.6
12	1.408	0.346	0.340	63.1	274.7
13	1.587	0.396	0.442	73.8	348.5
14	1.777	0.448	0.528	58.9	407.4
15	1.798	0.454	0.497	82	489.4
16	1.787	0.451	0.482	42.9	532.3

**Table 5 – Summary of axial and radial strain parameters, cumulative porewater displacement measurements and duration of test stages for specimen LTFD-1.**

The temporal evolution of water saturation can be estimated based on a simple mass balance using the difference in volumetric strain values obtained from volume change and porewater

displacement measurements (Figure 7). Examination of the data (uncorrected for closure of the initial air-filled microcracks discussed in Section 3.1) shows a rapid increase in water saturation of the specimen, reaching over 96% after just 2 days. Thereafter resaturation is characterised by a much slower upward progression which continues through stages [1] and [2].

Stage number	Average effective stress (MPa)	Volumetric strain (%)	
		From volume change	From porewater displacement
1	4.3	-0.686	-0.698
2	6.3	-0.421	-0.531
3	6.7	-0.316	-0.447
4	7.0	-0.191	-0.375
5	7.4	-0.059	-0.303
6	7.0	-0.071	-0.330
7	8.3	-0.033	-0.279
8	12.3	0.622	0.293
9	16.3	1.110	0.704
10	20.3	1.429	1.040
11	24.3	1.773	1.376
12	28.3	2.100	1.676
13	32.3	2.378	1.913
14	36.3	2.673	2.070
15	32.3	2.705	2.008
16	28.3	2.689	1.981

**Table 6 – Summary of average effective stress and volumetric strain data from volume change and porewater displacement measurements for each test stage. From stage [11] onwards, volumetric strains determined from volume change observations are based on an assumed principal strain ratio of 0.2764.**

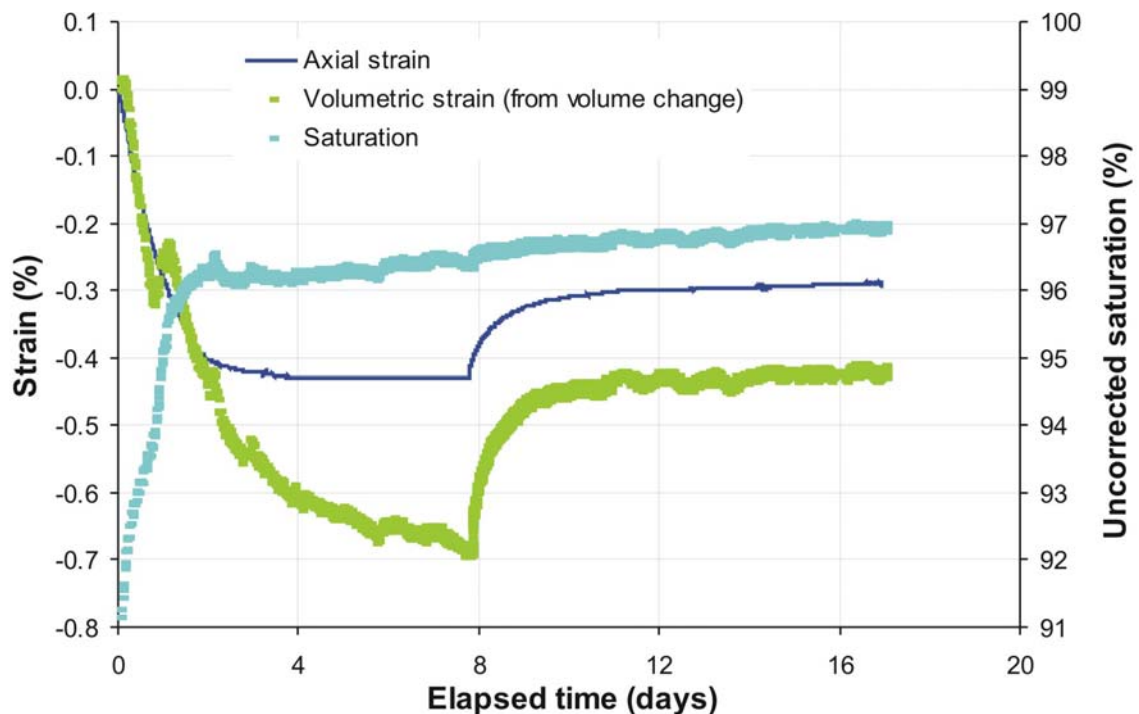


**Figure 7 – Time-dependent evolution in water saturation during test stages [1] and [2]. Rapid hydration occurs in the early section of the test, followed by a slow progressive increase in water saturation.**

The data suggests it could take a significant period of time to fully saturate the specimen. However, uncertainties in both the selection of initial parameters and the assumptions underpinning the saturation calculation mean that this observation should be treated with caution. Since no correction for crack-closure has been applied to the data, absolute values of water saturation are likely to be somewhat conservative.

For stage [2], axial stress and confining pressure were raised to 8.0 and 7.0 MPa respectively. This resulted in a consolidation transient lasting approximately 9.2 days (Figure 7). During this period, axial strain, radial strain and porewater displacement evolved to -0.289%, -0.066% and -0.848 cm<sup>3</sup> respectively (Table 5). After an initial period of consolidation, the direction of volumetric strain (based on measurements of porewater displacement only) reversed, illustrative of a small background swelling response. The observed change in volumetric strain of 0.02% is extremely small and can be explained by the continued movement of residual gas into solution. Volumetric strain data from volume change measurements did not exhibit a similar response.

At this stage of the test history the drained creep response of the specimen was examined by increasing axial stress in 1.0 MPa increments (test stages [3], [4] and [5]), followed by a decrease in axial stress of 1.0 MPa (stage [6]), while confining pressure was maintained constant at 7.0 MPa. Figure 8 shows a plot of visco-plastic strain and differential stress during this test period. Instantaneous loading strains have been subtracted from the creep data. As the differential stress increases, the specimen undergoes axial deformation. By comparison, radial strain appears to be relatively insensitive to the change in differential stress. Cross-plotting radial strain against axial strain (Figure 9) provides an estimate for the principal strain ratio during differential loading, yielding a value of -0.0681 for an OPA specimen undergoing creep deformation. Examination of volumetric strain data (Figure 10) clearly shows that creep is not a constant volume process and changes in the stress deviator can result in either the expulsion or inflow of porewater. A full interpretation of the creep stages is presented in Sections 4 and 5.

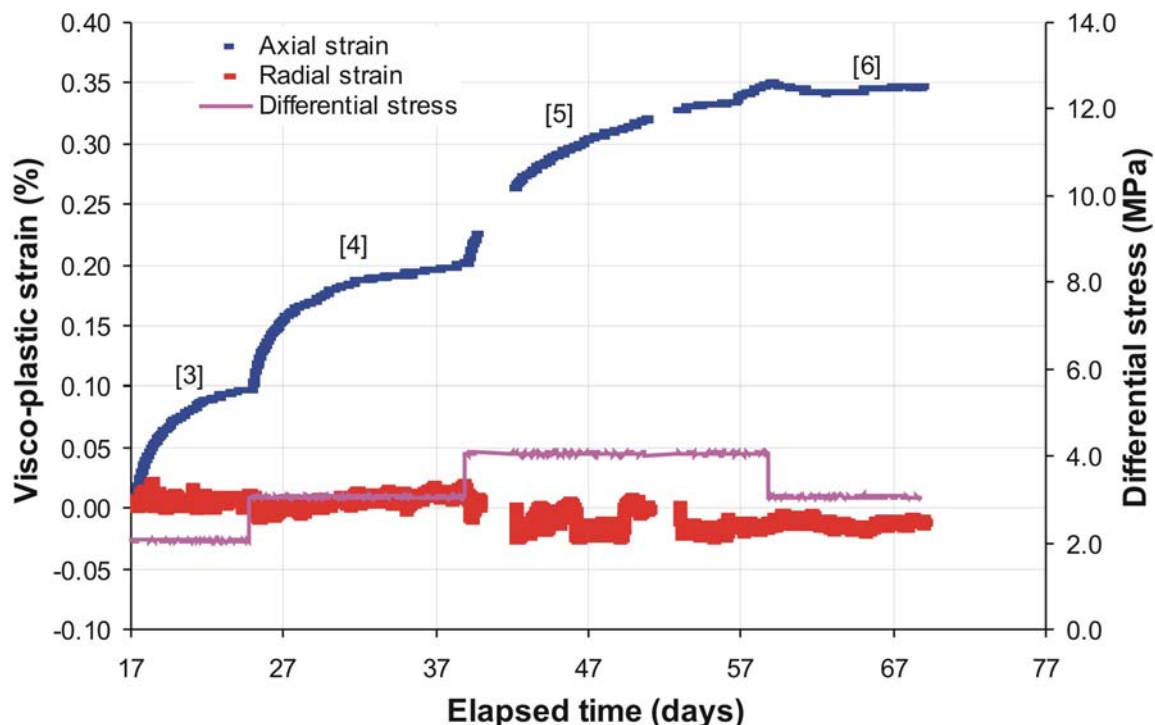


**Figure 8 – Visco-plastic strain and stress deviator during drained creep test stages [3], [4], [5] and [6]. Instantaneous loading strains have been subtracted from the data.**

At the end of the drained creep stages, confining pressure was raised to 9.0 MPa (test stage [7]), re-imposing the initial differential stress of 1.0 MPa. This resulted in radial consolidation of the

specimen with axial strain also exhibiting a minor consolidation response indicating the specimen may not have been fully drained at the end of stage [5].

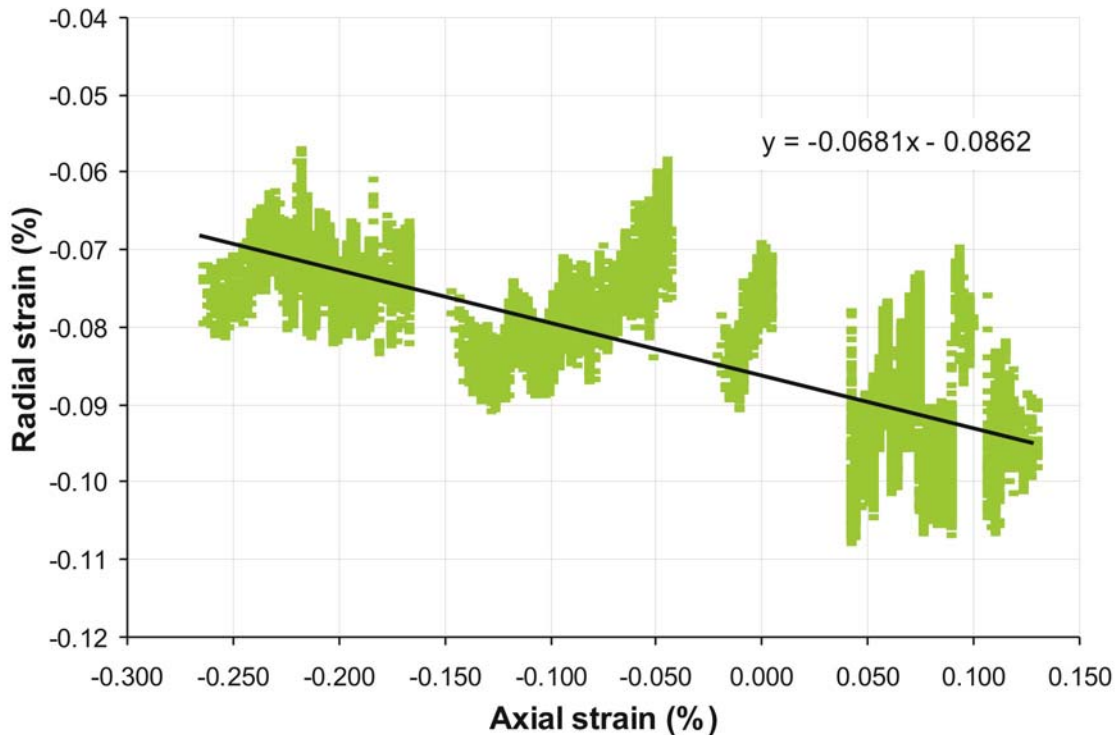


Figure 9 – Cross-plot of radial and axial strain for the determination of the principal strain ratio during creep deformation.

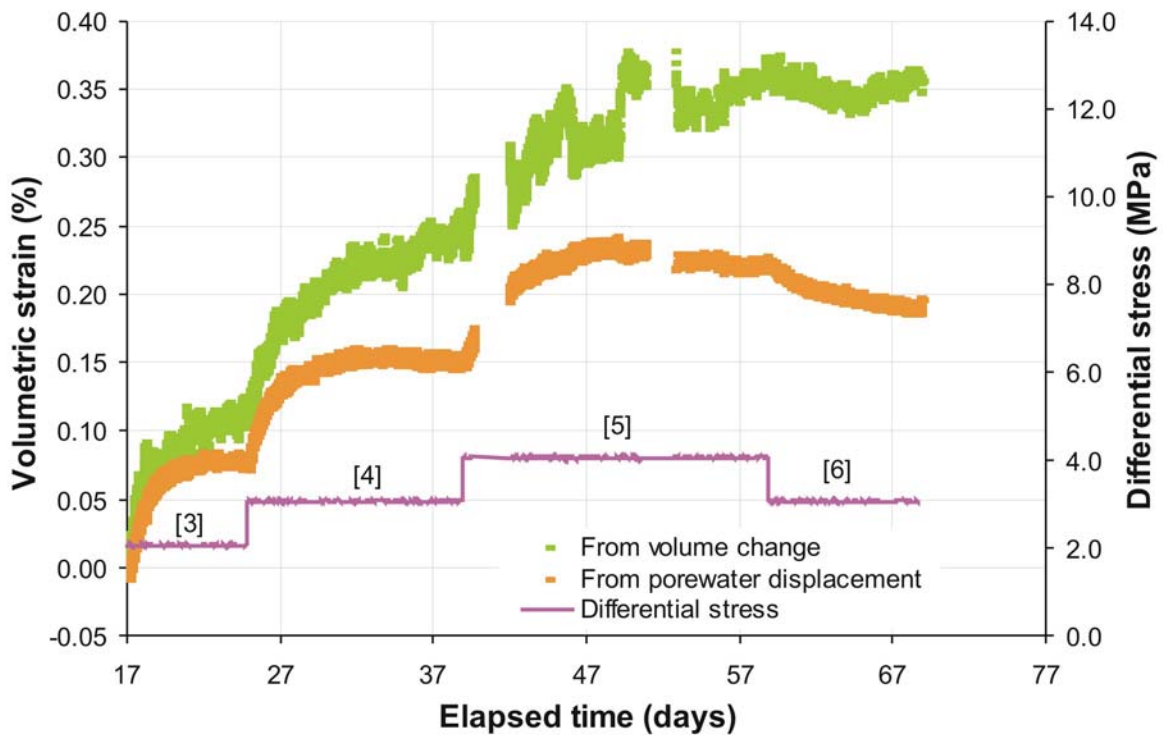
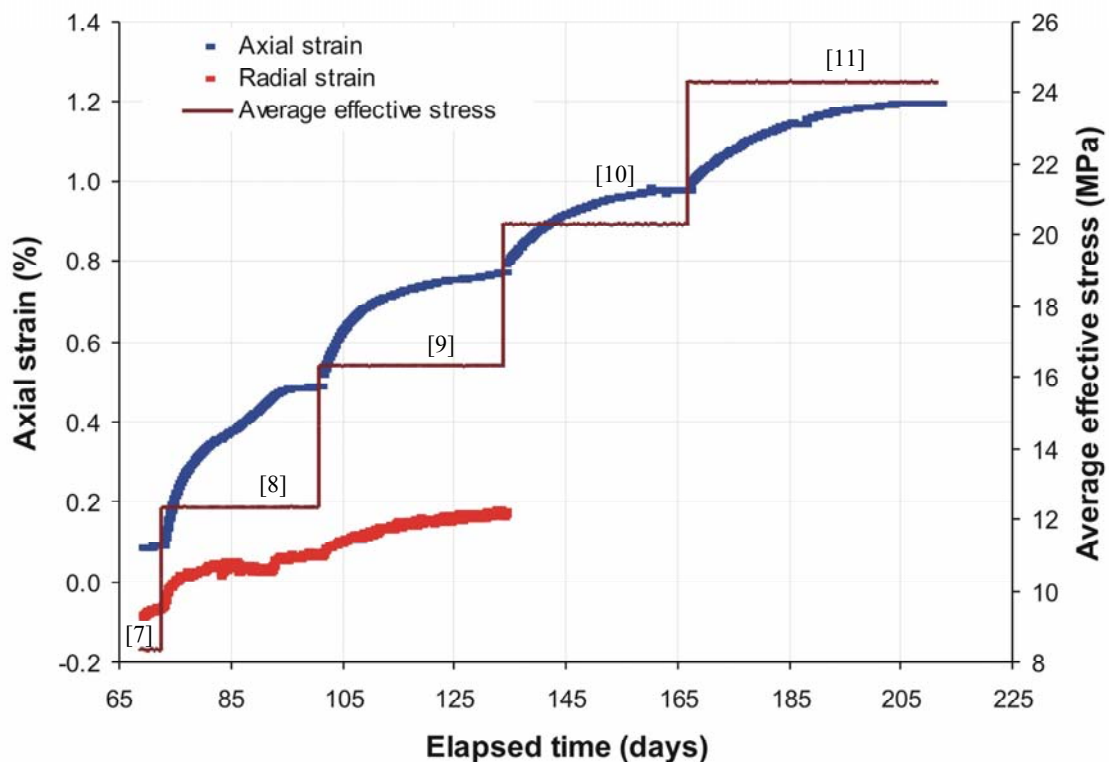


Figure 10 – Corrected volumetric strain data for creep stages [3], [4], [5] and [6]. As differential stress increases, dewatering of the clay is clearly observed.

Axial stress and confining pressure were then raised incrementally in 4.0 MPa steps. Axial strain, radial strain and effective stress parameters for test stages [8] through [11] inclusive are shown in Figure 11. Examination of the data shows well-defined axial strain transients approaching clearly-defined asymptotes. In contrast, radial strain is rather poorly defined and during stage [9] the confining system appeared to develop a small background leak - preventing further measurement of radial strain. The net effect of this leak was to predict principal strain ratios (PSR) that were unrealistically high or physically impossible. For test stage [10] onwards values of radial strain were calculated from axial strain measurements taking a drained PSR of 0.2764. This value was derived from analysis of the principal strain ratios (Figure 12) and is based on the average slope for test stages [1], [2], [8] and the initial section of stage [9]. One consequence of selecting a PSR value in this manner is that it assumes that radial deformation is linearly proportional to axial strain and that the parameter is constant throughout porosity-stress space. In addition the apparent trend of increasing PSR ratio from stage [8] to stage [9] is not accommodated within the calculation of volumetric strain from volume change measurements.

Volumetric strain data from volume change and porewater displacement measurements shows a progressive decrease in specimen volume under an increasing applied load, resulting from compression of the specimen and dewatering of the clay (Figure 13). A closer inspection of the data highlights a small offset in volumetric strain trends obtained from volume change measurements and that derived from monitoring of porewater displacement. This behaviour could relate to a number of factors such as mineral compressibility or compliance of the apparatus, although the latter has been demonstrated to have only a minor effect.



**Figure 11 – Axial strain, radial strain and average effective stress plotted against elapsed time for test stage [7] to [11] inclusive. The strain transients are clearly delineated and approach well-defined asymptotes.**

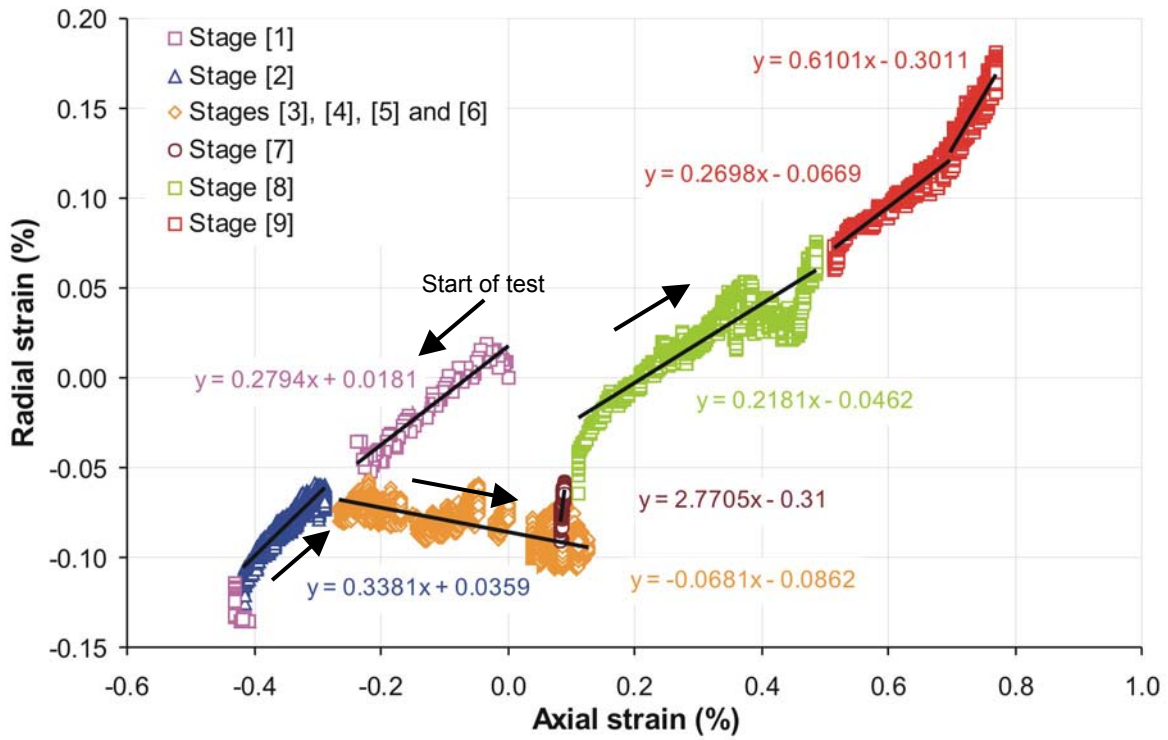


Figure 12 – Principal strain ratio analysis for test stages [1] to [9] inclusive. Arrows indicate the direction of the test history.

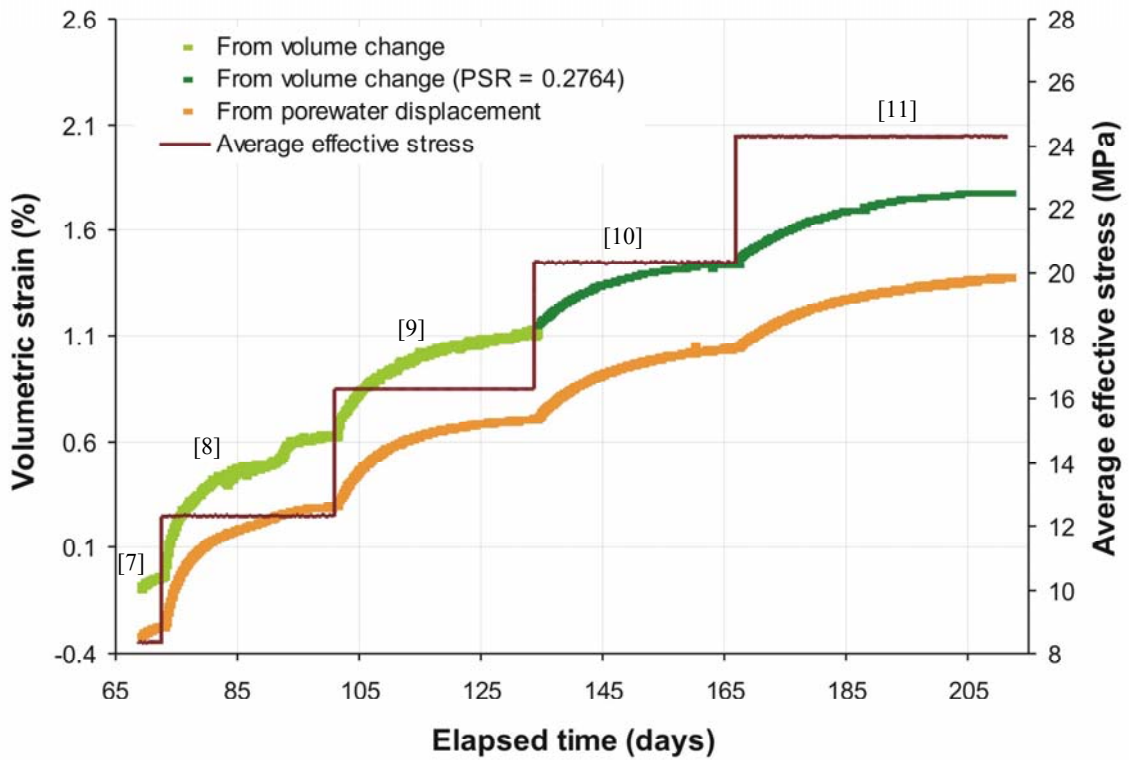
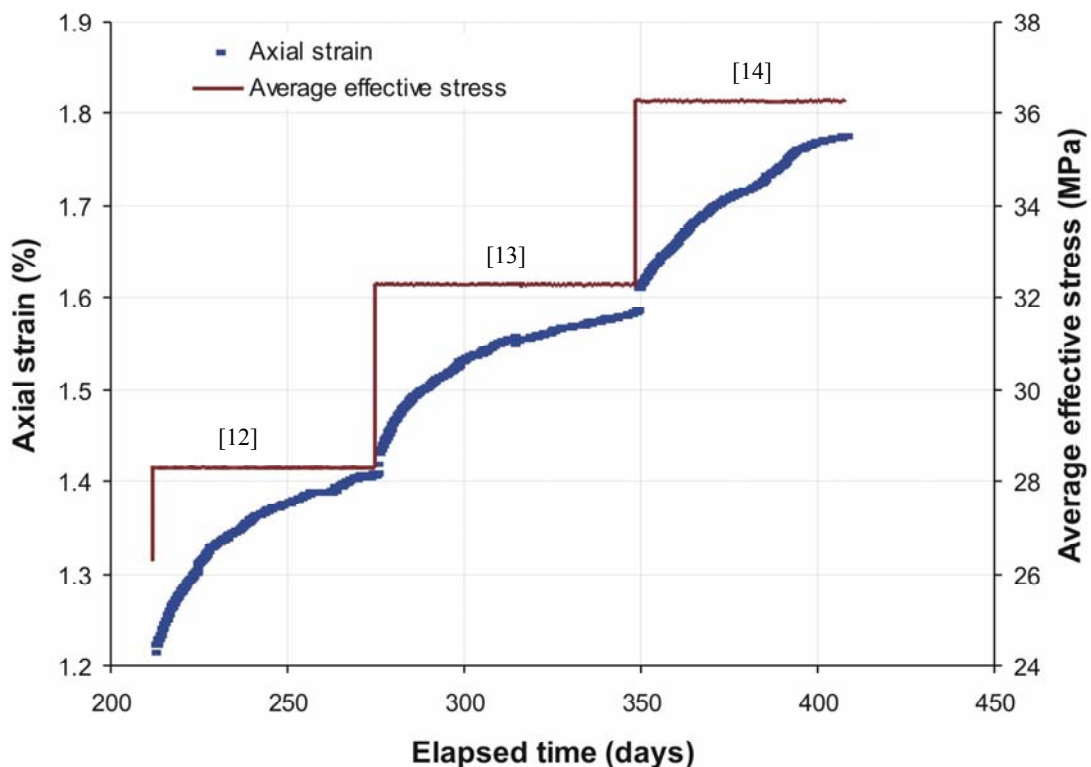


Figure 13 – Volumetric strain data from volume change and porewater displacement measurements during test stages [7] to [11] inclusive.

In test stages [12], [13] and [14] axial stress and confining pressure were again increased in a step-wise manner in 4.0 MPa increments, reaching a maximum net mean effective stress of 36.3 MPa. The length of the axial strain transients (Figure 14) have doubled in comparison to early test stages and are now characterised by less well-defined transients. This could be indicative of time-dependent visco-plastic yielding at high effective stresses. The volumetric strain data for both volume change and porewater displacement measurements shows a similar transient response (Figure 15). By the end of stage [14], the specimen has undergone 1.777% axial strain, around 0.448% radial strain and between 2.070% and 2.673% volumetric strain. The difference in the latter measurements could relate to a number of factors including apparatus compliance and grain-straining of the mineral fabric. Values of volumetric strain from porewater displacement measurements are not sensitive to problems caused by apparatus compliance. However, such measurements are unlikely to detect a significant component of volumetric strain related to mineral compression at high effective stresses.

Figure 16 shows a cross-plot of the cumulative flow data in Table 6 plotted against average effective stress. Examination of the data clearly demonstrates that until the specimen is subjected to an average effective stress in excess of 20 MPa, the total volume of porewater expelled from the specimen is equivalent to the volume injected during the initial resaturation and swelling (stage [1]). The strength of the swelling (suction) response noted in stage [1] is related to the average interparticle spacing and therefore the depth of burial. Given that previous volumetric strain is assumed non-recoverable when a specimen moves along the rebound-reconsolidation line i.e. elastic behaviour, the current interparticle spacing should primarily be determined by the previous maximum depth of burial. If correct, this suggests that the pre-consolidation stress for this test specimen is in the region of 20 - 25 MPa.



**Figure 14 – Axial strain and average effective stress plotted against elapsed time for test stages [12], [13] and [14]. The length of the strain transients for each stage has doubled compared to earlier test stages.**

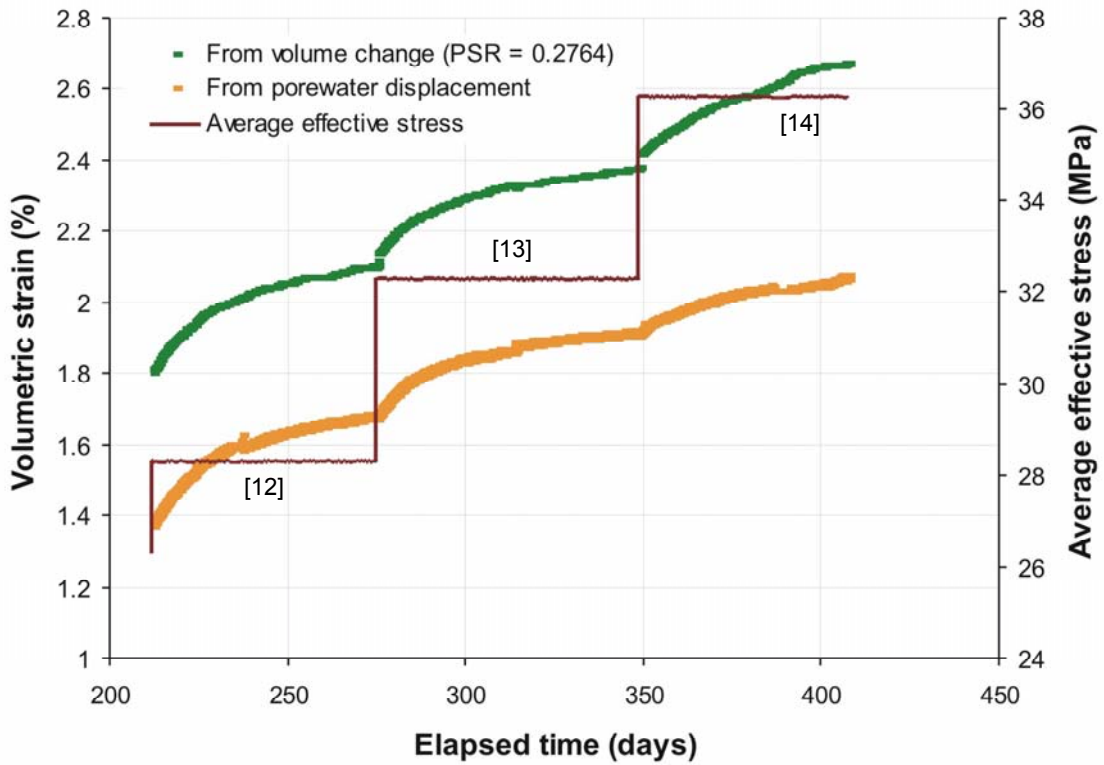


Figure 15 – Volumetric strain data from volume change and porewater displacement measurements for test stages [12], [13] and [14] inclusive.

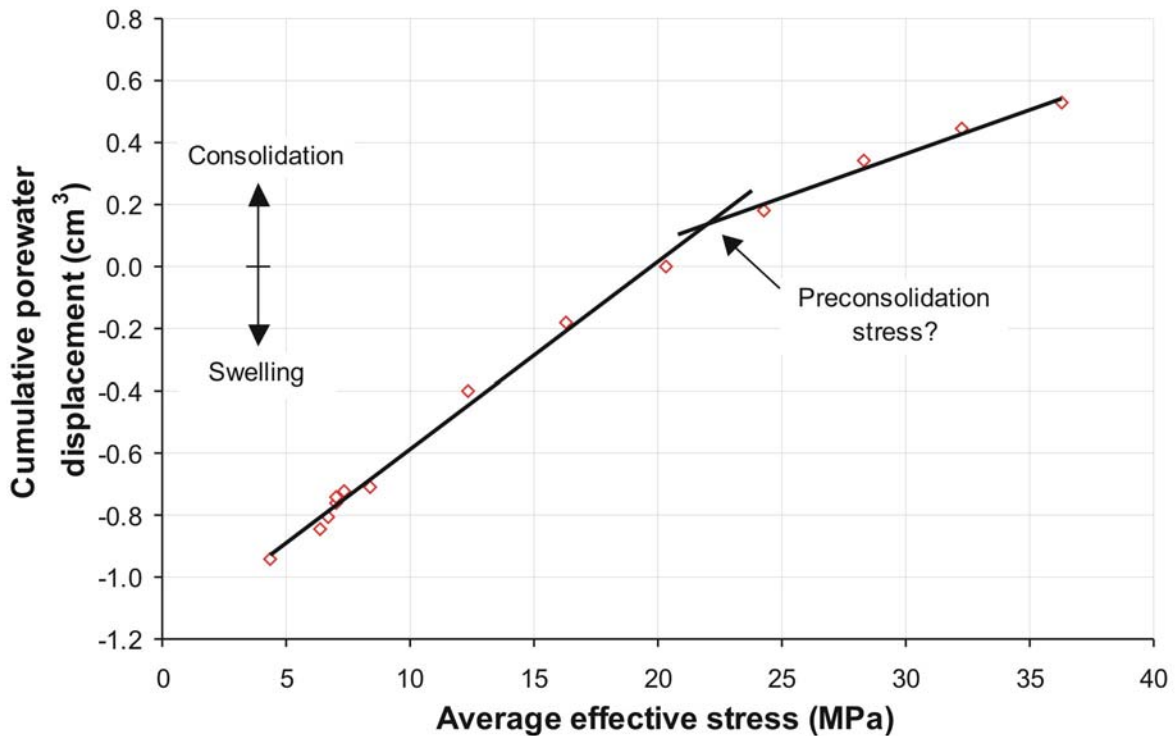


Figure 16 – Cross-plot of cumulative porewater displacement against mean normal effective stress. The convergence of the linear trend lines between 20 MPa and 25 MPa may provide an estimation of the preconsolidation stress.

In order to examine the rebound properties of the specimen, axial stress and confining pressure were reduced by 4.0 MPa (test stage [15]). Axial strain initially levelled at a value of 1.781% for a period of around 20 days (Figure 17). A slight upward trend was then observed reaching a

maximum strain of 1.804% before spontaneously declining to a value around 1.798% by the end of the stage.

Axial and radial stress was again reduced by 4.0 MPa resulting in a small negative transient in axial strain (Figure 17), which, by an elapsed time of 532 days had declined to 1.787%. Figure 18 shows a plot of volumetric strain based on porewater displacement measurements against elapsed time for test stages [15] and [16]. The reduction in effective stress results in small but well-defined negative transients commensurate with swelling of the specimen.

At this point in the test history the laboratory suffered a major power cut which extended beyond the capacity of the existing UPS systems. The net result of this unforeseen event was that the specimen was subject to an extensile stress regime as axial stress decreased to around 20.6 MPa while confining pressure remained high at 29.0 MPa. Examination of subsequent test stages clearly showed that the specimen had experienced significant disturbance, which dominated subsequent system responses. At this point the test was terminated and the apparatus decommissioned. Drift in the transducer outputs for the backpressure and confining system was relatively small given the duration of the test history (-0.57 MPa and 0.1 MPa respectively). In contrast the pump transducer connected to the axial ram exhibited a larger drift in pressure of around -2.4 MPa. This would equate to an axial “under-pressure” on the specimen of -9.7 MPa under test conditions. The data clearly indicates this offset is not manifested within the experimental stages reported above and is therefore most likely to have occurred very late in the test history after the interruption in electrical power or during the final decommissioning process.

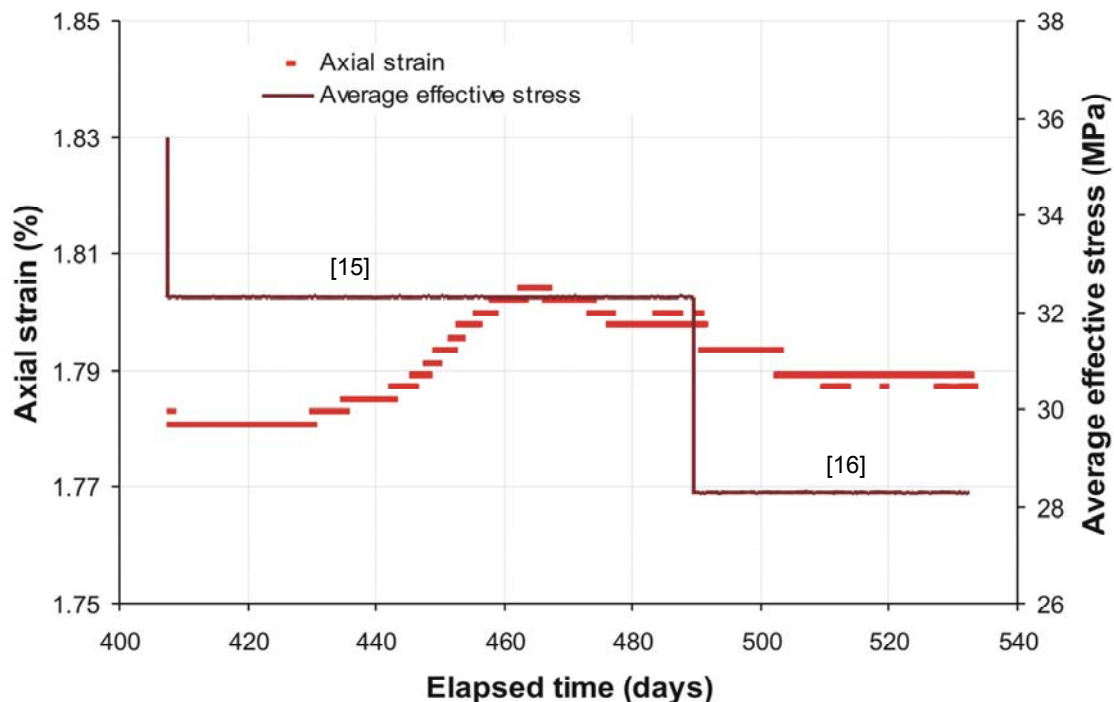


**Figure 17 – Axial strain and average effective stress plotted against elapsed time for test stages [15] and [16].**

To remove the specimen from the apparatus, axial stress and confining pressure were gradually reduced in a step-wise manner in 1.0 MPa decrements. Deflection of the axial push rod was recorded at each stage of the unloading history and at the end of the procedure, axial, confining and porewater pressure were vented to atmospheric pressure. The total deflection observed during this time was around -0.082 mm (the minus sign denoting an apparent swelling of the specimen) representing a recoverable strain of around -0.17%. When the specimen was extruded from the apparatus it sheared under its own weight along a number of inclined failure planes

(Figure 19). It is not possible to determine with any certainty when these features formed, but given the atypical experimental data following the triaxial extension event in stage [16], it seems probable that one or more of these features formed at that time. The specimen was weighed, oven dried and reweighed to determine the basic geotechnical properties.

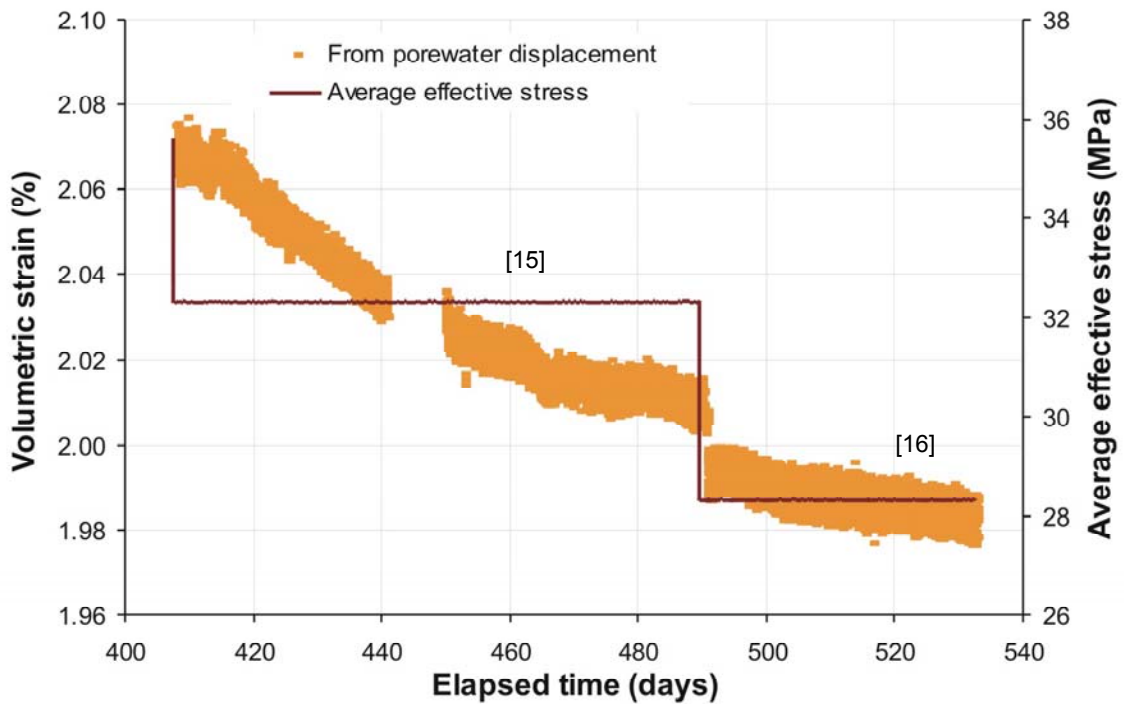


**Figure 18 – Volumetric strain (from porewater displacement measurements) and average effective stress data for test stages [15] and [16].**

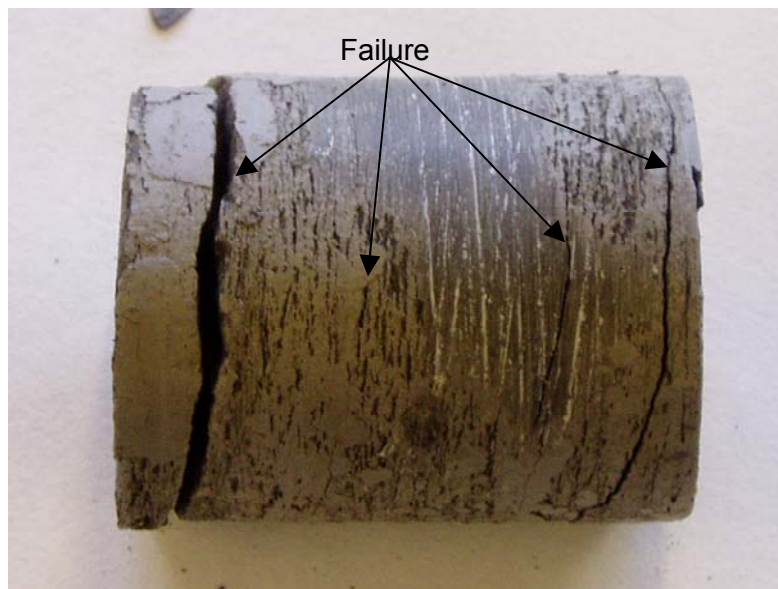


**Figure 19 – Post-test photograph of specimen LTFD-1 showing inclined failure planes.**

Post-test analysis of interstitial fluids showed a significant increase in major ions in the backpressure system either side of the specimen. This provides clear evidence for the expulsion of interstitial fluids from the specimen during the loading history. The distilled water contained within the pump reservoir remained fairly unchanged.

## 4 Interpretation

### 4.1 CONSOLIDATION BEHAVIOUR

Figure 20 shows the standard geotechnical plot of void ratio against the logarithm of effective stress (Schofield and Wroth, 1968; Atkinson and Bransby, 1978). The orange and green lines represent the behaviour of the specimen when axial stress and confining pressure are increased with backpressure held constant. The early curvature of both lines is assumed to relate to perturbation of the specimen during field sampling and specimen manufacture. From test stage [7] onwards the lines are sensibly linear in the log-linear parameter space up to an average effective stress of 36.3 MPa. The linear section of any part of a consolidation curve can be represented by the general relationship:

$$e = e_0 - \alpha \ln\left(\frac{\sigma'}{\sigma_0'}\right) \quad (\text{Eq4-1})$$

where  $-\alpha$  is the slope,  $\sigma'$  is the effective stress acting on the specimen, and  $e_0$  is the void ratio intercept at an effective stress,  $\sigma_0'$ , equal to 1.0 MPa. Values of void ratio and  $\alpha$  are given in Table 7 for each test stage. Detailed analysis of the consolidation transients indicates secondary consolidation (*i.e.* time-dependent volumetric creep of the fabric) still in progress at the end of most test stages. The superposition of the hydraulic and rheological responses will have a minor effect on the calculated consolidation parameters, but this is unavoidable given the practical constraints on test duration.

Inspection of the void ratio data for porewater displacement indicates that a very small inflection exists at an average effective stress of around 20 MPa. A similar response is also observed in the volume change data at around 21 to 22 MPa. The subtlety of this response demands care in its interpretation. If the inflection represents the preconsolidation stress it suggests that the parameter is rather poorly defined. However, due to extenuating circumstances, insufficient load was applied to the specimen to observe sufficient volumetric plastic yielding after the inflection point in order to confidently determine the preconsolidation parameter.

Figure 20 shows the early stages of the unloading response for the specimen when subjected to a reduction in average effective stress (test stages [15] and [16]). Unfortunately, only a small section of the unloading history is delineated due to the premature termination of the test (Section 3). However, inspection of the data clearly indicates that the majority of the strain for these early stages is non-recoverable. Unfortunately, given the lack of subsequent data it is not possible to give a quantitative interpretation in order to provide additional information on the current consolidation state of the clay.

Due to the loss of the radial strain measurement system during test stage [9], the void ratio measurements from volume change observations are best estimates only, based on axial strain measurements and an assumed PSR. The difference in void ratio – log effective stress response between volume change and porewater displacement measurements can be explained by a number of factors including compressibility of the mineral constituents, changes in pore morphology and to a very minor degree, compressibility of the apparatus (Section 2). Since estimates of volume change from porewater displacement measurements do not incorporate mineral compressibility, prediction of volumetric strain behaviour based on these observations alone is likely to be somewhat conservative in nature.

The  $\alpha$  values in Table 7, based on volume change measurements, exhibit a general trend of increasing magnitude as effective stress rises (Figure 21). An increase in  $\alpha$  value would be anticipated with the onset of plastic yielding. Examination of the porewater displacement data

shows a similar progressive upward trend to an average effective stress of around 30 MPa, at which point  $\alpha$  values begin to decrease. This reduction in value could be explained by grain-strain of the mineral fabric at high effective stresses. Even though the data do not exhibit the sharp increase in  $\alpha$  values indicative of classic virgin consolidation behaviour, it would appear that plastic yielding is occurring as average effective stress increases.

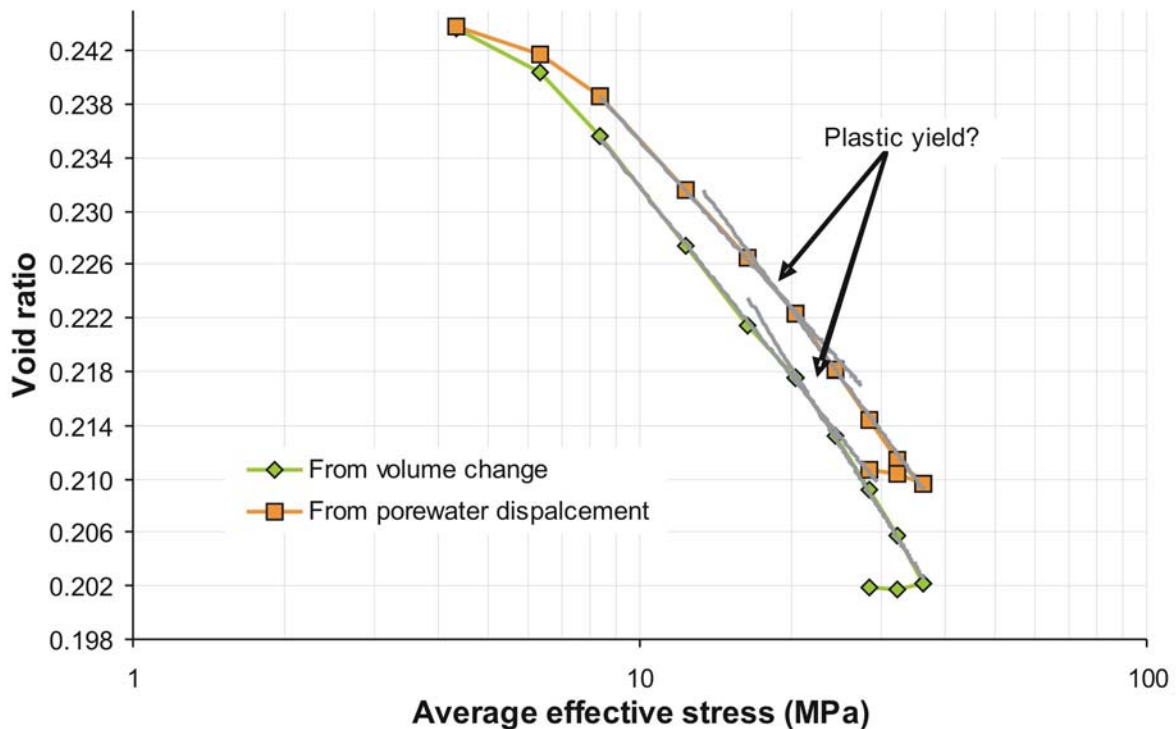


Figure 20 – Void ratio against logarithm of effective stress for volume change and porewater displacement measurements.

Stage number	Average effective stress (MPa)	Void ratio		Negative slope of consolidation curve ( $\alpha$ )	
		From volume change	From porewater displacement	From volume change	From porewater displacement
1	5.3	0.244	0.244	-	-
2	7.3	0.240	0.242	0.0087	0.0054
7	9.3	0.236	0.239	0.0174	0.0114
8	13.3	0.227	0.232	0.0206	0.0180
9	17.3	0.221	0.226	0.0215	0.0181
10	21.3	0.217	0.222	0.0180	0.0190
11	25.3	0.213	0.218	0.0237	0.0231
12	29.3	0.209	0.214	0.0266	0.0244
13	33.3	0.206	0.211	0.0260	0.0222
14	37.3	0.202	0.210	0.0313	0.0166
15	33.3	0.202	0.210	-0.0034	0.0066
16	29.3	0.202	0.211	0.0015	0.0025

Table 7 – Average effective stress, void ratio and  $\alpha$  parameters for each test stage.

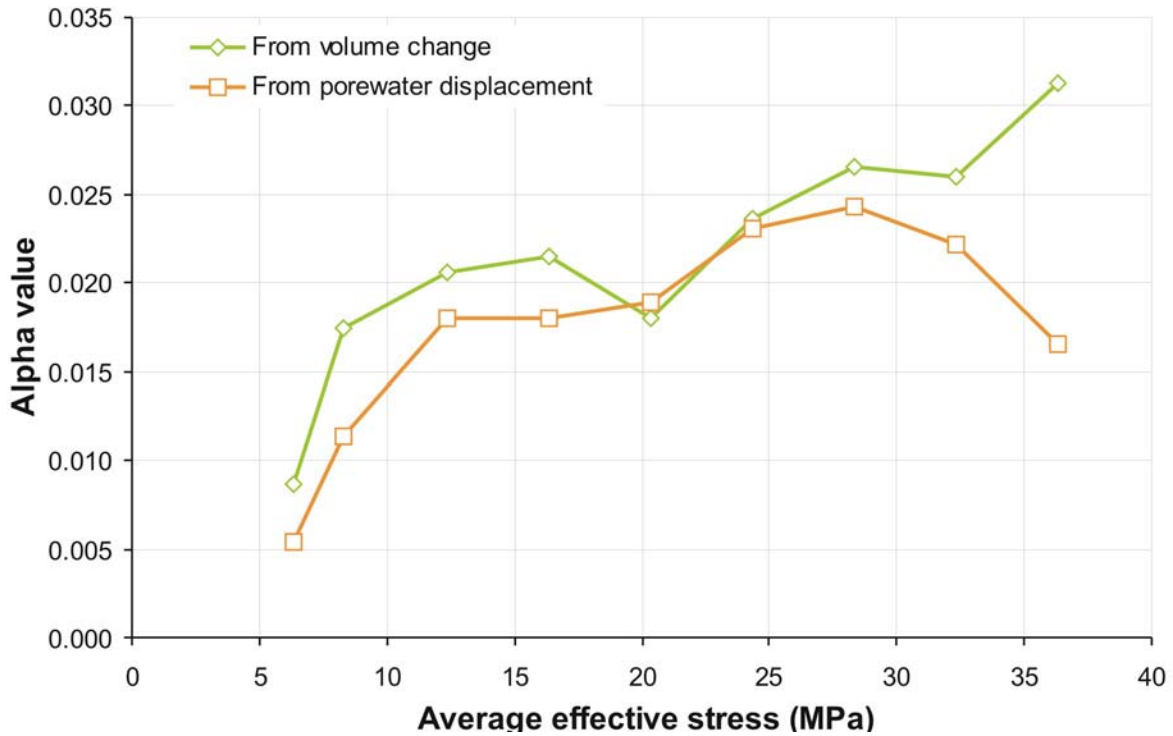


Figure 21 – Cross-plot of alpha ( $\alpha$ ) values for test stages [2] and [7] to [14] inclusive. Data shows a general trend of increasing  $\alpha$  values as average effective stress rises suggesting the onset of plastic yield.

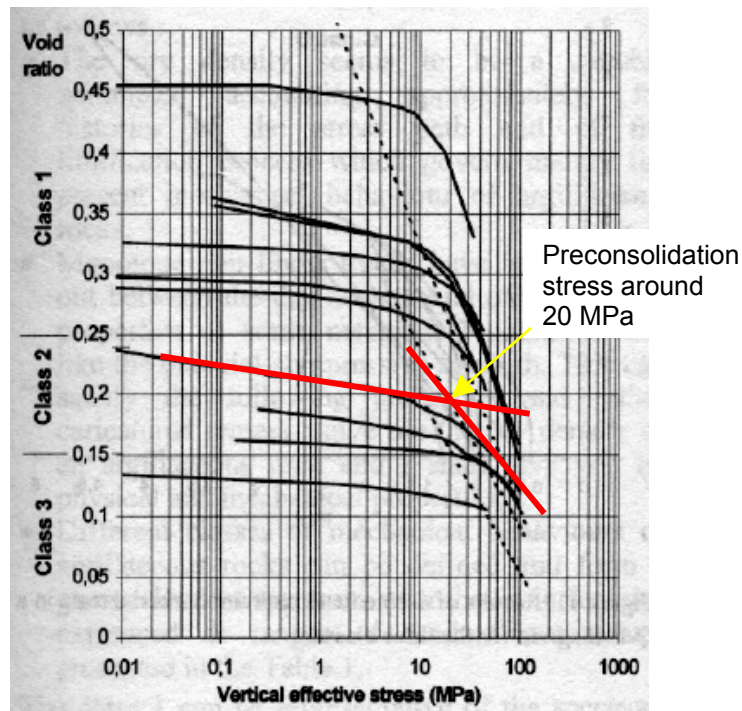


Figure 22 – A series of void ratio – vertical effective stress curves for a range of geological materials. The preconsolidation stress for a specimen in similar porosity-stress space (shown by red trend lines) suggests a value of around 20 MPa.

Figure 22 shows a series of void ratio - log effective stress plots for a range of argillaceous rocks from France (Heitz et al., 1998). Selection of a material in a similar porosity – stress space tentatively suggests a value for the preconsolidation stress of around 20 MPa, though the

identification of this point is only really possible having mapped the deformation behaviour to high effective stresses (in this case 100 MPa). The onset of plastic yielding occurs well before this value (around 10 MPa), which is qualitatively similar to the observations noted in our test history.

Analysis of the cumulative porewater displacement, void ratio and published data trends suggest that the preconsolidation stress for Opalinus clay is in the region of 20 to 25 MPa. Even though it is difficult to specifically identify this value from the current test history, the data from Table 5 can be used to predict volume change in response to increasing applied load.

#### 4.2 PARAMETER ESTIMATES FROM CONSOLIDATION DATA

The specific storage ( $S_s$ ) of a porous medium is the volume of water that is released or taken into storage by a saturated medium, per unit volume, per unit change in hydraulic head. For overconsolidated clay under an isotropic stress, the specific storage ( $m^{-1}$ ) is given by:

$$S_s = \frac{\rho_w g}{1 + e} \left[ \frac{e}{K_w} + \frac{\kappa}{\sigma_{\text{eff}}} \right] \quad (\text{Eq4-2})$$

where  $\rho_w$  is the density of water,  $K_w$  the bulk modulus of water,  $\kappa$  is a dimensionless parameter representing the gradient of the rebound-reconsolidation line in void ratio effective stress space and  $\sigma_{\text{eff}}$  is the effective stress. Substituting  $\kappa$  for the  $\alpha$  parameter in Table 7, an estimate for the specific storage for each consolidation state can be obtained. These values are given in Table 8.

Stage number	Average effective stress (MPa)	Specific storage ( $m^{-1} \times 10^6$ )	
		From volume change	From porewater displacement
2	6.3	11.7	7.6
7	8.3	17.5	11.7
8	12.3	14.2	12.5
9	16.3	11.4	9.7
10	20.3	7.9	8.3
11	24.3	8.6	8.4
12	28.3	8.4	7.7
13	32.3	7.3	6.3
14	36.3	7.8	4.5
15	32.3	-	2.4
16	28.3	1.2	1.5

**Table 8 – Estimates for specific storages based on  $\alpha$  values derived from consolidation measurements. For calculation purposes the bulk modulus of water is taken as 2.2 GPa.**

It can be seen from the data in Figure 23 that from test stage [8] onwards, specific storage values derived from porewater displacement measurements show a general decreasing trend with increasing average effective stress. Data from volume change exhibits a similar trend up to stage [10] at which point the line begins to level and specific storage becomes less sensitive to increases in average effective stress.

Drained and undrained consolidation parameters for the test specimen are given in Tables 9 and 10 respectively. Undrained values, determined at the start of each test stage (Section 2.7), are significantly higher (around an order of magnitude) than those for drained parameters. Examination of the data in Table 8 shows a clear change in response centred around an effective stress of approximately 20 MPa.

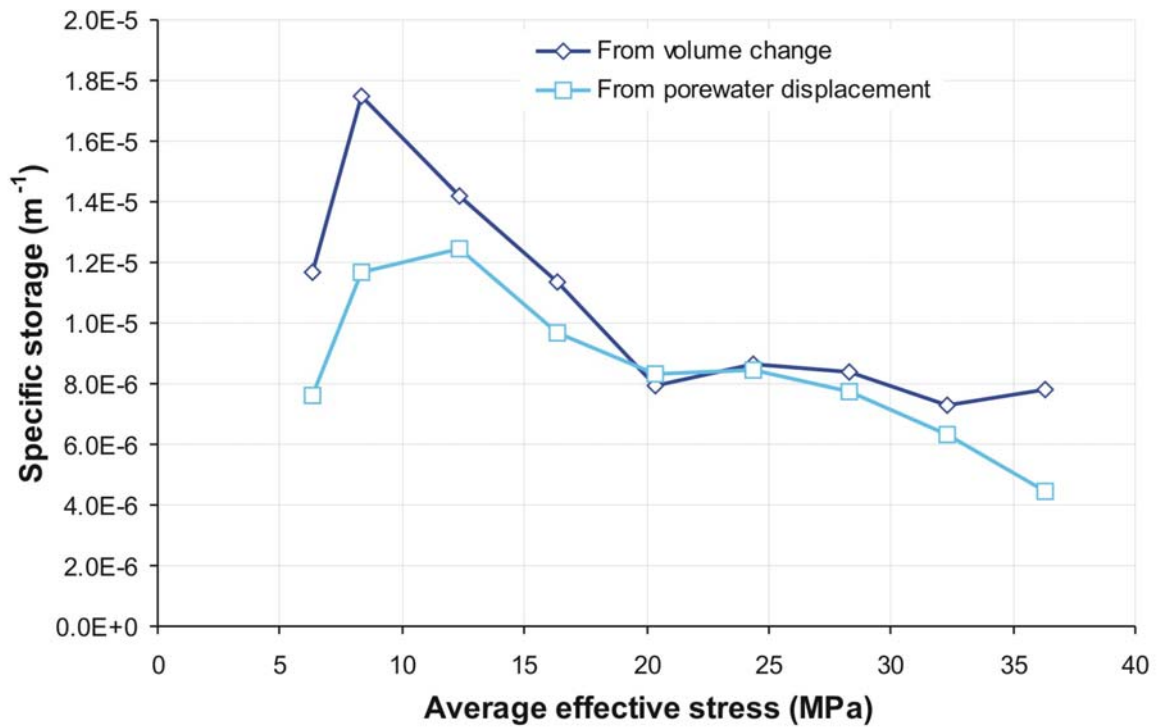


Figure 23 – Specific storage against average effective stress for test stages [2] and [7] to [14] inclusive.

Stage number	Bulk Modulus (GPa)	PSR	Youngs Modulus (GPa)	Shear Modulus (GPa)
2	0.8 (1.2)	0.338	0.7 (1.2)	0.3 (0.4)
7	0.5 (0.8)	0.276 <sup>#</sup>	0.7 (1.1)	0.3 (0.4)
8	0.6 (0.7)	0.218	1.0 (1.2)	0.4 (0.5)
9	0.8 (1.0)	0.270	1.1 (1.3)	0.4 (0.5)
<b>Range</b>	<b>0.5 - 0.8 (0.8 - 1.2)</b>	<b>0.218 - 0.338</b>	<b>0.7 - 1.1 (1.1 - 1.3)</b>	<b>0.3 - 0.4 (0.4 - 0.5)</b>
10	1.3 (1.2)	0.276 <sup>#</sup>	1.7 (1.6)	0.7 (0.6)
11	1.2 (1.2)	0.276 <sup>#</sup>	1.6 (1.6)	0.6 (0.6)
12	1.2 (1.3)	0.276 <sup>#</sup>	1.6 (1.8)	0.6 (0.7)
13	1.4 (1.7)	0.276 <sup>#</sup>	1.9 (2.3)	0.8 (0.9)
14	1.4 (2.6)	0.276 <sup>#</sup>	1.8 (3.4)	0.7 (1.3)
<b>Range</b>	<b>1.2 - 1.4 (1.2 - 1.7)</b>	<b>0.276<sup>#</sup></b>	<b>1.6 - 1.9 (1.6 - 3.4)</b>	<b>0.7 - 0.8 (0.6 - 1.3)</b>

Table 9 – Drained elastic constants determined for each loading stage. Values in parentheses are based on porewater displacement measurements. PSR values marked # denote average values derived from previous test stages (Section 3).

Stage numbers	Youngs modulus (GPa)	Poisons ratio	Bulk modulus (GPa)	Shear modulus (GPa)
1 - 2	7.2	0.27	5.1	2.9
7 - 8	13.7	0.19	7.5	5.7
8 - 9	10.9	0.13	4.9	4.8
9 - 10	11.5	0.14	5.3	5.0
10 - 11	11.7	0.13	5.2	5.2
11 - 12	12.7	0.16	6.3	5.5
12 - 13	9.1	0.11	3.9	4.1

Table 10 – Average undrained elastic constants determined from each load stage.

### 4.3 CREEP ANALYSIS

The problem of neglecting time effects in rock deformation is highlighted by the observation that all rocks creep upon undergoing a load change. Commonly this transient behaviour terminates in a few minutes or hours. In many rocks, the time period involved is so small that it can be ignored, as the creep attenuates rapidly or is an inconsequential part of the total strain under load changes. The consequence of creep is slow time-dependent strain at differential stresses well below the rupture strength of the rock (Davis and Reynolds, 1996). In other words, permanent (non-recoverable) damage occurs at stresses well below those that traditional geotechnical experiments measure. Creep strain can seldom be recovered fully when loads are removed, and thus it is largely a plastic deformation (Dusseault and Fordham, 1993).

Predicting the long-term behaviour of underground structures is not a simple and straightforward task. It demands a reliable constitutive model, which can be used to interpret measurements of viscous phenomena (Boidy and Pellet, 2000). It is also well known that time-dependent properties and trends measured on specimens in the laboratory cannot be extrapolated directly to field scale problems without due caution (Boidy *et al.*, 2002).

Creep can be manifested in a number of ways: it can be simply observed as the time-dependent radial response of axial compression in a uniaxial loading test; it can be observed as time-dependent volumetric strain observed in triaxial experimentation as the specimen takes time to compress, or as a reduction in porosity over time often with no variation in overall specimen volumetric strain. Thus, creep can result in a complex response to stress and/or strain. The subtleties of this complexity are often neglected or overlooked in the literature, which can lead to inaccurate predictions of long-term behaviour.

#### 4.3.1 Methods of studying creep

A number of experimental methods have been developed to study rock creep. These can be split into four main categories:

1. Constant strain-rate experiments can determine creep parameters by testing over a range of strain-rates during the standard triaxial compression (or extension) test.
2. Constant stress tests can be carried out in configurations such as triaxial, beam bending, uniaxial compression, double torsion and direct torsion (Dusseault and Fordham, 1993). Applied stress is maintained at a constant level and strain is analysed as a function of time.
3. Relaxation tests are carried out by imposing an *instantaneous* strain (length change in specimen,  $\Delta l$ ) and monitoring stress decay and axial strain over time. These types of test can be conducted together with constant-displacement experiments, i.e. by stopping the constant displacement at set intervals and observing the stress relaxation.
4. Transient testing is designed to keep structure constant by quickly altering parameters during testing. For a constant-displacement experiment this may mean changing strain-rate ( $\dot{\epsilon}$ ), such that  $\dot{\epsilon}_1$  is used initially, followed by  $\dot{\epsilon}_2$ ,  $\dot{\epsilon}_3$ , and then perhaps  $\dot{\epsilon}_2$  again. In this method, the specimen structure is not given much time to adjust.

Tests conducted using these four methods will result in a complete knowledge of the creep parameters for a test material. Each method has advantages and limitations, so appreciation has to be given as to the experimental procedure, more so than for the traditional engineering testing methods. As rock creep tends to be a slow process, it may be expected that a singular creep test may last up to a year in duration, obviously restricting the range of parameters that can be investigated. It also makes detailed microstructural analysis at different stages of the experiment extremely difficult.

### 4.3.2 Experimental procedure

The creep investigation was conducted during the early stages of the overall experimental programme. The chosen experimental procedure was a stepped differential stress approach, following the constant stress approach in a triaxial testing rig with a total of four differential stress stages implemented, as summarised in Table 11. During the creep investigation, the confining pressure was kept at a constant 7 MPa, with each stage of the test completed by varying the axial stress on the specimen.

Three stages of increasing differential stress were conducted (C1 – C3). The final stage of creep investigation was a relaxation experiment (R1) in which the axial stress was lowered from the level of stage C3 to C2. Each stage of differential stress variation was conducted with a near-instantaneous increase or decrease of axial load.

During each stage, differential stress was changed and kept constant, with confining pressure maintained at a constant level. In maintaining a constant axial load, the loading piston of the experimental rig moves, providing a measure of axial strain. Radial strain measurements were derived from the change in volume of the confining system, caused by volumetric creep of the specimen. The volumetric strain for each test stage could then be calculated.

Table 11 shows the length of time taken for each creep stage ranging from between 8 and 20 days, which, in terms of a creep investigation, can be viewed as relatively short. The creep component of the study however, was not the primary focus of experimental investigation.

Stage number	Creep stage	Confining pressure (MPa)	Axial stress (MPa)	Differential stress (MPa)	Time (days)
3	C1	7	9	2	8
4	C2	7	10	3	14
5	C3	7	11	4	20
6	R1	7	10	3	10

**Table 11 – Summary of the experimental conditions for each of the four creep stages of investigation.**

### 4.3.3 Experimental results

Figure 24 shows the axial strain for the four stages of creep investigation, test stages [3] to [6] inclusive (C1 – C3). These data has been adjusted to show only the axial strain accumulated after the initial swelling and consolidation stages of the experiment.

Figures 25 – 28 show each creep stage in more detail, highlighting the difference in stability of the results obtained for axial and volumetric strain. As can be seen, considerable noise is observed in the volumetric strain data. There are a number of possible explanations for this observation including:

- Temperature variations resulting in expansion or contraction of the experimental rig and confining fluid. The Transport Properties Research Laboratory is a temperature controlled facility, yet very small changes in ambient temperature could result in volume change that could then be interpreted as volumetric strain. It can be noted that the volumetric strain recorded between days 4 - 8 of stage 3 (C1, Figure 24) has a periodicity of around 1 day. Such variation is not seen in the axial strain, which is a direct measurement from the specimen length. It is very difficult to calibrate temperature effects to the required level of accuracy in order to be able to allow accurate compensation during data processing.
- The method used to determine the radial component of volumetric strain is towards the limit of resolution of the electronic measuring equipment.

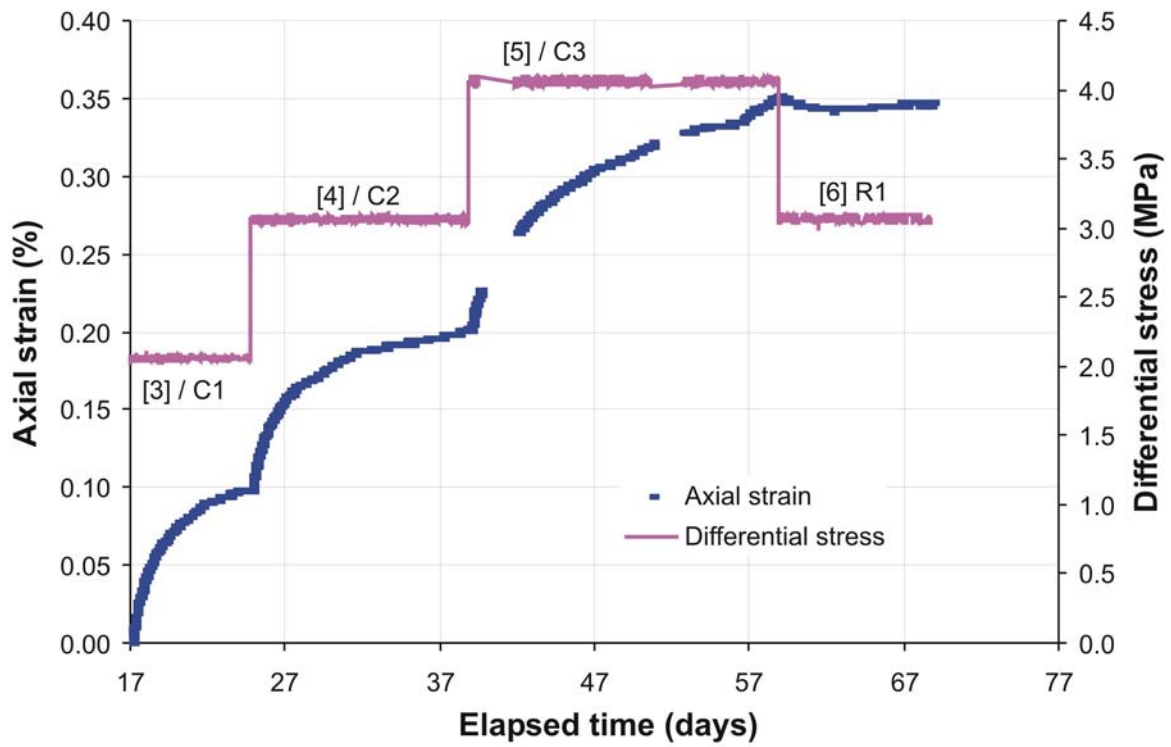


Figure 24 – Results of the complete creep study, showing the axial strain for the four stages of creep investigation.

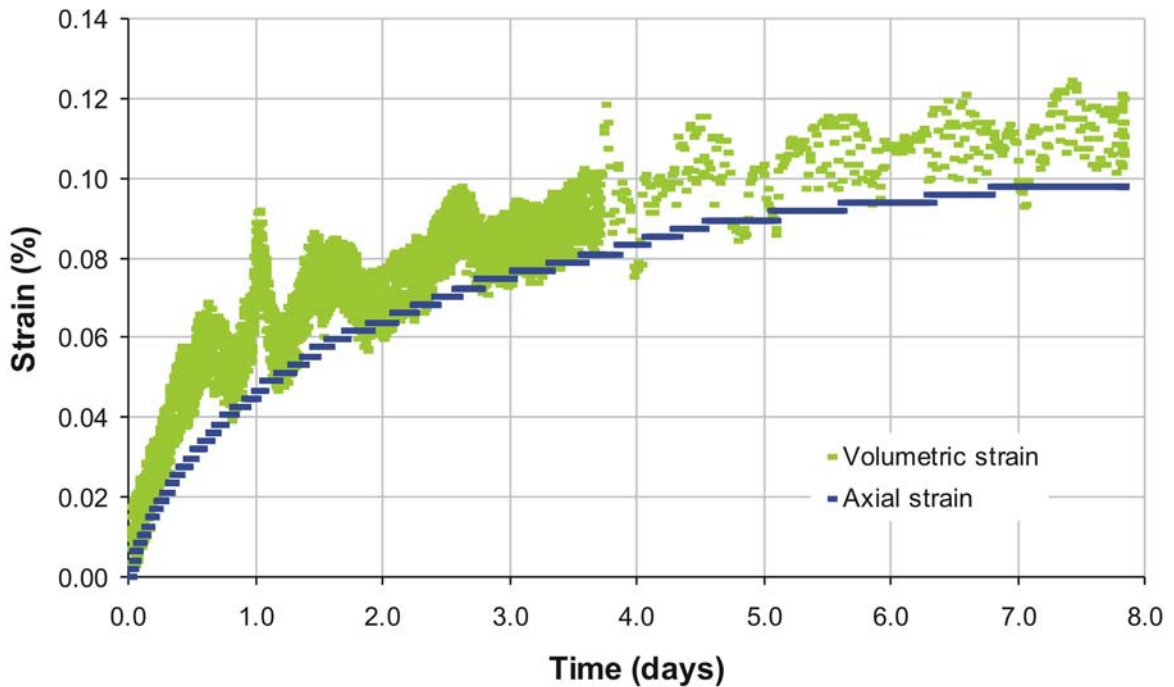


Figure 25 – Creep results for test stage [3] of the experiment (creep stage C1).

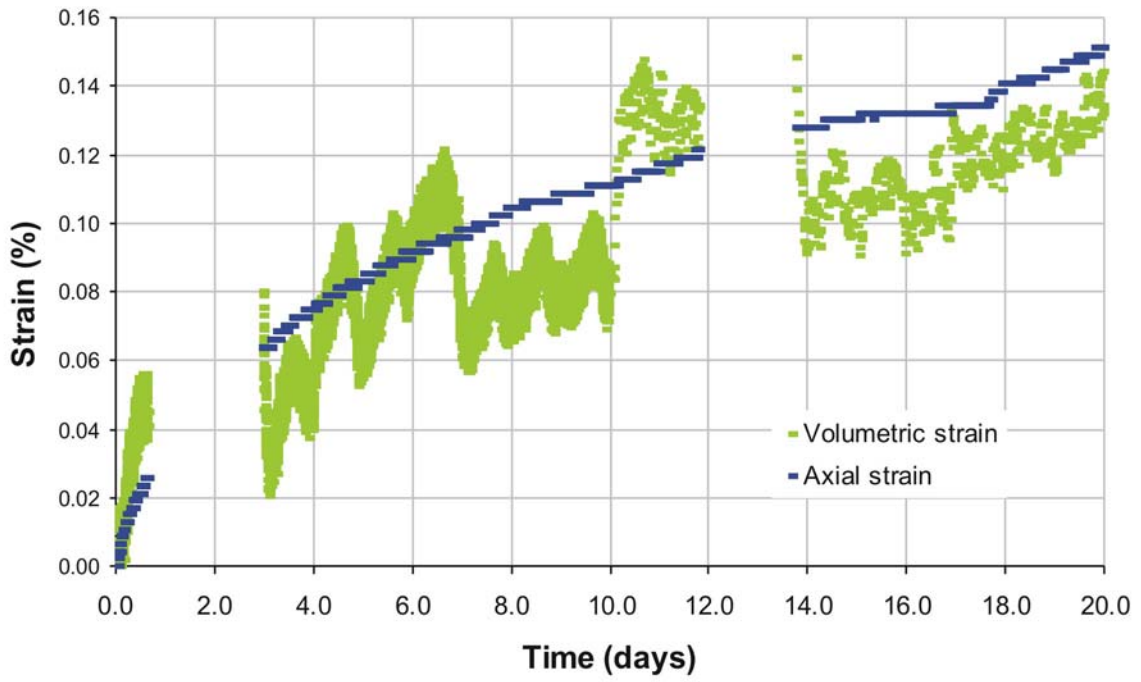


Figure 26 – Creep results for test stage [4] of the experiment (creep stage C2).

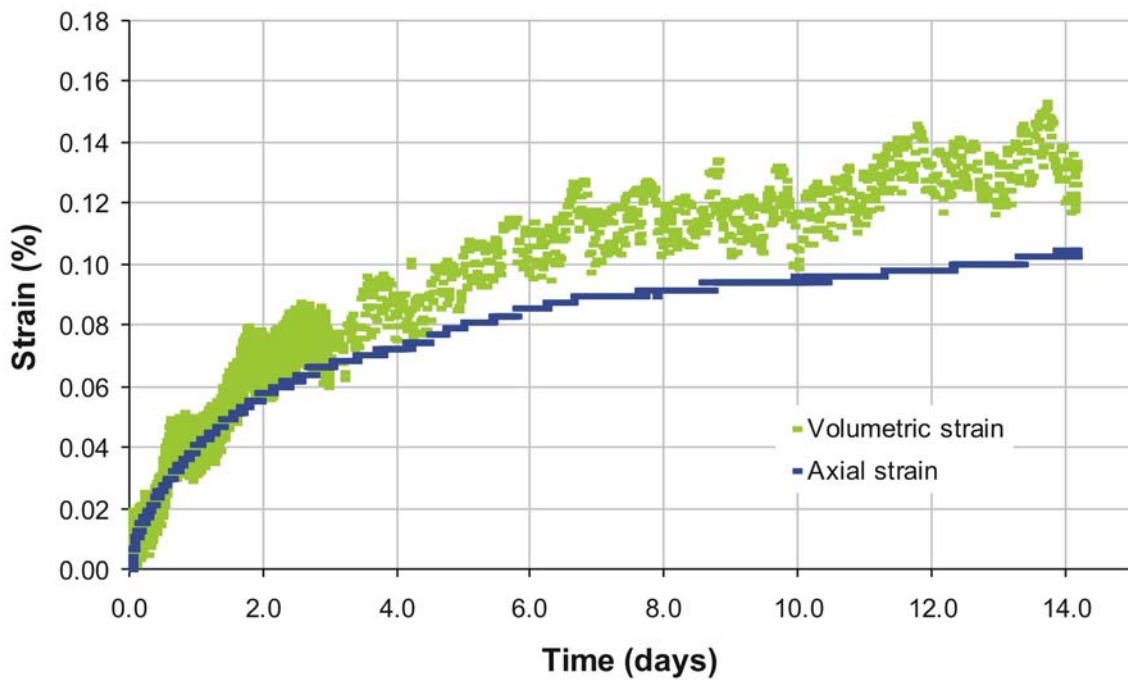
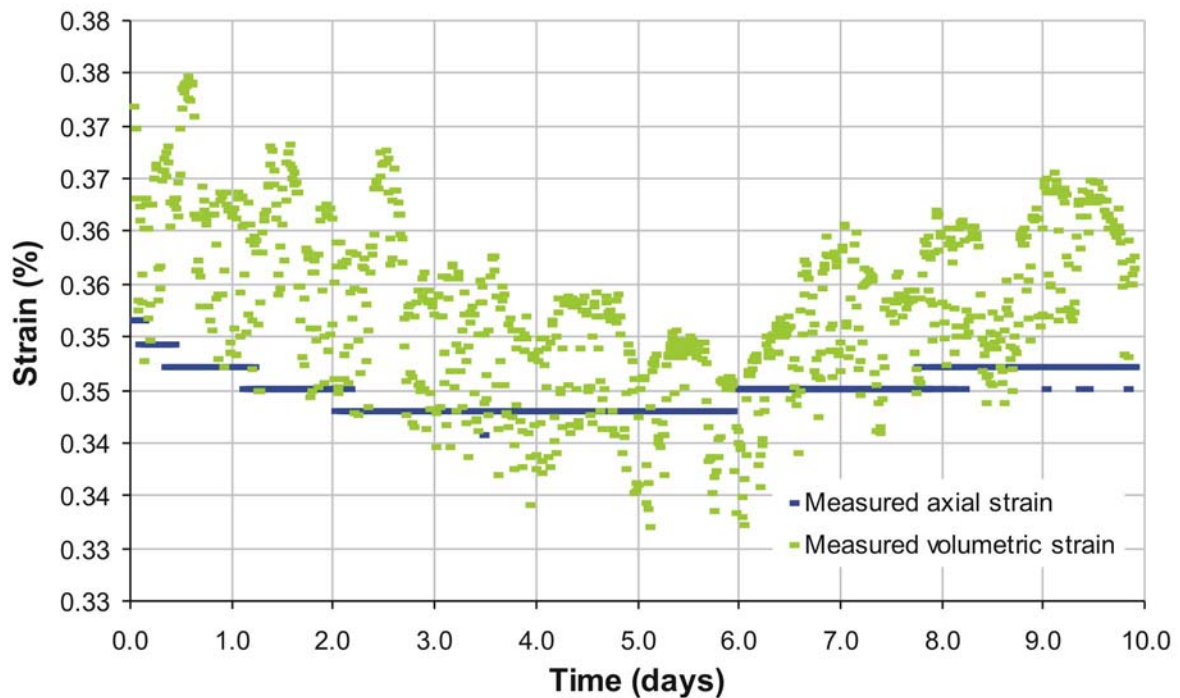


Figure 27 – Creep results for test stage [5] of the experiment (creep stage C3).



**Figure 28 – Creep results for test stage [6] of the experiment (creep stage R1).**

For all stages of creep, it is possible to see correlations between the stable axial strain and unstable volumetric strain results. However, notable changes can be seen for stage [5], as shown in Figure 27. This experimental stage has been affected by two intervals where data was unavailable (days 0.5 – 3 and 12 – 14). It would be possible to adjust the volumetric strain results to take account of this “drop-out”, but this has not been done. Noise in the volumetric strain data may relate to experimental artefacts such as voltage instability after temporary failure of the logging system. This problem is not apparent in any other stage of the experiment.

#### 4.3.4 General qualitative observations

In all three stages of creep experimentation it can be seen that the majority of strain occurs in the axial direction. If strain was homogenous, the axial component would represent only one third of the volumetric strain. As axial strain is observed as being approximately 80 % of the total volumetric strain in this test, it is clear that little axial stress is being translated into radial strain.

##### 4.3.4.1 CREEP STAGE C1 (STAGE 3)

As with all stages, the axial strain in stage [3] gives the “smoothest” result, as shown in Figure 25. Close examination shows that it may be possible to identify three stages to the creep:

- I. The first stage is seen approximately between days 0 and 2. Within this period the time-dependent creep is observed as a slowly decaying response.
- II. Between days 2 and 4.5 an almost linear response can be seen.
- III. From 4.5 days, until the end of the experimental stage at day 8, a secondary linear region of creep, with a slower response, can be seen.

These general observations are possibly over-simplifying the results, for example it could be argued that between stage II and III (at time = 4), there is an acceleration in the creep.

#### 4.3.4.2 CREEP STAGE C2 (STAGE 4)

As with stage C1, it is possible to describe three clearly defined stages of creep within stage 4 (C2), as seen in Figure 26:

- I. The first stage can be observed between 0 and 3 days, identified as a slowly decaying creep response.
- II. Between days 3 and 7 an almost linear response is seen.
- III. From day 7, until the end of the experimental stage at day 14, a secondary linear region of creep is seen. It could be interpreted that creep is slowly accelerating towards the end of this stage, although data are insufficient to conclusively state this.

As with stage C1, these general observations may be an over-simplification, but in this stage, it is possible to see the general stages described in both axial and volumetric strain. The data for volumetric strain after day 10 suggests that the possible observed acceleration in axial strain might be more prominent in volumetric strain. This may reflect some event whereby axial stress is being better translated into radial strain, such as the closure of pore space.

#### 4.3.4.3 CREEP STAGE C3 (STAGE 5)

As described earlier, the volumetric strain results for this stage are confusing due to the “drop-out” times where no data was available, as shown in Figure 27. However, it is possible to identify the same three regions of creep as previously seen, with a fourth region also now obvious:

- I. The first stage is seen between days 0 and 4, identified as a slowly decaying creep response.
- II. Between days 4 and 8 an almost linear response is seen.
- III. Between 8 and 17 days a secondary linear region of creep is seen. Creep can be interpreted as decelerating towards the end of this stage.
- IV. From day 17, until the end of the experimental stage at day 20, it appears that creep is accelerating. However, it should be noted that this region appears linear with a slope that is similar to stage II.

As previously highlighted, there are many complexities to the data that could be interpreted as real. These complexities are beyond the standard stages of creep, they may be real rock events, or they may derive from experimental observations. In modelling the long-term creep behaviour we have to decide how significant these events are.

#### 4.3.4.4 CREEP STAGE R1 (STAGE 6)

The purpose of this experimental stage was to examine the specimen response to a reduction in axial stress from 11.0 to 10.0 MPa. True plastic creep should be non-recoverable, although a certain amount of elastic creep should be present. As shown in Figure 28, there are two clearly identifiable regions of deformation:

- I. As axial stress was lowered, a certain amount of creep occurred, with the specimen recovering approximately 0.01% of the axial strain and 0.03% of the volumetric strain. The discrepancy between the two results can be explained by the hysteresis of the loading piston. This stage of deformation occurs between 0 and 6 days.
- II. Between days 6 and 10, positive creep is resumed, both axially and volumetrically.

The fact that creep is initially negative in sign and becomes positive mid-way through this experimental stage illustrates that the interpretation of these results is greatly complicated by the

complexity of the number of features acting at any one time, this is discussed in the following section.

#### 4.3.5 Complexity of measured parameters

The interpretation of creep of argillaceous rocks is greatly complicated by the number of phenomena acting simultaneously. A thorough knowledge of each factor is required in order to isolate the true creep response of the specimen.

- Stage [1] of the experiment is aimed at quantifying the saturation and swelling response of the specimen. Throughout this period of experimental study, a degree of saturation change and swelling will occur. As seen in Figures 7 and 8, the majority of this effect has been observed by the time subsequent experimental stages have been started. It should be noted that swelling causes negative creep.
- During a change in stress, sediments undergo compaction which is a natural time-dependent phenomena. Stage [2] of the experiment aimed to quantify the compaction of the clay in response to a change in axial and confining pressure. Creep tends to decrease with compaction as the material becomes indurated and more difficult to compact.
- Argillaceous rocks are inherently difficult to test in the laboratory. Their low permeability means that it takes a protracted period of time to re-equilibrate porewater pressure within the specimen when boundary stress is altered. The step-increase of axial load may have occurred at a rate that meant high-pore fluid pressures were created within the specimen, which then take time to dissipate. This would create a time-dependent response as effective-stress evolves in response to the dissipation of porewater pressure.
- True plastic or viscoplastic creep. This part of the experimental study is aimed at quantifying the true time-dependent plastic or viscoplastic deformation of the material. This is likely to be a slow response.
- There are also several experimental artefacts that may be contributing to an observed time-dependent deformation (e.g. the experimental stress-path, temperature fluctuations and instrument drift). However, these artefacts have been considered or deemed insignificant.

Each of the phenomena above will contribute to the observed strain to some degree. It is possible to quantify each one, but that takes a considerable amount of experimental data, which is far beyond the scope of this study. As conditions of the specimen are similar to those encountered *in situ*, it is possible to leave the data un-corrected, as similar influences would be expected to occur under *in-situ* conditions.

#### 4.3.6 Quantitative approaches to interpreting creep

As insufficient data and time is available to isolate the true creep component, one approach to modelling the current data is to apply methodologies used by other individuals. These can be extended to better fit the current data. Two such approaches have been applied:

- The Lemaitre model, as applied to the Opalinus clay by Boidy
- Power-law creep

##### 4.3.6.1 VISCOPLASTIC LEMAITRE CREEP MODEL

Boidy successfully applied the Lemaitre creep model to Opalinus clay (Boidy, 2002; Boidy and Pellet, 2000; Boidy *et al.*, 2001; Boidy *et al.*, 2002). This method aims to model the transient response of rocks as viscoplastic and is a viscoplastic constitutive model (Lemaitre and Chaboche, 1996; Boidy and Pellet, 2002). Other viscoplastic models exist based on extended elastoplastic models (Rizkalla and Mitri Hani, 1991).

The work of Boidy is a comprehensive study using the Lemaitre viscoplastic model to predict creep around the Mont Terri gallery. Boidy presents a back-analysis of time-dependent behaviour over a period of 8 years, with specific attention given to a section of tunnel that was left without any support for approximately 3 months. Once a stiff concrete ring lining had been added, the time-dependent convergence was also examined.

The Lemaitre creep model is based on the overstress theory formulated by Perzyna (1966) for rate-sensitive plastic materials. These equations describe the transient creep phase, which is defined by a decrease of the viscoplastic strain rate versus time under a constant stress level. The total strain rate ( $\dot{\epsilon}$ ) is divided into an instantaneous reversible (elastic) part and an irreversible (viscoplastic) part, as shown in Eq.4-3:

$$\dot{\epsilon}_{ij} = \dot{\epsilon}_{ij}^e + \dot{\epsilon}_{ij}^{vp} \quad (\text{Eq.4-3}) \quad \text{where: } \dot{\epsilon}_{ij}^{vp} = \gamma \langle \Phi(F) \rangle \frac{\partial G}{\partial \sigma_{ij}} \quad (\text{Eq.4-4})$$

Where the irreversible strain rate includes both viscous and plastic effects (Eq.4-4),  $\gamma$  is the viscosity coefficient,  $G$  is the viscoplastic potential,  $F$  corresponds to the static yield function, and  $\Phi$  is the flow rule. The brackets defined by Macaulay,  $\langle \rangle$ , control the function in the following way:

$$\begin{aligned} \Phi(F) &= 0 \quad \text{if: } \Phi(F) < 0 \\ \Phi(F) &= \Phi(F) \quad \text{if: } \Phi(F) > 0 \end{aligned} \quad (\text{Eq.4-5})$$

Function  $F$  depends on the second invariant of the stress tensor  $q$ , by assuming a von Mises loading surface, and on the strain-hardening parameter  $\kappa$ . The strain hardening parameter is a function of accumulated viscoplastic strains (second invariant of the stress tensor), which can be expressed by:

$$\epsilon_{ij}^{vp} = \int_0^t \left( \frac{2}{3} \dot{\epsilon}_{ij}^{vp} \cdot \dot{\epsilon}_{ij}^{vp} \right)^{1/2} d\tau \quad (\text{Eq.4-6})$$

The assumption of isotropic hardening is also invoked. In practical terms, the law is simplified by considering two further assumptions. Firstly, the constitutive law can be defined as being associated, in which case the viscoplastic potential,  $G$ , corresponds to the second invariant of the stress tensor  $q$ . This assumption implies that viscoplastic strains are developed without any volume changes. Secondly, in order to get a representative model, power laws have been introduced for the flow rule,  $F$ , and for the strain-hardening parameter,  $\kappa$ , as proposed by Lemaitre. Boidy (2002) gives the following expression for the viscoplastic strain rate:

$$\kappa(\epsilon_{vp}) = (\epsilon_{vp})^{-m/n} \quad (\text{Eq.4-7}) \quad \dot{\epsilon}_{ij}^{vp} = \frac{3}{2} A \cdot q^{n-1} \cdot (\epsilon_{vp})^m s_{ij} \quad (\text{Eq.4-8})$$

where  $s_{ij}$  is the deviatoric part of the stress tensor and  $q$  is the second invariant of the stress tensor. This law requires three parameters to be quantified: the viscosity coefficient  $A$ , the stress exponent  $n$ , and exponent  $m^*$  defined by:

$$m^* = -\frac{m}{n} \geq 0 \quad \text{where } 0 \leq m^* \leq (1-1/n) \quad (\text{Eq.4-9})$$

The main limitation of the Lemaitre creep model is that swelling phenomena and the effects of pore pressure and seepage are completely neglected.

### Application of Lemaitre by Boidy

Boidy (2002) used the Lemaitre creep law to fit experimental stepped strain rate data, as shown in Figure 29. The good fit of these data shows that the Lemaitre creep model, with carefully calibrated parameters, can predict strain-rate sensitivity of rock deformation.

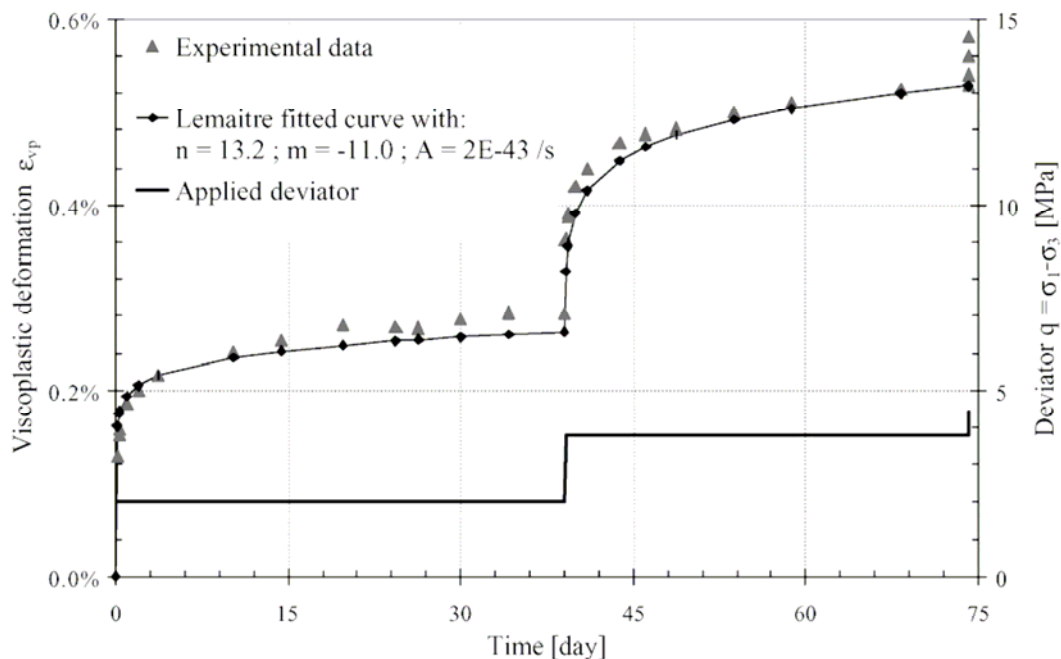


**Figure 29 – Lemaitre’s model fitted to triaxial creep data for the shaly facies of the Opalinus Clay. The confining pressure was 0.6 MPa. Test data from Kharchafi and Descoedres (1995) and the data fit from Boidy *et al.* (2002).**

In order to obtain a value for Young's modulus,  $E$ , that is representative of decompression of the rock, Boidy *et al.* (2002) performed a back-analysis of the convergence data using the methodology proposed by Sulem *et al.* (1987). The *in situ* elastic unloading modulus was found to be approximately 8 GPa.

Boidy *et al.* (2002) used triaxial experimental data of the shaly facies, supplied by École Polytechnique Federale de Lausanne (EPFL) and reported by Kharchafi and Descoedres (1995). The water content of the test material was quite high (near 8%), but the degree of saturation was less than 95%. Results shown in Figure 29 are representative of the overall data set. This specific test was performed in four steps:

- 1) Consolidation stage under 0.6 MPa of isotropic confining pressure, maintained for 24 hours.
- 2) Axial compression stage with a constant stress rate of  $0.25 \text{ MPa}\cdot\text{min}^{-1}$  up to 2 MPa differential stress.
- 3) Creep stage at 2 MPa fixed differential stress.
- 4) Creep stage at 3.8 MPa differential stress.

The Lemaitre creep parameters were obtained from the EPFL data by simultaneously fitting both stages of the test. Results are shown in Table 12. According to Kharchafi and Descoedres (1995), parameter  $\beta$  is slightly less than 1.

Parameter	From gallery convergence measurements			From EPFL lab test
	Set No. 1	Set No. 2	Set No. 3	
$N$	15.7	15.7	15.7	13.2
$M$	-13.3	-13.3	-13.3	-11.0
$A$	$3 \times 10^{-63}$	$3 \times 10^{-62}$	$3 \times 10^{-61}$	$2 \times 10^{-43}$
$\alpha$	0.07	0.07	0.07	0.083
$\beta$	1.1	1.1	1.1	1.1
$a$	$5 \times 10^{-3}$	$6 \times 10^{-5}$	$7 \times 10^{-5}$	$3.4 \times 10^{-4}$

**Table 12 – Lemaitre viscoplastic model parameters for the Opalinus Clay based on gallery convergence and a laboratory creep test performed at ÉPFL. Parameter Set No. 2 gives the best representation of the measured gallery convergences (from Boidy *et al.*, 2002).**

#### *Application of Lemaitre to the current study*

The programme used by Boidy was not available, so a simple calculation was conducted using Microsoft Excel. As an initial test, the model parameters stated in Table 9 were used and experimental parameters selected to ascertain that the model had been correctly programmed. Results comparable to those published by Boidy were obtained.

Figure 30 shows the results for the Lemaitre model (Table 12) and the current experimental data. Note that the relaxation stage R1 is not modelled. As can be seen, the four models published by Boidy *et al.* (2002) do not adequately describe the current test data. It should be noted that data set No. 1 gives a result that in Figure 30 appears to be zero strain, no error could be found in the code to determine why such a result was being achieved.

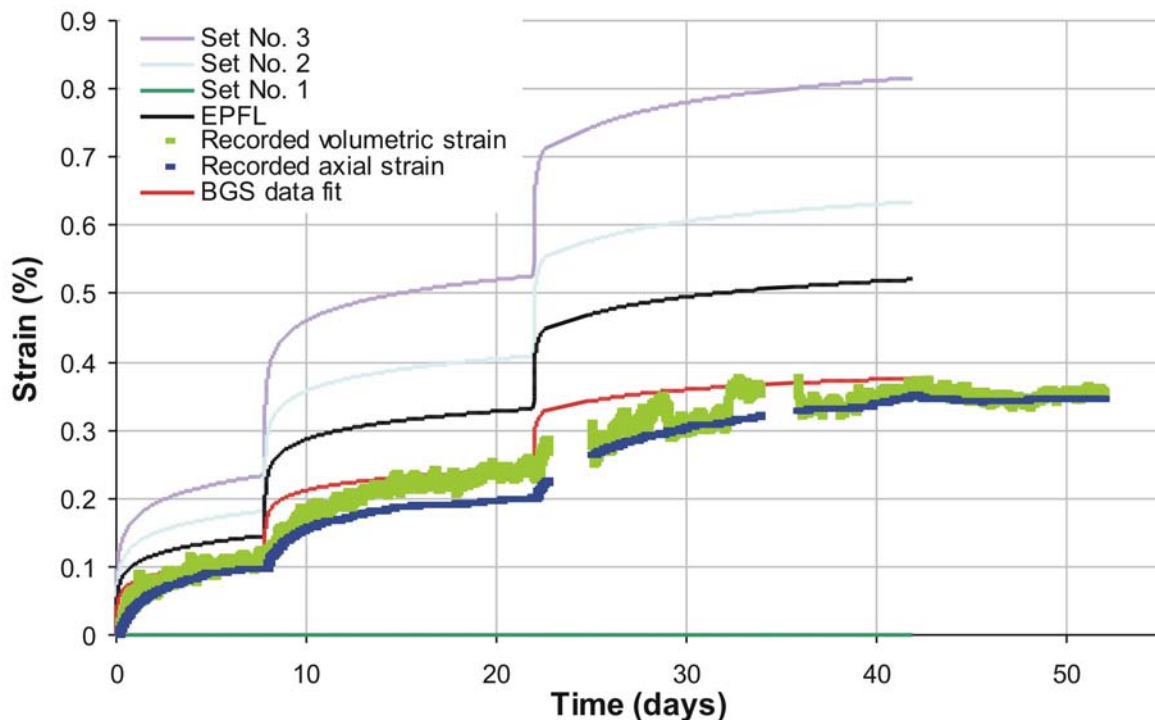


**Figure 30 – The application of the Lemaitre model to the current study. The experimental parameters published by Boidy *et al.* (2002) are shown, along with a fit produced for the current study [Lemaitre:  $N = 15.7$ ;  $M = -13.3$ ;  $A = 3 \times 10^{-61}$ ;  $\alpha = 0.07$ ;  $\beta = 1.1$ ;  $a = 7.42 \times 10^{-5}$ ].**

It had been hoped that at least one of the set of model parameters would fit the current data set. The current approach did not allow an iterative approach in determining ideal model parameters. A trial-and-error approach of adjusting model parameters showed that the general “form” of the curve is unaltered and is merely “squashed” or “stretched” in the direction of the Y-axis. Therefore, data for Set No. 3 was taken as a starting point and parameter  $a$  was varied until a satisfactory fit was achieved.

As shown in Figure 31, the Lemaitre model adequately describes the longer-term time-dependent deformation of the specimen after the differential stress was increased at approximately 5 – 7 days. It is important to note that the Lemaitre model is designed to describe volumetric creep and that a fit has been achieved for these data. During the initial part of each creep stage, the recorded strain is much lower than the prediction made by the Lemaitre model. This could be explained by the low permeability of the specimen and the resulting time taken to equalise porewater pressure.

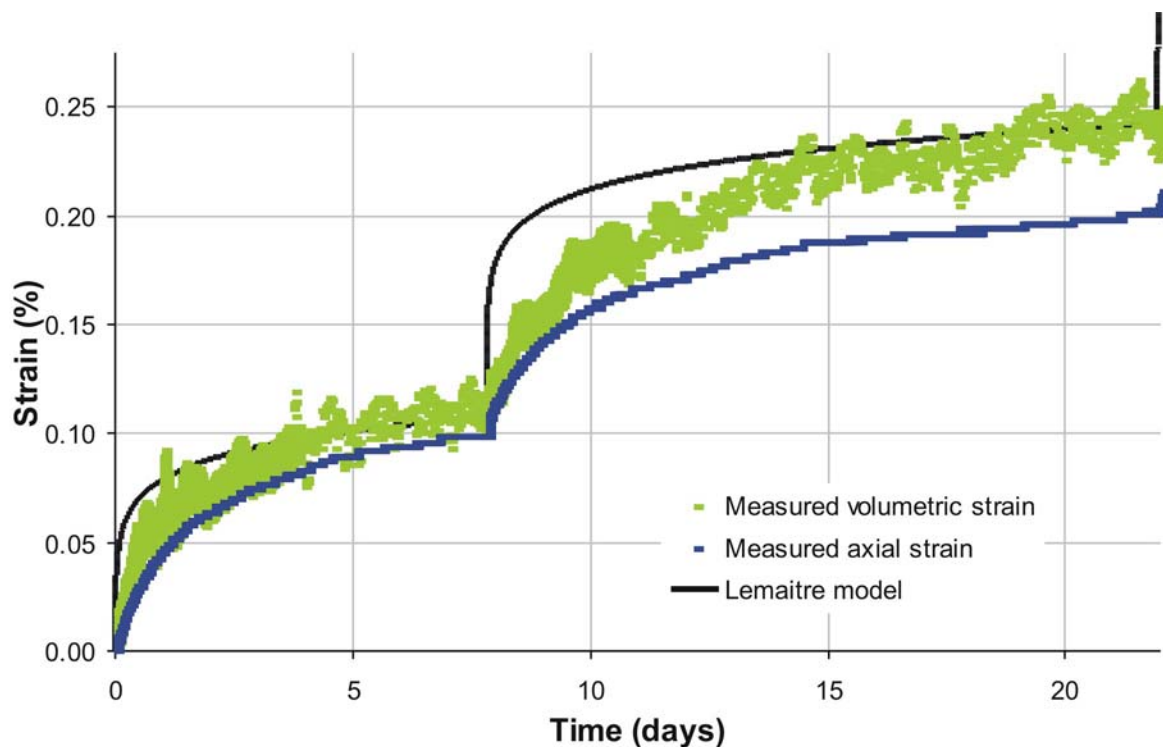


**Figure 31 – Comparing the form of the Lemaitre result with the strain data from the current study. [Lemaitre:  $N = 15.7$ ;  $M = -13.3$ ;  $A = 3 \times 10^{-61}$ ;  $\alpha = 0.07$ ;  $\beta = 1.1$ ;  $a = 7.42 \times 10^{-5}$ ].**

In relation to the long-term safety-case, the initial response of the rock may be unimportant. The Lemaitre model does seem to model the observed strain on the longer term. It should be noted that the Lemaitre fit for the data of Kharchafi and Descoedres (as reported by Boidy *et al.*, 2002) is very close.

It may be possible that the Lemaitre model is adequate at modelling the viscoplastic component of creep once the effects of pore-fluid pressure dissipation and specimen compaction have been accounted for. However, verification of this observation would require further work.

#### 4.3.6.2 POWER-LAW CREEP

Empirical creep laws derive from simple curve fitting of experimental data. A number of mathematical functions have been devised for a wide range of materials. While the fit of the

data may be perfect, this method of describing creep has no physical basis and this could lead to inadequacies due to oversight of important parameters.

The first creep laws described extensional deformation of metals in tension (pulling of metal rods). Phillips presented a logarithmic creep law in 1905 (Eq.4-10), and Andrade proposed a transient creep law in 1910 (Eq.4-11):

$$\text{Phillips: } \dot{\epsilon} = Bt^{-1} \tag{Eq.4-10}$$

$$\text{Andrade: } \dot{\epsilon} = \frac{B}{3}t^{-(2/3)} \tag{Eq.4-11}$$

where  $\dot{\epsilon}$  is strain rate,  $B$  is a constant and  $t$  is time (Dusseault and Fordham, 1993). These two equations are fitted curves to extensional strain data, and have specific inadequacies: predictions at small time intervals give large strain rates; there is no differentiation between compressive and tensile stresses; they reflect no physical mechanisms and do not include temperature effects. A rock will not show both steady state and tertiary creep if its state remains unaltered.

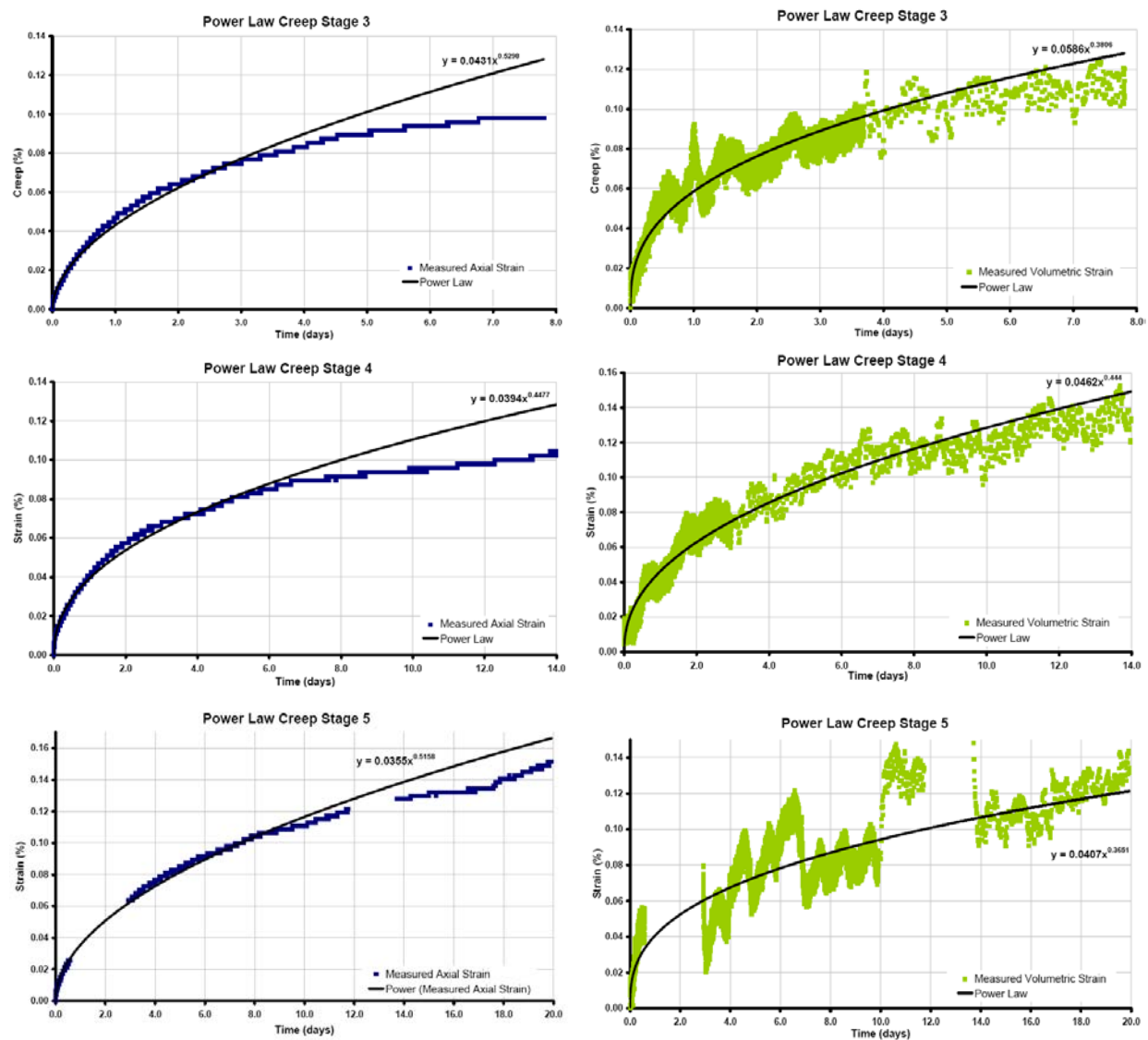


Figure 32 – The fit of each creep stage using a power-law relationship.

Power-law creep is often assumed for rocks and is an underlying assumption in the Lemaitre model which has also been applied to Boom Clay (Thimus and De Bruyn, 1998). Figure 32

shows a very simple fitting of the recorded data with a power-relationship. Examination of the data shows a satisfactory fit is achieved for the volumetric strain, although this may be due to the considerable scatter of these data. In contrast, the fit for the generally “cleaner” axial strains is rather poor by comparison. Several modifications of the power-law relationship were attempted in order to fit the data. Splitting the data into the sub-stages described above, and fitting these separately was also attempted. However, a good fit was not achieved in any of the modelling runs.

#### 4.4 HYDRO-MECHANICAL MODELLING

This study uses the coupled flow and elastic deformation finite element code STAFAN (INTERA, 1983) to try to model several of these changes to the stress state in order to extract values for apparent rock properties, primarily hydraulic permeability and Young’s modulus, as the test progresses and to assess the extent of departures from the assumptions of isotropic linear elastic deformation.

##### 4.4.1 The data

The data that have been considered for modelling are divided into two experimental phases. During the first phase, the radial, or confining, stress was held constant at 7 MPa whilst the axial stress was changed as shown in Figure 33. Here it can be seen that there is also an initial period to the test, stage [1], during which the specimen is swelling (-ve axial strains). It has been assumed that modelling of Phase 1 should be made relative to the state at the end of this step. For modelling purposes elapsed time was set to zero. Thus, the specimen is maintained with confining stress at 5 MPa, axial stress at 6 MPa, and porewater pressure at the drainage hole at 1 MPa for nearly 8 days, at which point the confining and axial stresses are both raised by 2 MPa to mark the start of Step 2 of the test. Axial stress is then raised three more times by increments of 1 MPa to give Steps 3, 4, and 5, before being reduced by 1 MPa for Step 6 at a test duration of about 59 days.

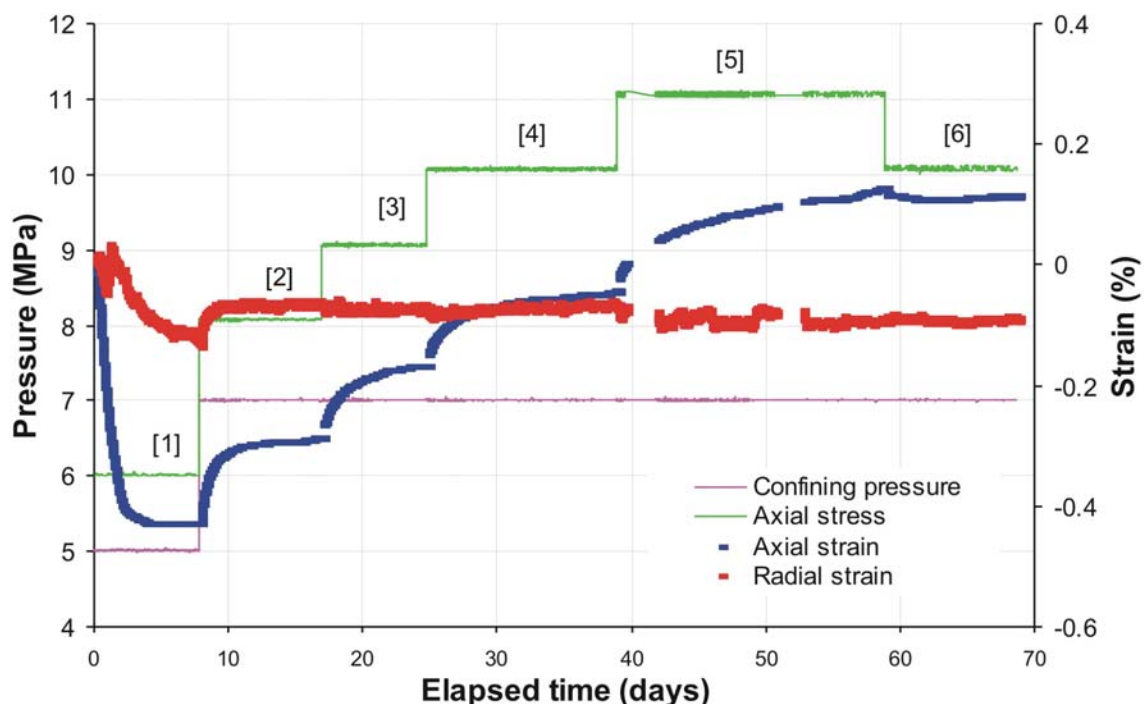
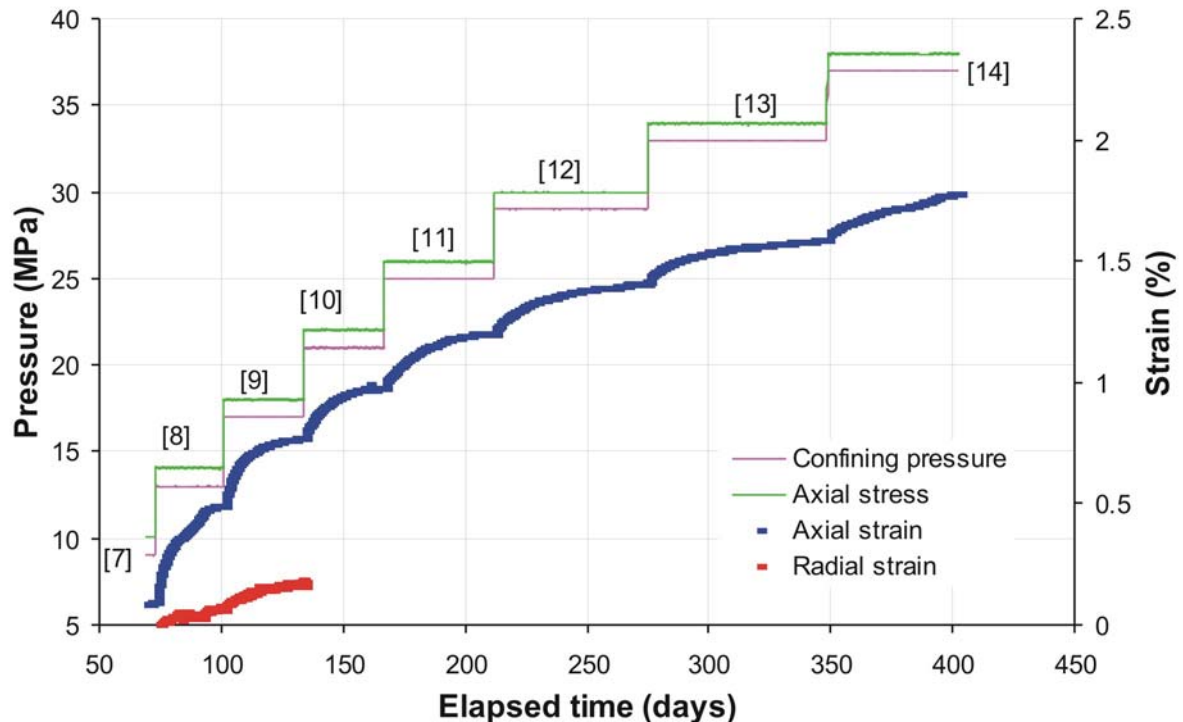


Figure 33 – Data for Phase 1 of the hydro-mechanical testing during which the confining pressure is held constant while the axial stress is changed. The steps in the test are numbered for ease of reference.

At approximately 70 days into the test the confining pressure was raised to 9 MPa, keeping the axial stress at 10 MPa, in order to commence Phase 2 of testing. During this second phase, shown in Figure 34, the axial and confining stresses were raised together by increments of 4 MPa to create steps 8 to 14, which was completed after approximately 405 days. It will be noted that the radial strain data have only been plotted up to about 170 days. This is because a leak developed in the confining pressure system and it became impossible to use volumetric flow in this circuit to estimate the radial strain.



**Figure 34 – Data for Phase 2 of the hydro-mechanical testing during which the confining and axial pressures are changed together in steps of 4 MPa. The stages in the test are numbered for ease of reference.**

#### 4.4.2 Model definition and boundary conditions

The experimental system has been modelled using the coupled elastic deformation and porous medium flow finite element code STAFAN (INTERA, 1983). The symmetry in the system allows the use of a 2D axi-symmetric model over half of the length of the specimen. Figure 35 shows the stress and flow boundary conditions that were applied. Thus, no-flow and no radial deformation conditions were applied to the specimen axis, and no-flow and no axial deformation to the base of the model (the mid-length plane of the specimen). The confining pressure was applied as a set of specified radial forces on the outer face of the specimen, together with no-flow. The axial pressure was applied as a set of specified axial forces acting on the top face, together with no-flow except at the centre of this face where the drainage hole is located. Here a specified fluid pressure condition is defined. The drainage hole has a diameter of 0.36mm.

Initially, a uniform mesh of elements 1mm square was adopted but it was found that this was inadequate to accurately represent the flow close to the drainage hole. A series of runs with successively refined meshes was made seeking convergence in the axial strain and pressure fields leading to the adoption of a mesh composed of 2200 nodes on 2106 quadrilateral elements, the smallest of which were 20x50 $\mu$ m, close to the drainage hole. Even with this refinement, the calculated cumulative flows from the drainage hole differed slightly (6%) between the two most

refined meshes tried, but it is to be expected that there will be slower convergence in this quantity since it is obtained from the derivative of the porewater pressure solution.

The main rock property parameters required by the model are the Young's modulus, the Poisson's ratio, and the radial and axial components of hydraulic permeability. The calculations done here all assumed an isotropic hydraulic permeability and a Poisson's ratio of 0.2. The modelling approach taken was to try to fit, by trial and error, the model output to the axial deformation data. The value of Young's modulus was adjusted to give the long-term magnitude of the deformation and then the permeability was used to fit to the transient build-up to that long-term value.

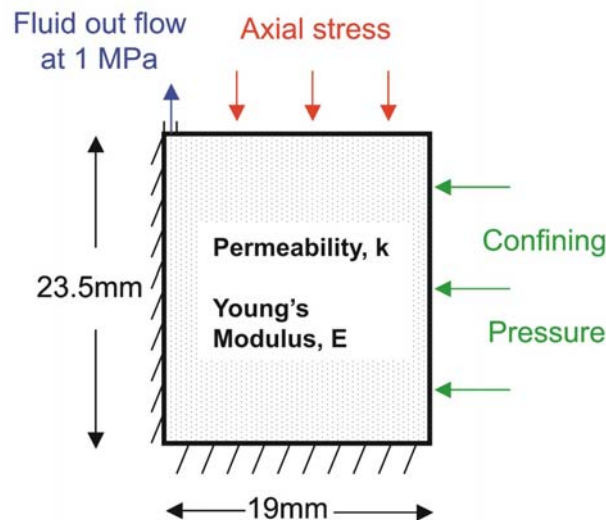


**Figure 35 – Schematic diagram of the main elements of the model and boundary conditions.**

#### 4.4.3 Modelling of Phase 1 data

The approach taken to modelling the Phase 1 data was to find values for the permeability and Young's modulus that gave a good fit to the axial strain response to stage [2] of the test and to continue the simulation to show the extent and nature of the deviation of the data from the model solution as the test progressed. It was found that values of  $2.0 \times 10^{-18} \text{ m}^2$  for the permeability and 450 MPa for the Young's modulus were suitable and the full simulation is compared to the data in Figure 36. It may be noted that the data have been offset in both time and axial strain to place the origin of the graph at the end of stage [1] of Figure 33.

It can be seen that the model provides a reasonable representation of the data for most of the duration of stage [2], but that towards the end of this stage the data starts to deviate from the prediction of the model. It would seem that the specimen is exhibiting some creep deformation in addition to the elastic deformation included in the model. As the test progresses beyond stage [2] it can be seen that the data deviates progressively further from the model response. The relatively rapid responses of the elastic model to changes in stress become less apparent in the data and are replaced with much longer transients and increasing amounts of creep, particularly in stage [4]. When the axial stress is reduced in stage [6], the model returns the axial strain to the level obtained at the end of stage [4] whereas the data shows very little reduction in strain. Indeed, towards the end of stage [6] the data show axial strain increasing again, providing a further indication that a creep process is occurring.

The longer transients seen in stages [3], [4], and [5] might be interpreted as indicating a reduction in the permeability of the specimen as the axial stress increases but, as noted, it is clear that a creep process is also involved and it is likely that this will be contributing to the duration of the transient responses.

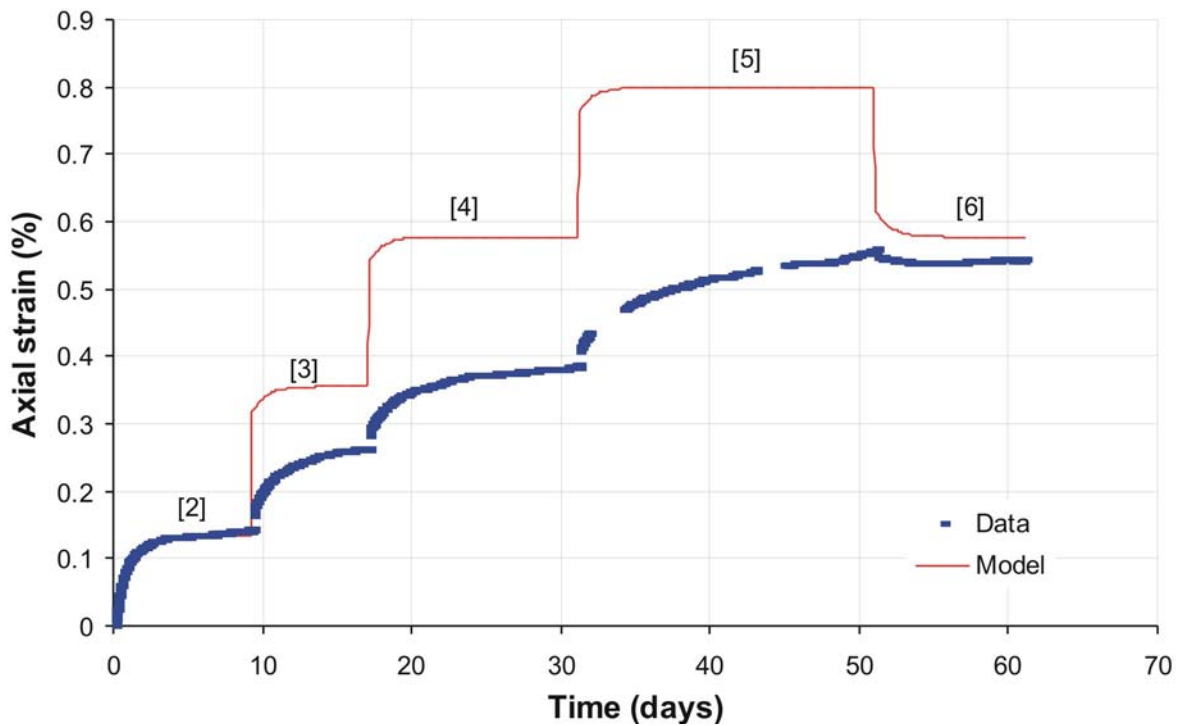


**Figure 36 – A comparison of data for the axial strain during Phase 1 of the test with the model response. The model parameters were set for fitting to stage [2].**

The radial strain data are compared to the model output in Figure 37. It can be seen that the response of the specimen to stage [2] of the test is less than half of that predicted by the model, despite the good fit of the model to the axial strain data. This may suggest that the assumption of isotropy used in the model is invalid. The specimen's response to the other stages of the test are also much smaller than predicted by the model, with some of the stress changes being barely discernable in the data.

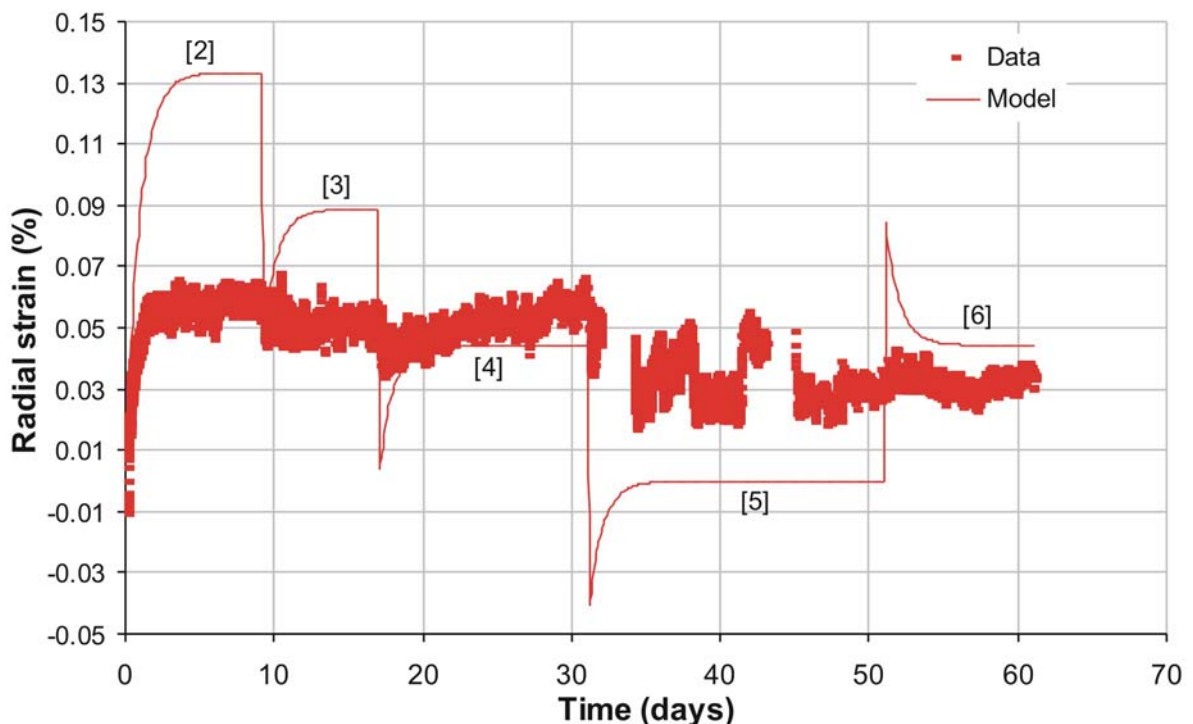


**Figure 37 – A comparison of data for the radial strain during Phase 1 of the test with the model response.**

The data for the flow of porewater from the specimen during testing are compared with the output from the model in Figure 38. Here it can be seen that the model predicts significantly greater flow volumes than are obtained from the specimen. Much of this offset arises during the first stage of the test, but additional offsets arise from subsequent stages too. As for the axial data, the rebound predicted by the model for stage [6] is barely discernable in the data.

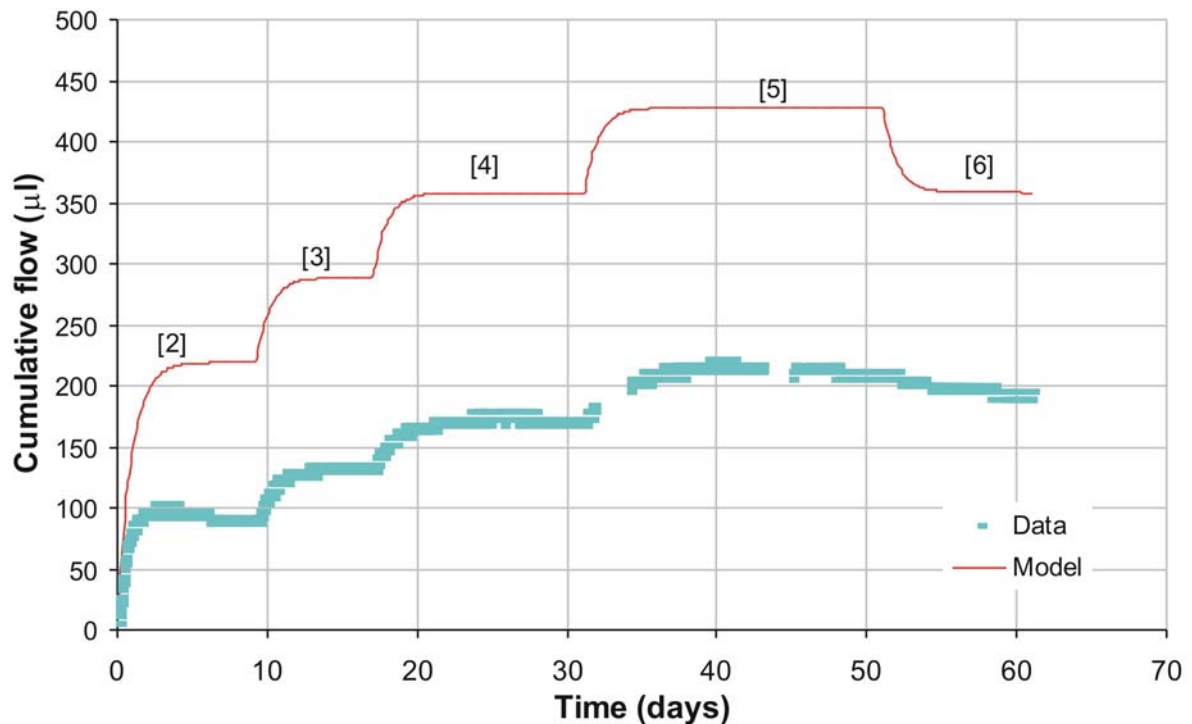


**Figure 38 – A comparison of data for the porewater flow during Phase 1 of the test with the model response.**

#### 4.4.4 Modelling of Phase 2 data

Phase 2 of the test program consists of seven stages with both axial and confining stresses increased by 4 MPa each time. The stages last for between 30 and 80 days. In view of the results of the Phase 1 modelling, where the linear elastic model was unable to represent multiple testing stages from a single set of rock property parameter values, it was decided to treat each stage of Phase 2 as a separate test and to use the model to parameterise the changing state of the specimen. Thus, the model was used to fit for permeability and Young's modulus at each stage, again using the axial strain data for the fitting. The results of this approach are shown in Figures 39 to 45 and the parameter values obtained are listed in Table 13.

Stage number	Permeability (m <sup>2</sup> )	Young's modulus (MPa)
8	2.7e-19	470
9	1.9e-19	700
10	8.2e-20	965
11	5.9e-20	865
12	4.0e-20	925
13	2.8e-20	1050
14	2.5e-20	950

**Table 13 – Parameter values determined for each stage of Phase 2.**

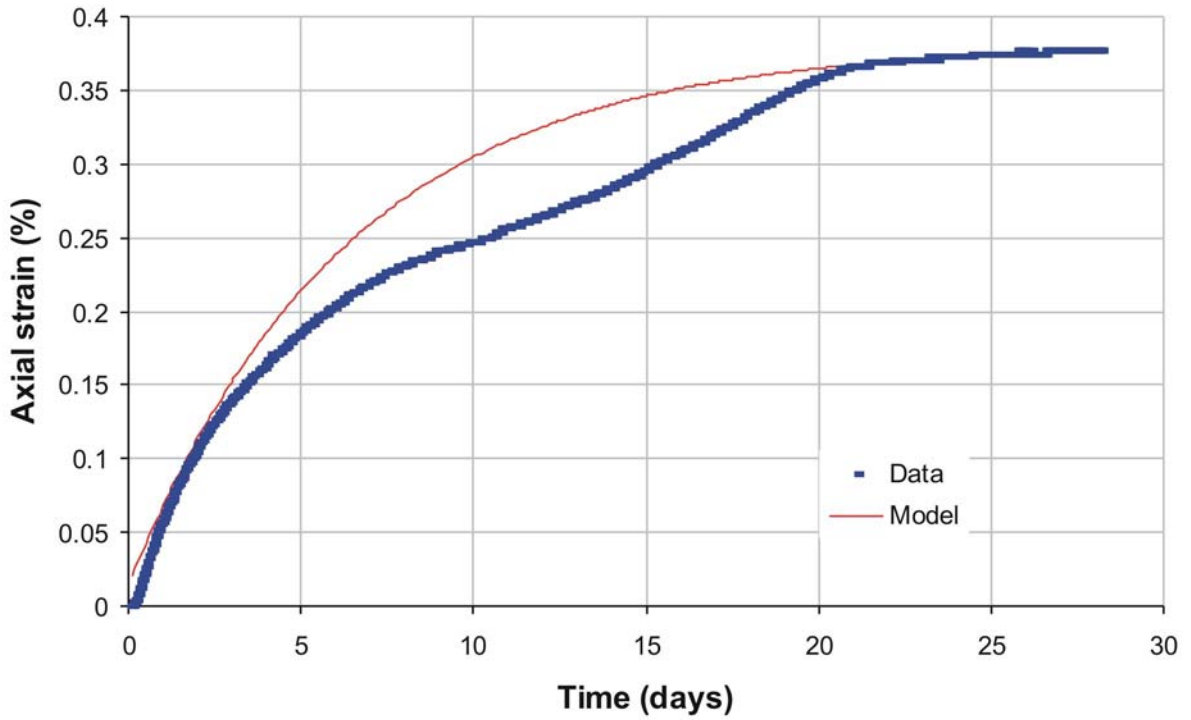


Figure 39 – Comparison of model to axial strain data for test stage [8].

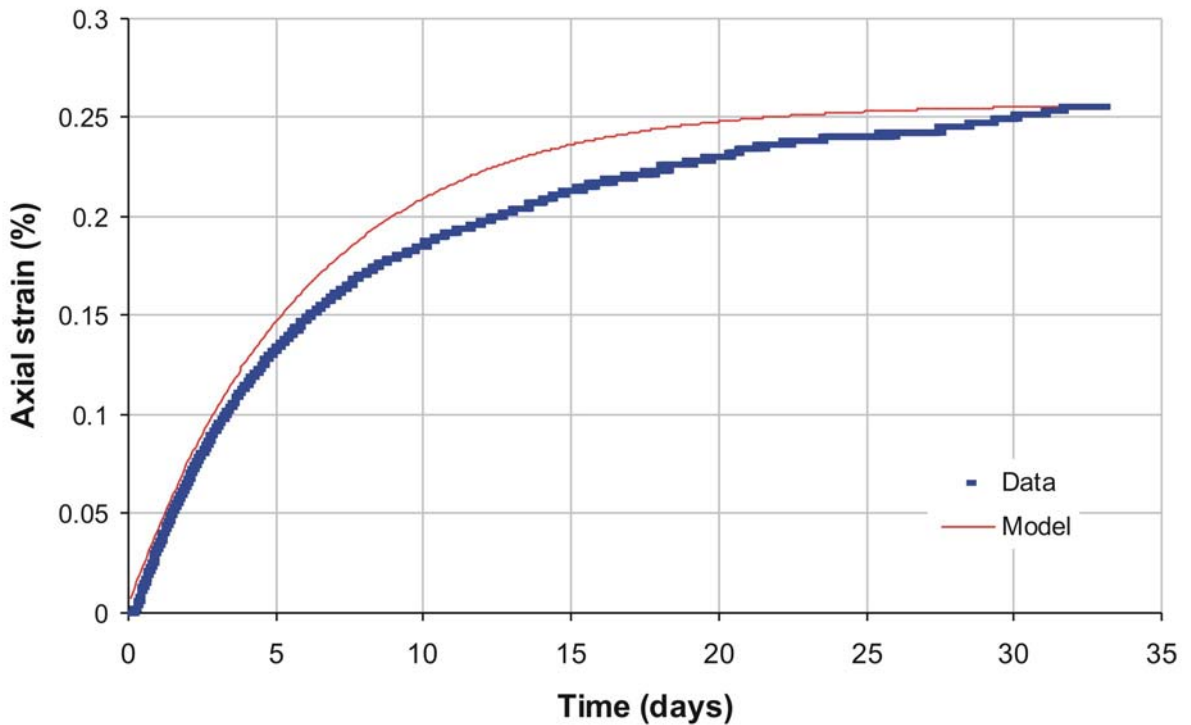


Figure 40 – Comparison of model to axial strain data for test stage [9].

It can be seen that generally good fits have been obtained in each stage, although in some the data deviates from the model curve in some regions, such as the middle of stage [8] and the end of stage [14]. Table 13 shows that the apparent permeability declines by an order of magnitude over the course of the test. The apparent values of Young’s modulus double during the test, but most of this change occurs over the first two stages with the remaining stages falling in the range

865-965 MPa, except for stage [13] which is slightly higher at 1050 MPa. The average value of Young’s modulus for the last 5 stages is 950 MPa.

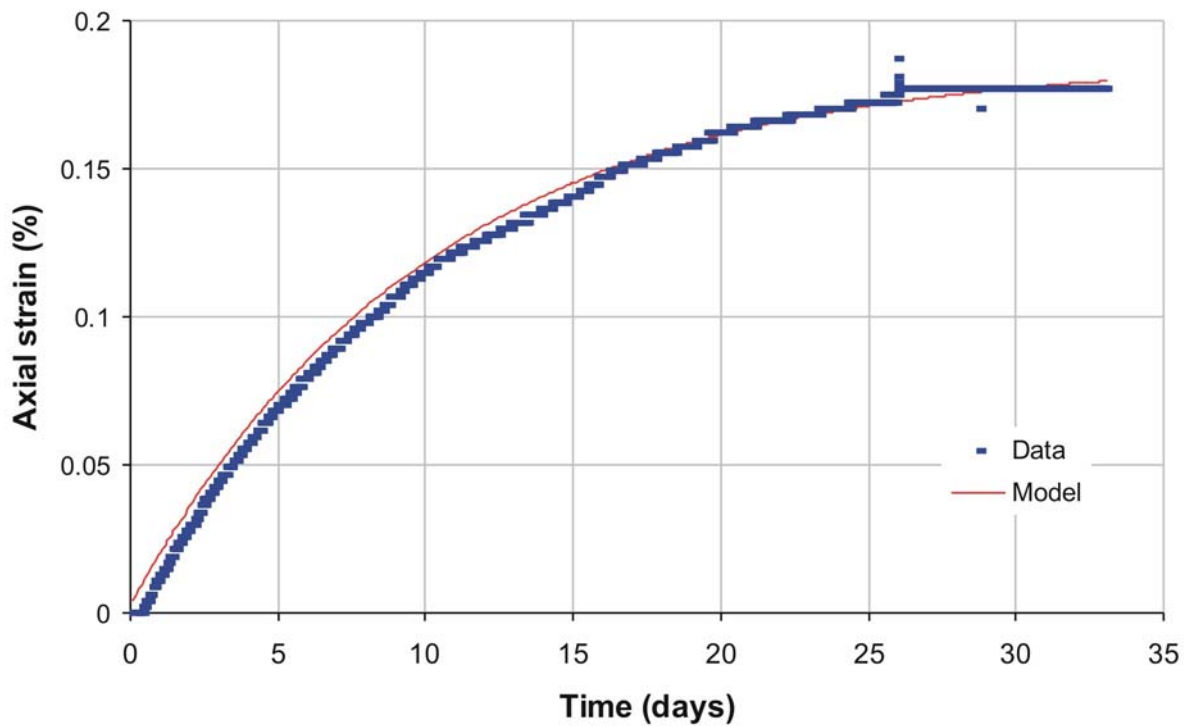


Figure 41 – Comparison of model to axial strain data for test stage [10].

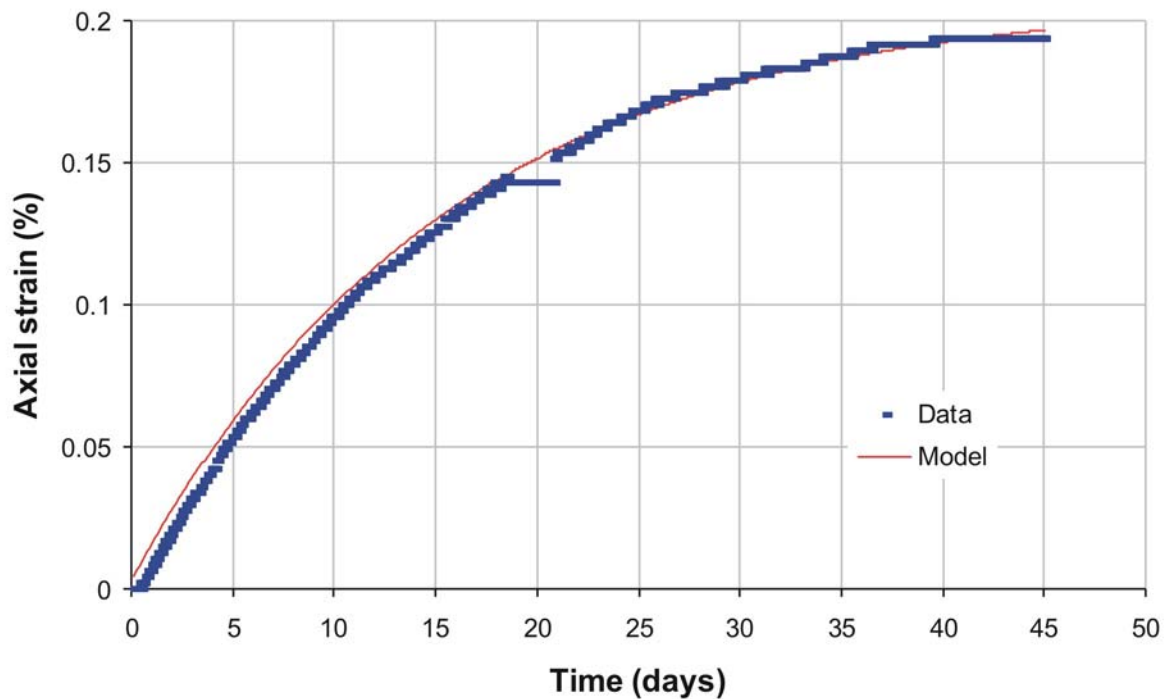


Figure 42 – Comparison of model to axial strain data for test stage [11].

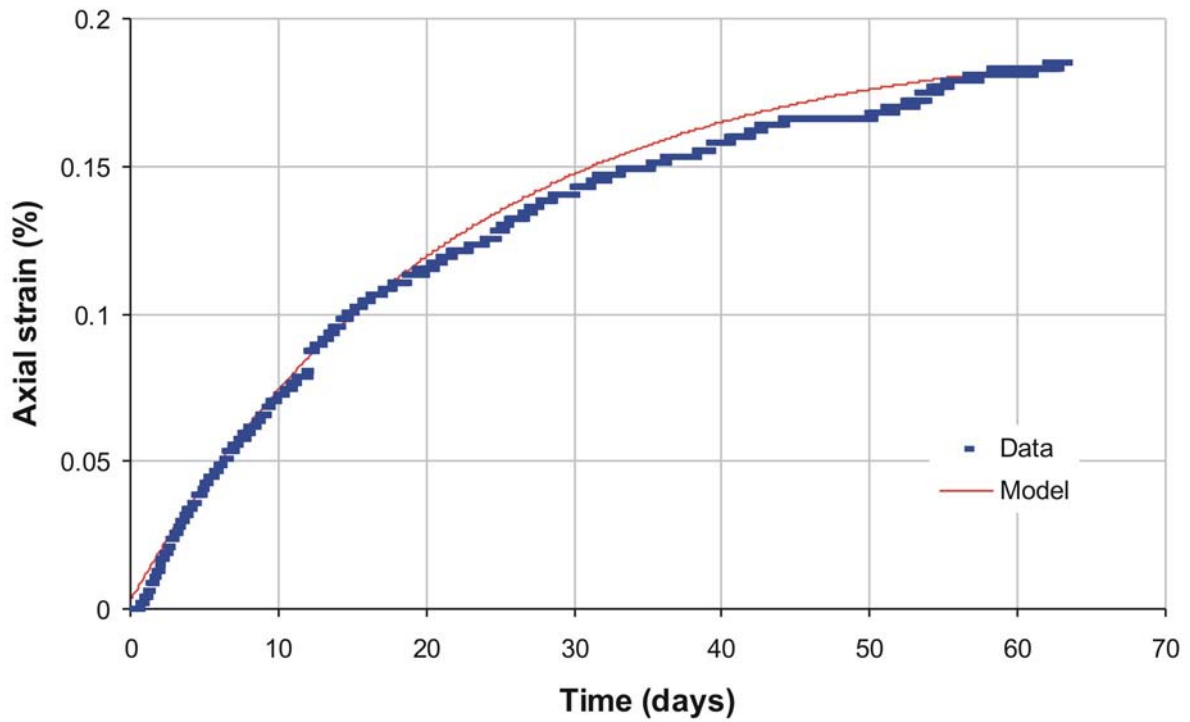


Figure 43 – Comparison of model to axial strain data for test stage [12].

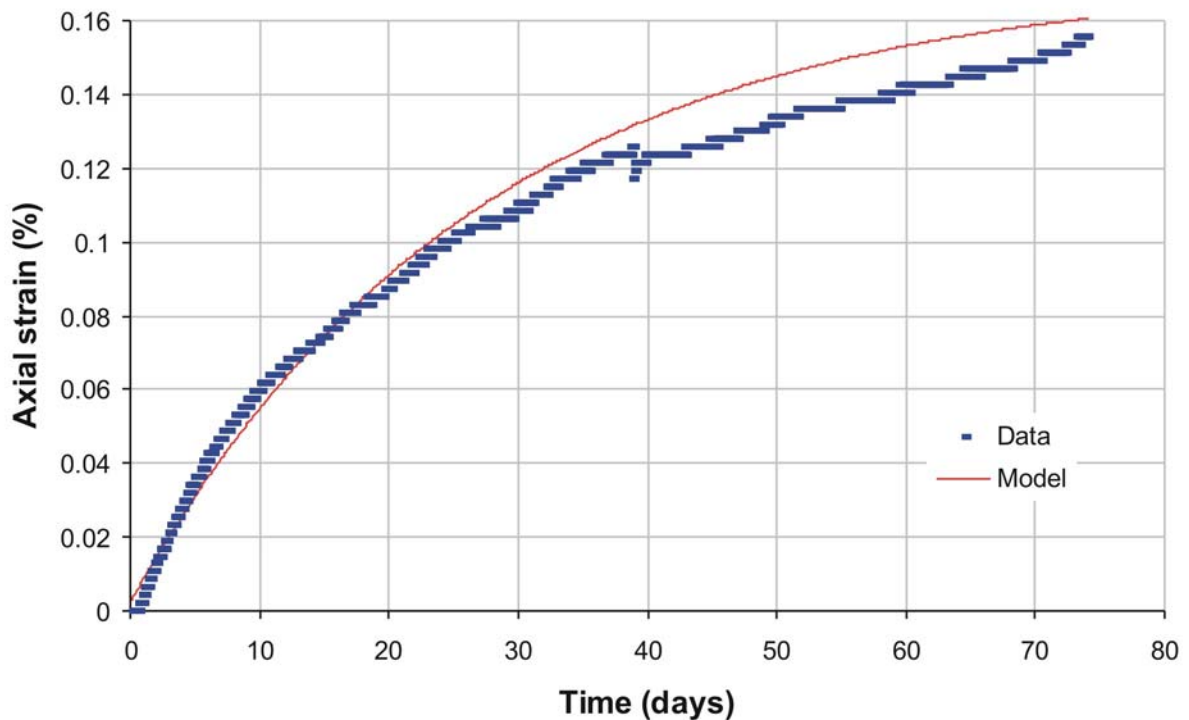


Figure 44 – Comparison of model to axial strain data for test stage [13].

The radial strain data, only available for stages [8] and [9], are compared to the model predictions in Figures 46 and 47. The model makes a rather poor representation of the Phase 1 data. In stages [8] and [9] the model predicts much larger strains than were observed.

The porewater flow data are compared to the model predictions in Figures 48 to 54. It can be seen that in all stages the model significantly over-estimates the volume of porewater that is expelled from the specimen. This would seem to be consistent with the radial strain differences noted above for stages [8] and [9]. Taken together, the comparisons of the model calculations with the radial strain and porewater flow data may indicate that the isotropic deformation assumption of the model is not appropriate and that an anisotropic model should be considered instead.

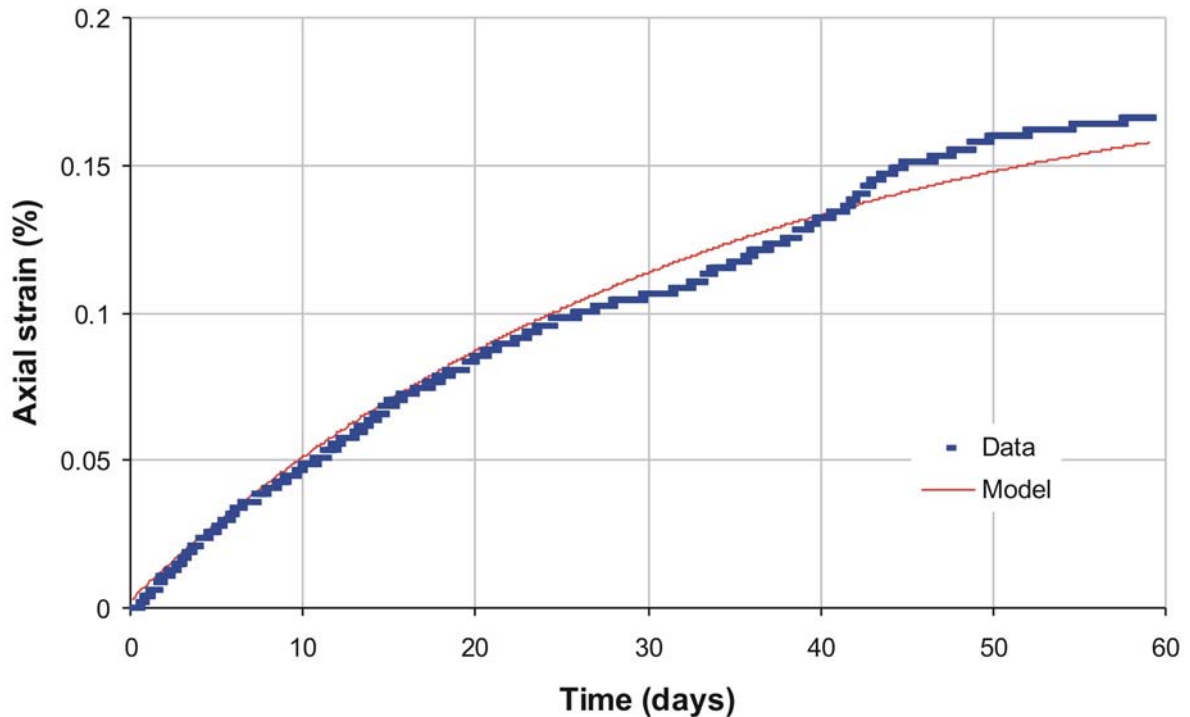


Figure 45 – Comparison of model to axial strain data for test stage [14].

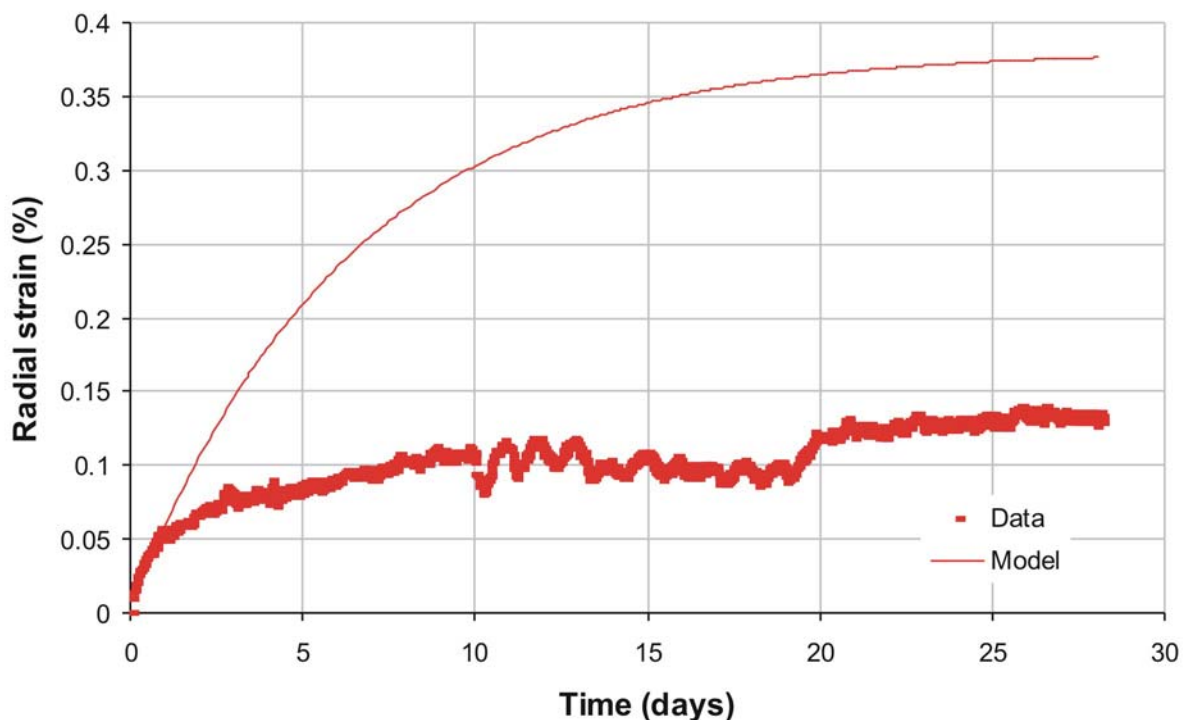


Figure 46 – Comparison of model to radial strain data for test stage [8].

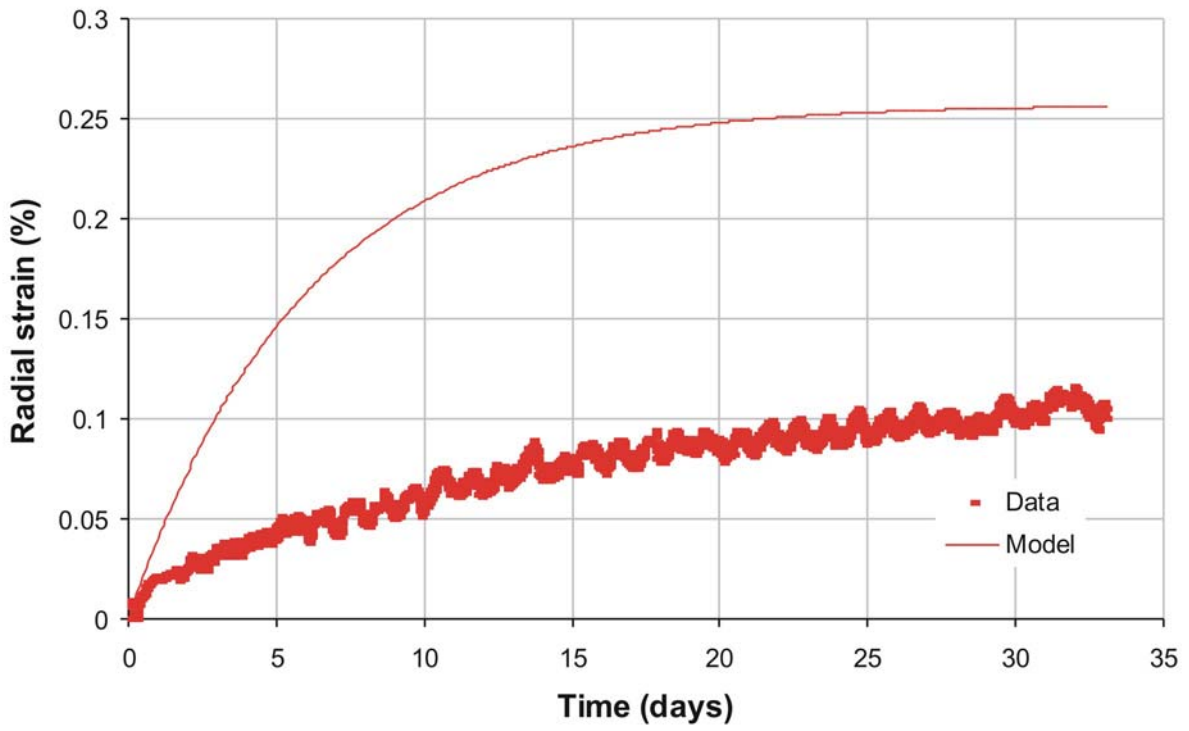


Figure 47 – Comparison of model to radial strain data for test stage [9].

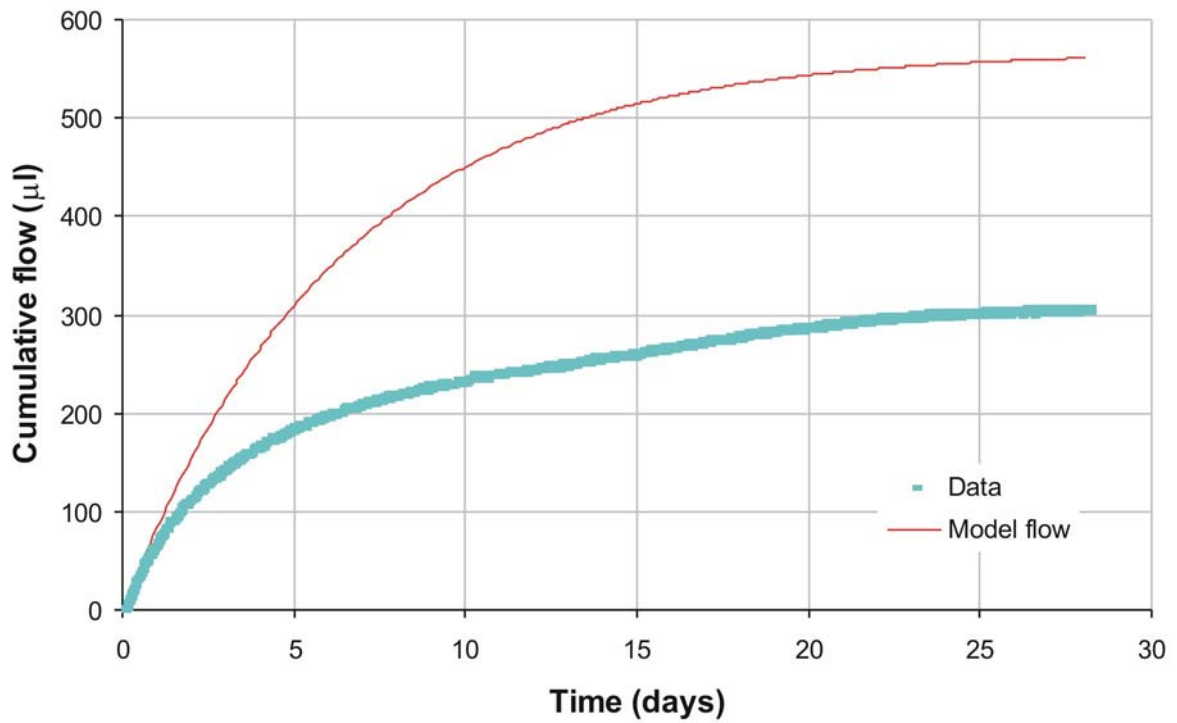


Figure 48 – Comparison of model to porewater flow data for test stage [8].

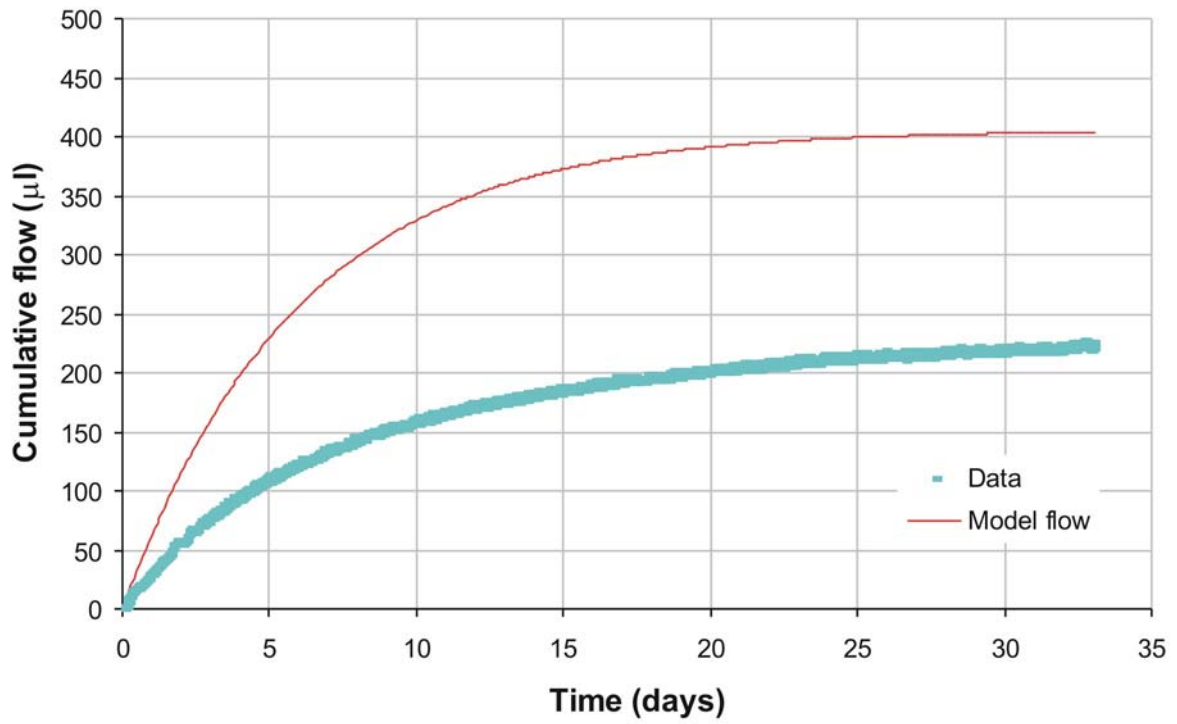


Figure 49 – Comparison of model to porewater flow data for test stage [9].

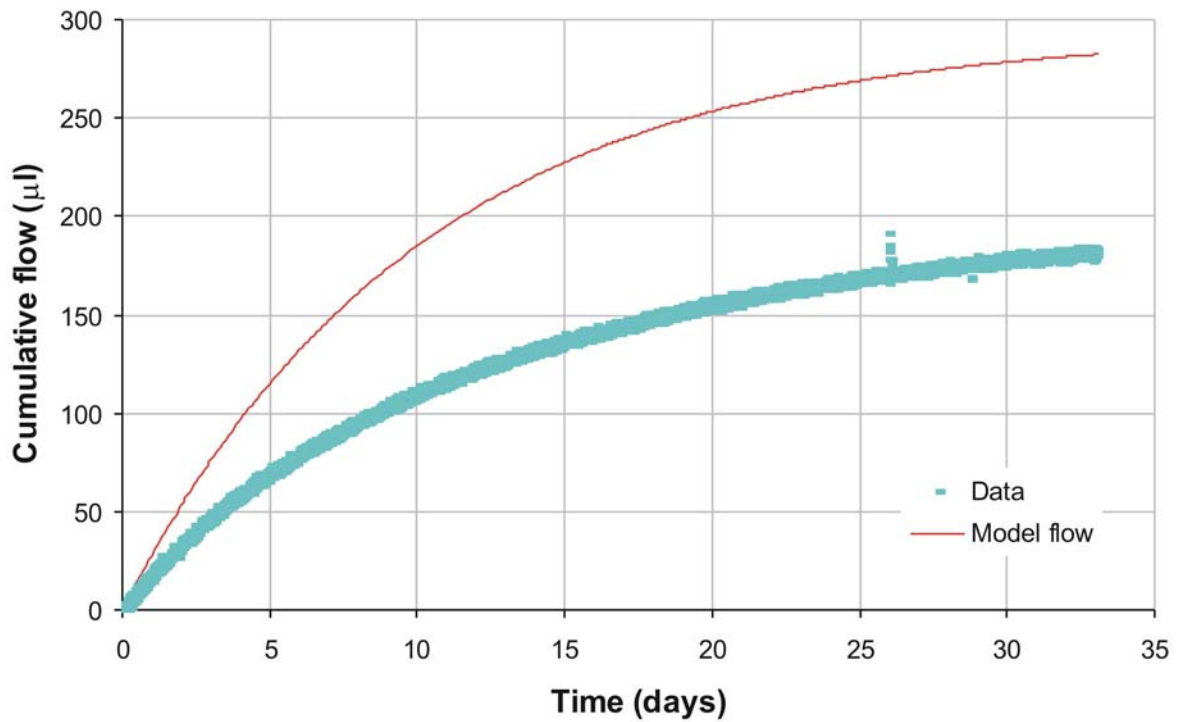


Figure 50 – Comparison of model to porewater flow data for test stage [10].

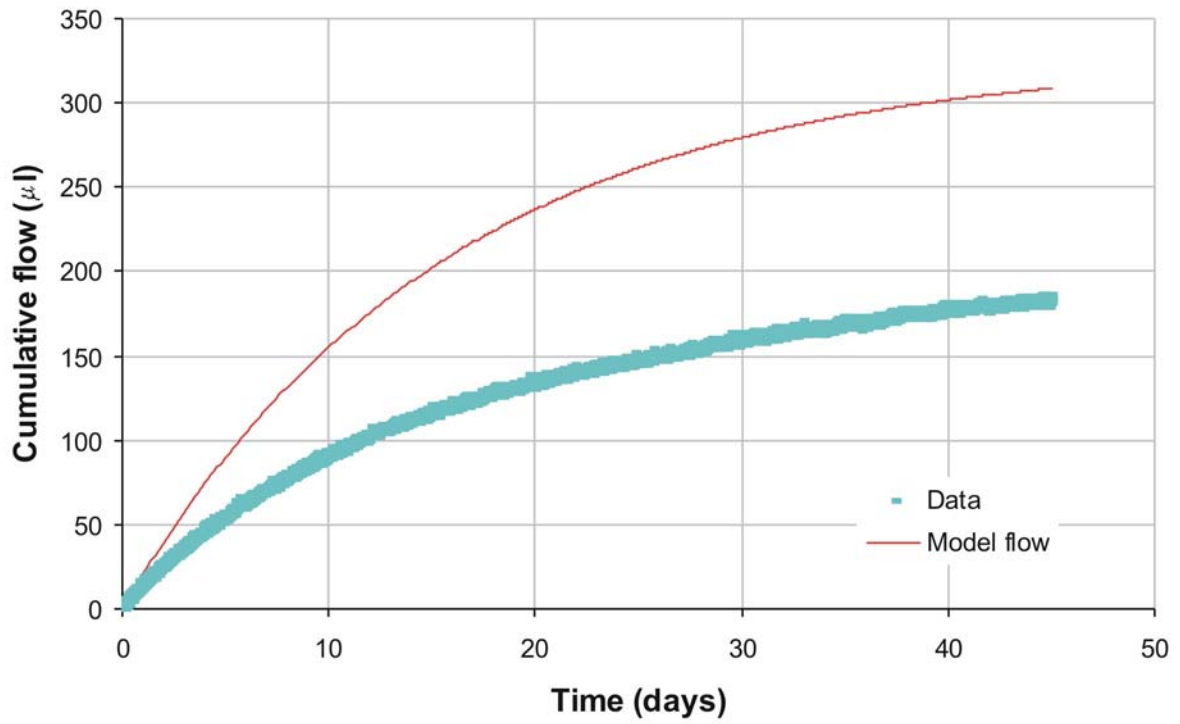


Figure 51 – Comparison of model to porewater flow data for test stage [11].

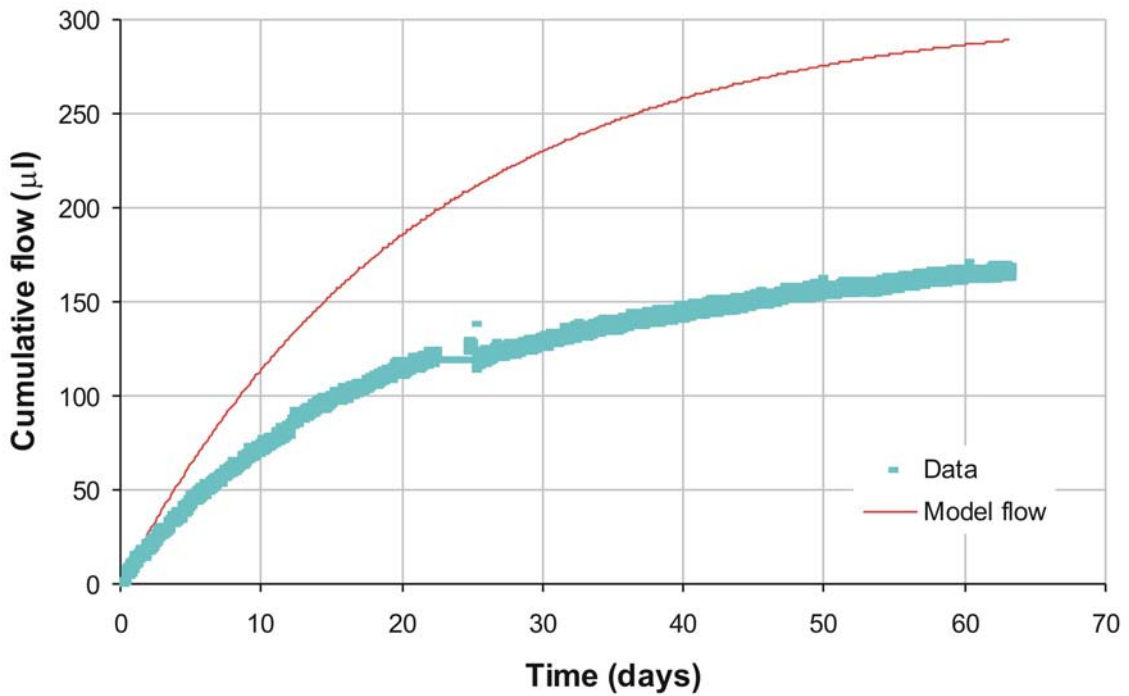


Figure 52 – Comparison of model to porewater flow data for test stage [12].

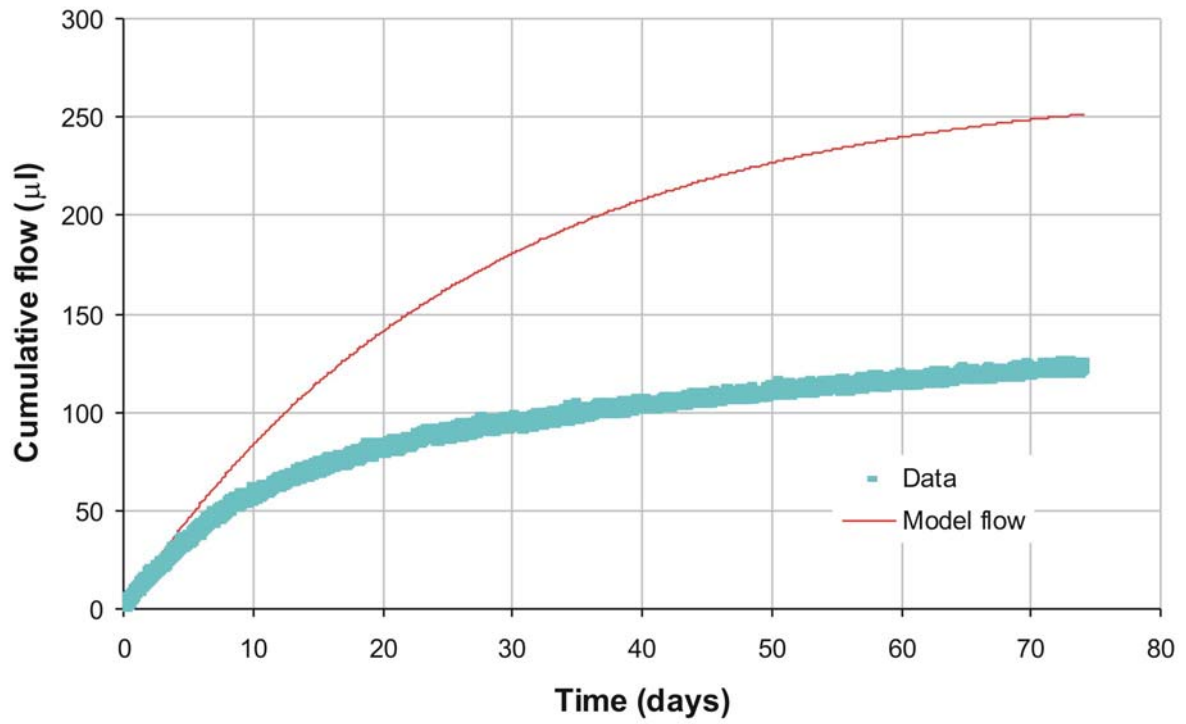


Figure 53 – Comparison of model to porewater flow data for test stage [13].

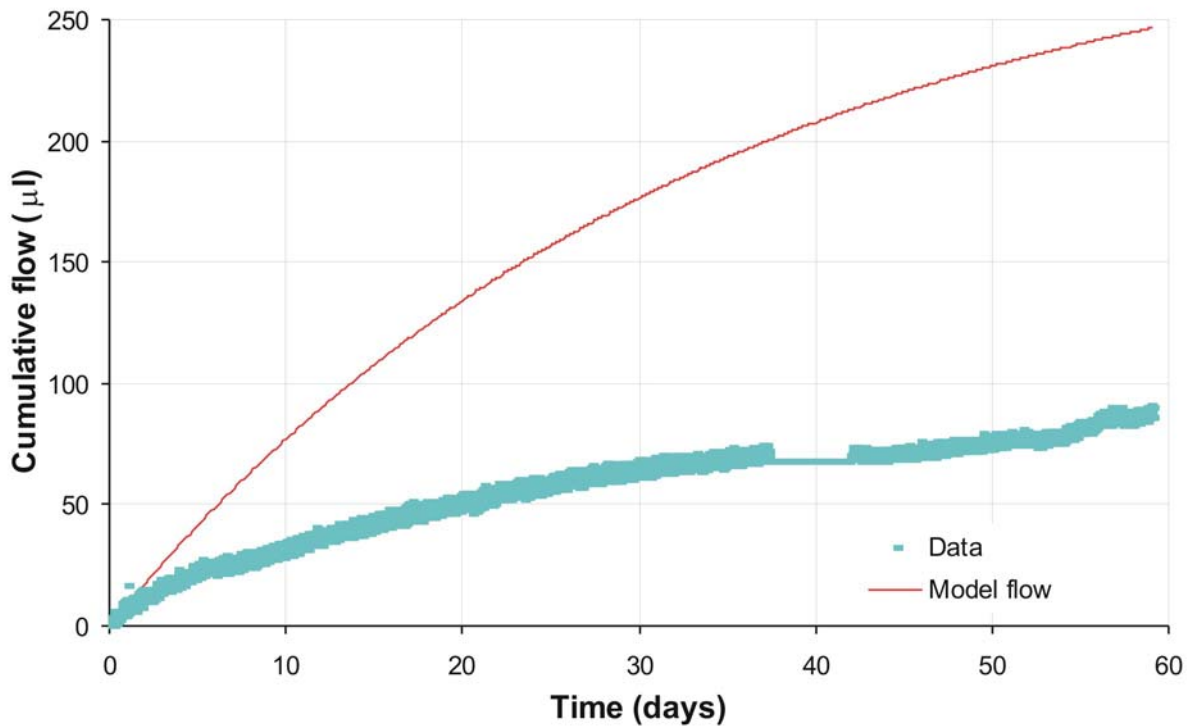


Figure 54 – Comparison of model to porewater flow data for test stage [14].

## 5 Conclusions

A specimen of Opalinus clay from Mont Terri has been subjected to stress testing over a period of 532 days with observations being made of strains (axial and radial) and of the volume of porewater expelled or injected into the specimen. Testing was undertaken by changing either (or both) of the axial and confining stresses in sharp steps followed by periods of between 4 and 82 days during which time the specimen was allowed to adjust to the new stress state. In this way, the drained consolidation, creep and rebound behaviour of an Opalinus clay specimen was examined. The test material was subject to a maximum average effective stress of 38.3 MPa.

At the onset of testing the specimen was found to have a significant air content. Initial measurements suggested that approximately 50% of the air was resident within dilatant microfractures which were sensitive to the applied level of confining stress and around 50% was located in the remaining pore space of the mudrock; it is uncertain from the available data whether the dilatant microfractures had closed completely. When exposed to test permeant (distilled water), the initial strain response was dominated by swelling and hydration of the mudrock. Volumetric strain based on volume change showed far less strain than measurements based on porewater displacement, suggesting residual air was present within the microstructure of the clay. To compensate for this phenomena, volumetric strain data from porewater displacement measurements were corrected for gas saturation at the end of test stage [1].

Examination of volumetric strain data for both volume change and porewater displacement measurements indicate a small inflection in the standard geotechnical plot of void ratio against the logarithm of average effective stress at a value between 20 and 22 MPa. The  $\alpha$  values based on volume change measurements exhibit a general trend of increasing magnitude as effective stress rises. An increase in  $\alpha$  would be anticipated with the onset of plastic yielding. Examination of the porewater displacement data shows a similar progressive upward trend to an average effective stress of around 30 MPa, at which point  $\alpha$  values begin to decrease. This reduction in value could be explained by grain-strain of the mineral fabric at high effective stresses. Even though the data do not exhibit the sharp increase in  $\alpha$  values indicative of classic virgin consolidation behaviour, it would appear that plastic yielding is occurring as average effective stress increases. The data suggest the onset of plastic yielding occurs before 20 MPa, which is supported by examination of data from Heitz et al. (1998).

Analysis of net porewater flow measurements indicate original interstitial fluid was not expelled from the specimen until average effective stress exceeded 20 MPa. While insufficient load was applied to the specimen to fully delineate the void ratio effective stress relationship, an estimate for the preconsolidation stress in the region of 20 to 25 MPa seems reasonable given the data available.

Due to the premature termination of the test only a small section of the initial unloading history is delineated. Reductions in average effective stress to 32.3 and 28.3 MPa resulted in only minor amounts of recoverable strain.

As effective stress rises there is a noticeable increase in the duration of the strain transients compared to earlier test stages. As the induration state of the mudrock increases, strain traces are characterised by less well-defined transients, indicative of time-dependent plastic yielding at high effective stresses. The volumetric strain data for both volume change and porewater displacement measurements shows similar transient behaviour. By the end of the loading cycle at an average effective stress of 36.3 MPa, the specimen had undergone 1.777% axial strain, around 0.448% radial strain and between 2.070% and 2.673% volumetric strain (depending on the method of calculation). These results give an average PSR ratio of 0.252, suggesting that the material is either mechanically anisotropic or behaving as a non-ideal elastic medium.

From test stage [8] onwards, specific storage values derived from porewater displacement measurements show a general decreasing trend with increasing average effective stress and are in

the range  $1.5$  to  $12.5 \times 10^{-6} \text{ m}^{-1}$ . Data from volume change measurements exhibit a similar trend up to stage [10] at which point they appear to level and specific storage becomes less sensitive to increases in average effective stress. These values are in the range  $1.2$  to  $17.5 \times 10^{-6} \text{ m}^{-1}$ .

Calculation of elastic constants clearly show that values derived for undrained quantities are significantly higher (around an order of magnitude) than those for drained parameters. Data suggest there is a transition in behaviour centred around an average effective stress of approximately 20 MPa. Below this value drained bulk modulus, Young's modulus and shear modulus based on volume change measurements range from 0.5 to 0.8 GPa, 0.7 to 1.1 GPa and 0.3 to 0.4 GPa respectively. Above this value (up to 36.3 MPa) these parameters range from 1.2 to 1.4 GPa, 1.6 to 1.9 GPa and 0.6 to 0.8 GPa. Values derived from measurements of porewater displacement gave consistently higher values.

Four experimental stages were dedicated to examining the creep behaviour of the specimen, with test stages lasting up to 20 days in duration. In terms of creep investigation, these stages are relatively short, but in each case it can be argued that steady secondary creep was observed.

A close examination of each stage shows that the creep curve can be broken down into three (or four in the case of stage C3) distinct responses. In the first, a steady decay in strain-rate is observed. This is followed by an almost linear region, which is succeeded by a secondary linear response with a slower creep rate. In the final creep stage (C3, stage [5]), a third linear response was observed, with a similar slope to that of the first linear region. However, there is insufficient data to ascertain whether this phenomenon can be attributed to accelerating creep.

In general, volumetric strain data in these test stages exhibits considerable noise in comparison to axial strain results. This can be predominantly explained by noise in the radial strain measurement.

The Lemaitre model, as applied to Opalinus clay by Boidy (Boidy *et al.*, 2002), was applied to the current test data, however the published model parameters failed to adequately fit the current data. Minor alteration of these parameters enabled modelling of the longer-term volumetric responses to be undertaken.

The Lemaitre model did not predict the initial stage of creep (from time = 0 to  $t = 5 - 7$  days) very effectively. A much slower response time was seen in the current data, which was absent in the work by Kharchafi and Descoedres (1995). The time-dependent nature of compaction and pore-pressure dissipation may account for these differences. The effect of compaction, swelling and pore-pressure transients were not removed from the current data.

Power-law creep has been applied to argillaceous rocks (e.g. Thimus and De Bruyn, 1998) and an attempt to formulate a power-law relationship was undertaken. In general the fit of these relationships was adequate for the volumetric strain observed, although these data are inherently noisy. Conversely, the fit of the axial strain data was not adequate and even the subdividing of the data into the individual creep stages failed to give an acceptable fit.

The power-law fit of the data for stage C3 was adequate, although a combination of power-law for the initial response and Lemaitre for the longer response may achieve a better prediction for this test stage.

The final stage of creep (R1) has not been quantitatively analysed. This stage of deformation shows an initial reduction in strain, which after 6 days exhibits a positive increase in net strain. This may be attributed to the complexity of the experiment and could be indicative of pore-pressure dissipation effects caused by swelling of the specimen.

In addition to the creep modelling described above, a numerical simulation was set-up using the 2-dimensional coupled flow and deformation code STAFAN, which assumes linear elastic and isotropic-deformation and porous medium flow of the porewater.

Two phases of the testing were modelled separately. During Phase 1, covering the first 70 days, the model was used in an attempt to fit the creep data. This phase was modelled by fitting the model response to the axial strain data for test stage [2] and then continuing the model to cover the remaining steps, i.e. a calibrate and predict approach was adopted. To make the calibration, the hydraulic permeability and Young's modulus were treated as adjustable parameters. A reasonable fit was made to the first step axial strain data using a permeability of  $2.0 \times 10^{-18} \text{ m}^2$  and a Young's modulus of 450 MPa, but the extrapolation to later steps showed a progressive deviation from the data. In addition, the model made poor predictions for the radial strain and porewater flow data in all steps. These observations indicate that both the assumptions of linear elasticity and isotropic deformation are probably invalid for this specimen supporting the evidence presented above, that plastic deformation was occurring. The high permeability and low modulus values for stage [1] may be caused by perturbation to the specimen noted as a possible cause for the curvature observed in the early section of the void ratio log effective stress plot.

During the second phase of testing, the axial and confining stresses were raised synchronously in a series of seven 4 MPa steps. In view of the results of the Phase 1 modelling, where the linear elastic approach was unable to represent multiple testing steps from a single set of rock property parameter values, it was decided to treat each step of Phase 2 as a separate test and to use the model to parameterise the changing state of the specimen. Thus, the model was used to fit for permeability and Young's modulus at each test stage, again using the axial strain data for the fitting. It was found that the Young's modulus rose from nearly 500 MPa in the first step to an average of 950 MPa over the last five steps. This value is significantly lower than those derived from volume and porewater displacement measurements and results from the over prediction of radial strain due to the simple linear-elastic assumption (i.e. isotropic properties) in the STAFAN model.

The apparent permeability was reduced steadily over the course of this phase of testing from nearly  $3.0 \times 10^{-19} \text{ m}^2$  in the first step to less than  $3.0 \times 10^{-20} \text{ m}^2$  in the final step. As for the first phase of testing, the model provides generally poor representations of the radial strain and porewater flow data.

It has been shown that the linear elastic deformation model is not a good analogue for the behaviour of this specimen. There are clear indications of non-linear responses to stress changes in the data and it seems likely that some form of viscoelastic or viscoplastic model should be adopted. In addition, the axial and radial strain responses would seem to be anisotropic, bringing further complexity to the model that should be employed.

## References

- ATKINSON, J. H. and BRANSBY, P. L. (1978). *The Mechanics of Soils: An Introduction to Critical State Soil Mechanics*. McGraw-Hill, New York.
- BEAR, J. (1986). *Dynamics of Fluids in Porous Media*. Environmental Science Series. Elsevier, New York, 764 p.
- BOIDY, E. (2002). *Modelisation numerique du comportement differe des cavites souterraines*. PhD thesis, Grenoble 1 University, 317 pp.
- BOIDY, E. and PELLET, F. (2000). Identification of mechanical parameters for modeling time-dependent behaviour of shales, ANDRA Workshop, Behaviour of Deep Argillaceous Rocks: Theory and Experiment; Proceedings International Workshop on Geomechanics, Paris, October 11–12, 2000, 13 p.
- BOIDY, E. and PELLET, F. (2002). Identification of mechanical parameters for modelling time-dependent behaviour of shales. In: Hoteit, N., Su, K., Tijani, M., and Shao, J.-F., eds., *Hydromechanical and Thermomechanical Behaviour of Deep Argillaceous Rock*. Lisse, Swets and Zeitlinger, 11-22.
- BOIDY, E., BOUVARD, A. and PELLET, F. (2002). Back analysis of time-dependent behaviour of a test gallery in claystone. *Tunnelling and Underground Space Technology*, **17**, pp.415–424.
- BOIDY, E., PELLET, F. and BOULON, M. (2001). Numerical modeling of deep tunnels including time-dependent behaviour. In: Desai et al. (Eds.), *Computer Methods and Advances in Geomechanics*, Balkema, Rotterdam, pp.1663–1668.
- BRITISH STANDARD METHODS (1990): *Soils for civil engineering purposes, Part 2, BS 1377: Classification test*, pp. 61.
- CARTER, N.L. (1976). Steady flow of rocks. Review. *Geophysics and Space Physics*, **14**, pp.301–360.
- DAVIS, G.H., and REYNOLDS, S.J. (1996). *Structural geology of rocks and regions*. 2nd Edition. John Wiley and Sons, New York.
- DUSSEAULT, M.B., and FORDHAM, C.J. (1993). Time-dependent behavior of rocks. In: Hudson, J.A., ed., *Rock testing and site characterization*. Oxford, United Kingdom, Pergamon Press, pp. 119-149.
- GAUTSCHI, A. (2001). Hydrogeology of a fractured shale (Opalinus Clay): Implications for deep geological disposal of radioactive wastes. *Hydrogeology Journal*, pp 99-107, Springer-Verlag, Heidelberg.
- HARRINGTON, J.F. AND HORSEMAN, S.T. (1999). Gas transport properties of clays and mudrocks. In: Aplin, A.C., Fleet, A.J. and Macquaker, J.H.S. (eds) *Muds and Mudstones: Physical and Fluid Flow Properties*, Spec. Pub. **158**, pp 107-124, Geological Society of London.

- HEITZ, J.F., HAUDEVILLE, A. and HOTEIT, N. (1998). Geomechanical spectrum of argillaceous rocks. In: *The Geotechnics of Hard Soils - Soft Rocks*, A. Evangelista and L. Picarelli (eds), Balkema, Rotterdam, pp 183-190.
- HORSEMAN, S.T. (2002). Approach to long-term evolution of host rock hydromechanical properties based on the dilatancy boundary concept. Technical Report RR/02/XX-Final Draft. British Geological Survey.
- HORSEMAN, S.T. (2001). Self-healing of fractures in argillaceous media from the geomechanical point of view. In: *Proceedings of a Topical Session on Self-healing held in Nancy, France*. IGSC Working Group on Measurement and Physical Understanding of Groundwater Flow Through Argillaceous Media. OECD/NEA Radioactive Waste Management Committee. NEA/RWM/CLAYCLUB(2001)5 (unclassified).
- HORSEMAN, S.T., WINTER, M.G. and ENTWISLE, D.C. (1993). Triaxial experiments on Boom Clay. In: *The Engineering Geology of Weak Rock*, Cripps, J.C. et al., (eds), Balkema, Rotterdam, 36-43.
- HUYAKORN, P.S. AND PINDER, G.F. (1983). *Computational Methods in Subsurface Flow*. Academic Press, New York, 473 pp.
- INTERA, 1983. STAFAN: A Two-Dimensional Code for Fluid Flow and the Interaction of Fluid Pressure and Stress in Fractured Rock for Performance Assessment. Report of the Office of Nuclear Waste Isolation, ONWI-427.
- INDERBITZIN, L. and MÉTILLE, J. (2004). HA Experiment / Borehole BHA-4: Documentation of Drilling and Sample Conditioning. Technical report TN 2004-82, Geotechnical Institute Ltd., Switzerland.
- KARIG, D. and MORGAN, J. (1994). Tectonic deformation: Stress paths and strain histories. Chapter 6. In: Maltman, A. (ed.) *The Geological Deformation of Sediments*. Chapman and Hall, London, 167-204.
- KHARCHAFI, M. and DESCOEUDRES, F. (1995). Comportement differe des roches marneuses encaissant les tunnels, Colloque Mandanum Craies et Schistes GBMR, Brussels, 10 pp.
- LEMAITRE, J. and CHABOCHE, J.-L. (1996). *Mecanique des materiaux solides*. Dunod, pp. 253–341.
- MARSILY, G. de (1986). *Quantitative Hydrogeology for Engineers*, Academic Press, San Diego, 440 p.
- PERZYNA, P. (1966) Fundamental problems in viscoplasticity. *Advances in Applied Mechanics*, **9**. Academic Press, New York, pp.243–377.
- RIZKALLA, M., and MITRI HANI, S. (1991). An elasto-viscoplastic model for stress analysis of mining excavations. In: Roegiers, J.C., ed., *Rock mechanics as a multidisciplinary science*, Balkema, Rotterdam, 597-606.

SCHOFIELD, A. and WROTH, P. W. (1968). Critical State Soil Mechanics. McGraw-Hill, London.

SULEM, J., PANET, M. and GUENOT A. (1987). Closure analysis in deep tunnels. International Journal of Rock Mechanics and Mineral Science and Geomechanical Abstracts, **24**, pp. 145-154.

THIMUS, J.F., and DE BRUYN, D. (1998). Long-term thermo-mechanical behaviour of Boom Clay. In: Evangelista, A. and Picarelli, L., eds., The Geotechnics of Hard Soils - Soft Rocks, Balkema, Rotterdam, pp.337-341.

WOOD, D.M. (1990). Soil Behaviour and Critical State Soil Mechanics. Cambridge University Press, 462 pp.

## Appendix 1 Glossary

**Accelerating creep** – stage of creep where the time-dependent strain continues to accelerate until ultimate failure, unusual in rocks. It is often referred to as **tertiary creep**.

**Average effective stress** – equal to mean stress minus porewater pressure.

**Axial displacement** – the movement of a loading piston creates a force on a sample by displacing a loading piston in the direction parallel to the samples length (axis).

**Axial force/stress** – the displacement of the loading piston in the axial direction creates a force in that direction. Stress is related to force as being force per unit area.

**Axial strain** – the resultant strain along the axis of the specimen.

**Bulk density** – defined as the ratio of the total mass (solid and liquid phases) to the total volume.

**Bulk modulus (K)** – defined as the ratio of the pressure on a body to its fractional decrease in volume. This parameter refers to elastic (recoverable) deformation.

**Compliance** – the inverse of stiffness. A measure of the ease with which a material may be deformed. For an experimental pressure vessel, the compliance should be very low compared with that of the test specimen, i.e. the force generated by the axial loading system should be translated to the specimen rather than the pressure vessel.

**Consolidation** – process by which a soil/rock loses water and becomes more compact, usually through the application of a total stress.

**Constant strain-rate experiments** - determination of creep parameters by testing over a range of strain-rates during the standard triaxial compression (or extension) test.

**Constant stress tests** – can be carried out in configurations such as triaxial, beam bending, uniaxial compression, double torsion and direct torsion (Dusseault and Fordham, 1993). Applied stress is maintained at a constant level and strain is analysed as a function of time.

**Constitutive creep model** - a constitutive flow/creep law is a generalised equation of the form:  $\dot{\epsilon} = A \cdot f_1(\sigma) \cdot f_2(T) \cdot f_3(s)$  where  $\dot{\epsilon}$  is strain-rate,  $A$  is a constant,  $f_1(\sigma)$  is a function of stress,  $f_2(T)$  is a function of temperature and  $f_3(s)$  is a function of structure. The constitutive nature of this form of flow law states that each function within the law is entirely separate, i.e. strain-rate is a function of stress and is also a function of temperature, but it is not a function of stress and temperature.

**Creep** – the continuous deformation of a solid material under constant stress that is well below its yield stress. Creep can also be defined as the time-dependent deformation of rock.

**Creep models** – there are many creep models (mathematical formulations) that are used to describe time-dependency. Each of these models has several parameters, some of which have physical basis while others are purely empirical.

**Differential stress** – defined as the difference between the maximum and minimum stress components, i.e.  $\sigma_1 - \sigma_3$

**Drained consolidation** – a consolidation (q.v.) experiment where interstitial fluid is allowed to drain from the specimen. The loading of the sample has to be at a suitably low strain-rate as to allow pore fluid to drain fully from the specimen. In an undrained test, the backpressure system is closed and interstitial fluid pressure rises as a consequence of pore compression.

**Dry density** - density of a unit block of rock after oven drying at 105°C for a period in excess of 24 hours.

**Effective stress** – the average normal force per unit area transmitted directly from particle to particle of a soil or rock mass. Under equilibrium conditions the effective stress in a saturated soil is equal to the difference between total stress and pore pressure.

**Elastic constants** – a series of coefficients that define the elastic properties of a material. Includes Young's modulus of elasticity (E), bulk modulus of compressibility (K), Poisson's ratio ( $\nu$ ) and shear modulus of elasticity (G).

**Finite element model** – a numerical method for solving differential equations by means of 'piecewise approximation'. As distinct from the finite difference method, which regards the solution region as an array of grid points, the finite element method envisions the region as being made up of many small interconnected subregions called 'finite elements'. Such elements, which generally take simple shapes (e.g. triangular, quadrilateral, and rectangular) are then assembled in various ways to represent a solution domain of arbitrary geometry.

**Hydraulic conductivity** - the constant of proportionality in Darcy's law. The volume of water that will move through a porous medium in unit time, under a unit hydraulic gradient, through a cross-section of unit area normal to the direction of flow.

**Hydromechanical test** – a test designed to examine the effect of mechanics on fluid flow (hydraulics).

**Interstitial fluids** – original fluid that is present within the pore space of a rock or soil.

**Lemaitre model** – viscoplastic model used to describe the creep behaviour of rock.

**Linear elasticity** – used to describe a material that has 'perfect' elastic properties. It is not uncommon for rocks to display a stress-strain result that is non-linear in the elastic region. Some studies have also shown that the elastic properties are pressure sensitive.

**Mean stress** – mean stress is the average of the three principal stresses i.e.  $\frac{1}{3} (\sigma_x + \sigma_y + \sigma_z)$ , or in the case of a triaxial experiment  $\sigma_c + \sigma_a/3$ , where  $\sigma_c$  is the confining stress and  $\sigma_a$  is the axial stress.

**Moisture content** - defined as the ratio of the mass of water to the mass of solids in a rock or soil.

**Net porewater displacement** – total amount of pore fluid expelled.

**Permeability** – the capacity of a porous rock, sediment or soil for transmitting a fluid; it is a measure of the relative ease of fluid flow under unequal pressure.

**Plastic yielding** – see yield stress

**Poisson's ratio ( $\nu$ )** - defined as the ratio of the radial strain to the axial strain. This parameter refers to elastic (recoverable) deformation and describes how much axial compression is translated into radial strain.

**Porewater displacement** – the movement of interstitial fluid into or out of a specimen subject to a change in boundary conditions.

**Porewater pressure** – defined for this experiment as the fluid pressure in the reservoir of the backpressure system, which is under equilibrium conditions and is assumed to be equal to the fluid pressure within the macro pores of a porous rock.

**Porosity** – the ratio of the aggregate volume of interstices in a rock or soil to its total volume.

**Power-law creep** – time-dependent strain (primary creep) that can be described mathematically by a power-law relationship, such as  $\dot{\epsilon} = Bt^{-1}$ .

**Preconsolidation stress** – the maximum stress-level that a sediment has experienced in its stress history. During a loading experiment, the preconsolidation stress is seen as a clear deviation in the consolidation response with increasing load. At stress levels above this value “new” plastic damage occurs within the specimen.

**Primary creep** – an observed condition of time-dependent strain where the creep rate reduces with time, sometimes referred to as decelerating creep. Primary creep is either superseded by steady-state creep or by zero creep.

**Principal strain ratio (PSR)** – defined as the ratio between the radial and axial strain components.

**Radial strain** – component of strain recorded in the radial direction. The radial direction is always perpendicular to the axial direction.

**Rebound/rebound-reconsolidation line (RRL)** - if the clay is unloaded, then only the elastic strains are recovered. The drained path then follows the rebound-reconsolidation line (*RRL*), also known as the swelling line. This is idealised as a straight line on a plot of  $\nu$  against  $\ln(p')$  with a negative slope (Schofield and Wroth, 1968).

**Relaxation tests** - carried out by imposing an *instantaneous* strain (length change in specimen,  $\Delta l$ ) and monitoring stress decay and axial strain over time. These types of test can be conducted together with constant-displacement experiments, i.e. by stopping the constant displacement at set intervals and observing the stress relaxation.

**Rupture strength** – the stress-level at which a specimen ruptures, or the stress level at which a fracture is formed.

**Saturation** – defined as the ratio of the volume of water to the volume of voids.

**Secondary consolidation** – time-dependent loss in pore volume occurring under a sustained, but not necessarily constant, effective stress.

**Shear modulus ( $G$ )** - defined as the tangential force per unit area divided by the angular deformation (in radians). This parameter refers to elastic (recoverable) deformation.

**Specific storage ( $S_s$ )** - the quantity of water that a unit volume of porous rock releases from storage under the effect of a unit decline in hydraulic head.

**STAFAN** - coupled flow and elastic deformation finite element code devised by Intera (1983).

**Steady-state creep** – a creep (strain vs. time) response that gives a linear response, i.e. the creep rate is constant for an indefinite period of time. It is often referred to as **secondary creep**.

**Strain ( $\epsilon$ ,  $\gamma$ )** - change in shape or volume of a body in response to a change in boundary conditions. Defined as the ratio of the change in length/volume to the original length/volume.

**Strain rate** – the rate at which strain is induced within a rock. In a laboratory, a large range of strain-rates can be used during the constant displacement axial loading experiment. In nature, strain-rates are several orders of magnitude smaller than those used in laboratory experiments. Strain-rates induced by engineering practices, such as tunnelling, may create high strain-rates, comparable with those of the laboratory.

**Strain transient** – a time-dependent strain response leading to a defined asymptote.

**Stress ( $\sigma$ )** – the force per unit area acting on a body causing it to deform (strain). Has various components such as deviatoric stress, differential stress, effective stress, mean stress, octahedral stress, normal stress and shear stress.

**Stress path analysis** – during deformation, the stress regime can change markedly. The aim of stress-path analysis is to replicate a given stress-path (or stress regime change). This may be a simple burial and exhumation stress-path, or can be a complex stress-path, such as those created by the advancement of a shaft during tunnelling.

**Swelling** – the increase in volume exhibited by a soil or rock due to the intake of fluid or the relaxation in confining stress.

**Transient testing** - designed to keep structure constant by quickly altering parameters during testing. For a constant-displacement experiment this may mean changing strain-rate ( $\dot{\epsilon}$ ), such that  $\dot{\epsilon}_1$  is initially used, followed by  $\dot{\epsilon}_2$ ,  $\dot{\epsilon}_3$ , and then perhaps  $\dot{\epsilon}_2$  again. Not much time is given for the specimen structure to adjust.

**Triaxial extension** – the conditions of extension should not be confused with tension (or pure tension). Extension is a special condition of compression. All forces are compressive, but specimen extension occurs in the direction where the compressive stress is least. This condition creates extensional fractures (not pure tension, or Brazilian-type fractures).

**Viscoelastic/viscoplastic** – the term visco refers to viscous (see viscosity) and represents the time-dependency of a particular process. Viscoelastic refers to a material that has both viscous and elastic properties, whereas viscoplastic materials have both viscous and plastic properties.

**Viscosity** – a measure of the resistance to flow that a fluid offers when subjected to shear stress.

**Void ratio** - ratio of the volume of void space to the volume of solid material in a sediment.

**Volumetric strain** – the change in total volume of the specimen during experimentation, usually expressed as a percentage.

**Water content** – see moisture content.

**Yield/yield stress** – the yield point marks the end of recoverable (elastic) deformation and occurs at the onset of permanent (plastic) deformation. It is observed as a clear deviation in the stress-strain results.

**Young's modulus (E)** - Defined as the ratio of the stress applied to a body to the strain produced. This parameter refers to elastic (recoverable) deformation.